ORIGIN AND FATE OF ARSENIC AND ASSOCIATED TRACE ELEMENTS IN THE RIVERS OF HOKUSETSU AREA, NORTHERN OSAKA PREFECTURE, JAPAN

（日本の大阪府北部北摂地域の河川水中のヒ素と関連微量元素の起源と移動）

平成 28 年度

Emilie EVEN
(エミリ　エベン)

ACKNOWLEDGEMENTS

The present study has been first of all a collaborative work involving the following people.
For supervision, discussion, major advices and thorough review: Prof. Harue Masuda (OCU).
For complementary scientific discussion, guidance on mineralogy, teaching on samples preparation and use of EDS and EPMA: Profs. Sakuyama T. (OCU), Shinoda K. (OCU), Kawakami T. (Kyoto U.), Okudaira T. (OCU), and Dr. Yoshida K. (Jamstec).
For guidance and use of LA-ICP-MS at Kyoto University: Prof. Hirata T. (Tokyo U.) and his students.
For guidance on S isotopes and Organic Carbon analysis at Okayama University: Profs. Chiba H. (Okayama U.) and Yamanaka T. (Okayama U.).
For extensive laboratory and analytical guidance: Shimonaka T. (OCU) and Okazaki K. (OCU).
For tremendous help on completing the field survey: OCU students Shibata T., Sakamoto Y., Murasaki T., Shintani T., and Dr. Fuchita S.
First samplings and analysis of the geochemical mapping work were initiated by Nojima A., under the supervision of Prof. Harue Masuda.

ABSTRACT

Since 1994, arsenic contamination has been chronically reported in the Hokusetsu river and ground waters that have sometimes been used for domestic purposes. The contamination has been thought to be natural, meaning that the geological settings caused the contamination. Dissolution of As-rich pyrite hosted in the Paleozoic/Mesozoic sedimentary rocks was proposed as the mechanism responsible for the contamination. These sedimentary rocks are the dominant geological formations of the region, and the As contamination may thus appear in other areas where the same formations are found. The study area is also a part of the important Tungsten-Tin-Copper mineralized Province. Numerous ore deposits were formed in association with the magmatic activities of the Late Cretaceous and Early Paleogene. Beside the mining commodities of W, Sn and Cu, many other trace elements, especially hazardous trace metals such as As, Ni, Co, Pb, are found in these deposits. Previous studies did not make clear the origin of the As-bearing pyrite, nor the possible release of the aforementioned elements from the ore-deposits into the environment. Such an uncertainty and the need to address the spread of the contamination of As and its associated elements in rivers of the Hokusetsu area motivated the present study. In order to document the whole process of As contamination of river, the river waters and sediments were analyzed to draw geochemical maps of an area of the Hokusetsu Mountains wider than in previous studies. The sulfide ore minerals recovered from the study area were mineralogically and geochemically studied in the context of the source(s) of As and its related elements. Then, the transportation process of these elements in river waters was investigated in relation to the attenuation or accumulation of concentration along the river flow.

The geochemical mapping showed that the highest concentrations of As in riverwaters and riverbed sediments appeared in the sedimentary rock areas, as a halo around the Ibaraki granitic complex, especially nearby faults. The As concentrations were comparatively low in the sedimentary areas far from the granitic complex. The waters flowing through the granitic rocks were remarkably depleted in As. The analogous patterns of As in water and sediments indicated that the element distribution of riverwaters was controlled by the base flow, i.e., the interaction between subsurface water and host rocks. The highest concentrations were also prominent in fractures zones, emphasizing the role of the fracture in increasing the specific surface area (SSA) of rock mass, infiltrating oxic water and promoting the water-rock interaction. Sulfur isotope ratios of dissolved sulfate showed that the ambient river waters were impacted by sulfur inputs from soils, while the higher sulfate concentrations were attributed to the dissolution of pyrite and/or other sulfide ore minerals, as observed by Ito et al. (2003). The sulfur isotopes from sulfides in rocks showed that two kinds of ore-deposits existed in the contaminated areas, i.e., deposits from the Late Paleozoic/Mesozoic submarine volcanogenic, and hydrothermal ore deposits from the Late Cretaceous to Early Paleogene magmatic activities. The consistency of sulfur isotopic ratio from these ore deposits with those from high-sulfate concentrations of highly As contaminated waters showed that the As contamination was related to the dissolution of sulfide ores in the area.

In order to characterize the As-bearing sulfide minerals and their origins, sulfide minerals recovered from rocks and ore deposits were mineralogically and geochemically examined. The Late

Paleozoic/Mesozoic submarine ore-deposits were rare in the study area, despite being an important source of the As contamination. The Late Cretaceous to Early Paleogene ore deposits were common, and categorized into two subtypes: the plutonic type disseminated in contact-metamorphosed rocks (i.e., pneumatolytic and skarn type deposits in quartzite and other meta-sedimentary rocks) by the granitoids intrusion, and the subvolcanic type deposits comprising hydrothermal veins related to granitic cupolas and porphyry dikes. Laser ablation-ICP-MS revealed the presence of As in sulfides from all types of ore deposit, but was the highest (up to 0.8wt%) in the pyrite from some of the subvolcanic type deposits located in sedimentary rocks intruded by granite porphyry dikes. Associated hazardous elements such as Pb, Ni, Co were also observed in sulfides. These elements would also be released into the study hydrosphere from the sulfide dissolution, similarly to As.

The influence of geology and ore-deposits of the study area and the fate of As and its associated trace elements in the studied river system were assessed through an extensive geochemical mapping, multivariate statistical analysis and assessment of the trace elements behavior in the water column. Mapping and statistical analysis showed that most of trace elements (Ni, Co, V, Cr) originated from the clay-rich Ultra-Tamba formations, while the influence of ore deposits was unascertained on Zn, Cu, Pb distribution, but strong for As. Upon its release into the river systems, As did not undergo complexation with large particulate matter (>0.45μm). Analysis of the fractionation of studied trace elements was metered via the dissolved transport index (DTI) that indicates the percentage of an element in the dissolved fraction. DTI calculations showed that As preferentially remained as a dissolved species in the water column, together with the trace metals Ni, Cu and Cd that showed a similar behavior. These observations are dissimilar to what has been emphasized in most of river water studies in which As has been described as binding onto Fe-, Mn- and Al- oxides and hydroxides and detrital clays. These later elements, as well as Ti, are the major constituents of the mineral-binding phases and their DTI were indeed low. However, the binding of Co and Pb (DTI<50), and Cr to a lesser extent (DTI<75) onto those mineral particles was demonstrated, which implied an removal from the water column of these metals as they precipitated with the particulate phase. The binding inability of As and other hazardous trace metals issued from the dissolution of ore minerals would increase their mobility, and may thus involve an extension of contamination. But the inflow of As-free, trace-metal-free groundwater into the streams contributed to lower the high As concentrations and those of other trace-metals.

The present study helped understanding the origin and behavior of As, and associated trace elements, in the hydrosphere of mountainous shallow rivers in an area of heavily mineralization, as part of the As geochemical cycle in the Earth's crust.

要　旨

大阪府北部の北摂山地では河川水に環境基準値の 0.01mg/L を超えるヒ素が含まれることが以前から知られていた。この地域でのヒ素汚染は、堆積岩中の黄鉄鉱の化学的風化作用によると説明されてきたが、黄鉄鉱がヒ素を濃縮している理由とヒ素汚染の拡大状況については不明であった。これらを明らかにするために、本研究を計画した。

最初に、悉皆調査により、大阪府北部とそれと接する京都府と兵庫県の一部の 163 地点から河川水を、そのうちの 84 地点からは河床堆積物を同時に採取し、主成分化学組成とヒ素とヒ素に関連する微量元素を定量した。分析結果は地球化学地図として、濃度分布を検討した。河川水の化学成分濃度分布は表層地質や河床堆積物の化学組成と明瞭な関係があり、河川水の化学組成は基底流出する地下水が最大の規制要因であることが明らかであった。河川水と河床堆積物のヒ素濃度は調査地域中央に分布する茨木花崗岩体の周辺部で高かった。

次に、硫化鉱物の化学的性質を検討した。本地域西部には多くの熱水性とマグマ性の鉱床がある。また、堆積岩中には硫化鉱物による鉱染が見られることがある。これらのヒ素を含む硫化鉱物は、産状やイオウ同位体比、ニッケルやコバルトなどの微量元素組み合わせなどから、付加体内部の海底熱水活動と白亜紀～新生代初期の花崗岩体に関連するマグマ性の交代鉱床作用の２つに起源を持つことが示唆された。どちらもヒ素汚染の原因となりえるが、海底熱水活動に起源を持つものの方が高濃度の汚染を発生させていた。

ヒ素汚染発生地点には好気的地下水の涵養経路となる古い断層があり、化学的風化作用を促進する要因となっている。さらに、硫化鉱物の分解後、鉄・マンガンなどは酸水酸化物・酸化物として沈殿除去されるが、ヒ素は溶解度の高いヒ酸として懸濁物に吸着されることなく表層水中を流下する。このことが、ヒ素汚染の拡大の原因である。

本研究の結果は、ヒ素が、火成作用やそれに伴う熱水活動を通じて海洋・大陸地殻に濃縮され、陸域では水圏を通して移動することを明らかにした。

TABLE OF CONTENTS

LIST OF FIGURES

infiltrations to δ 34S (< 0‰) from pyrite in rocks. After Mizota & Sasaki, 1996 (soil data), Sato & Kase, 1996 (stratiform deposits) and Ishihara and Sasaki, 1991 (igneous sulfur).

Fig. 4.7 – Summary model of As contamination in the study area, in relation with the geological settings. Highest contamination appears in zone of rocks disseminated with As-bearing sulfides and fractured by fault

Fig. 4.8 –Arsenic concentrations and isotopic sulfur ratio of river waters from the present study (gray symbols) and Ito et al. (2003) (open symbols). The general evolution shows a decrease of the isotopic signal with the increase of As concentrations

Fig.4.9 - Weathered mineral in the wacke sandstone of Todoromi area

Fig. 4.10 - Photomicrographs in reflected light of a) magnetite (mag) and chalcopyrite (cp), and hematite (brown red) in Todoromi sandstone, b) back-scatter electron (BSE) detail image of the magnetite/chalcopyrite assemblage with colloform texture. c) Todoromi sandstone with magnetite (mag) and pyrrhotite (po), and titanite (ttn) with Ti oxide (Ti Ox), d) scanned electron image (SEI) of Todoromi shale with headspear-shape marcasite (mrc) and sulfarsenide (sulfAs) of gersdorffite-cobaltite solid solution. Photomicrographs in reflected light e) in quartzite of pyrrhotite (po), chalcopyrite (cp), ilmenite (ilm) and garnet (gnt), (f) Otani Mine assemblage with stannite (stn), native Sn (Sn), sphalerite (sp), pyrite (py) and chalcopyrite (cp), Kawaura mine sulfides with (g) pyrite, chalcopyrite (cp) rimed with digenite (dg) and (h) chalcopyrite surrounded by Ag-sulfides (Ag sulf), and covellite (cv, blue), (i) scanned electron image (SEI) of pyrite (py) in shale gauge (dark grey) of Satsukiyama fault (Fushio). Photomicrographs in reflected light of (j) deformed pyrite (py) and magnetite (mag; grey) in hornfels nearby Hirao mine, (k) assemblage of chalcopyrite (cp) rimed with covellite (cv, blue) from Hirao hydrothermal ore deposit, (l) assemblage of chalcopyrite (cp) and sphalerite (cp) with chalcopyrite disease (cp blebs in sp) at Hirao mine, (m) pyrrhotite (po) and magnetite (mag) in hornfels near Osugahara mine, and (n) Tada mine massive sulfide of chalcopyrite (cp), bornite (bn), sphalerite (sp), galena (gl) and covellite (cv, blue), o) sphalerite (sp) and galena (gl) in Hatano skarn deposit, p) authigenic TiO2 mineral (rutile, bright areas) overgrown by titanite (ttn, gray areas).

Fig. 4.11 - Time resolved ablation line of a) across a weathered chalcopyrite/magnetite assemblage in Todoromi sandstone, b) marcasite sulfide in Todoromi shale, c) sulfides assemblage of chalcopyrite (cp) and pyrrhotite (po) in contact-metamorphosed quartzite sample, d) pyrite sulfide in hornfels rocks nearby Hirao mine. Time resolved ablation line of e) massive pyrite from Hirao hydrothermal deposit (the black arrow marks the firing of the laser), f) veinlet of pyrite in massive pyrite from the Hirao hydrothermal deposit, g) pyrrhotite with magnetite exsolution in hornfels rocks near Osugahara Mn mine (the black arrow marks the firing of the laser), and h) sulfide assemblage of bornite (bn, galena (gl) and chalcopyrite (cp) for the Tada xenothermal ore-deposit.

Fig.4.12 - Element mapping of ^{32}S and ^{75}As by LA-ICP-MS of the quartzite sample. The mapping of sulfur delimited well the sulfide minerals of the sample. Arsenic appeared in minute places scattered all over the sulfides, mainly in pyrrhotite

Fig.4.13 - Element mapping of ^{32}S, ^{55}Fe, ^{118}Sn and ^{75}As by LA-ICP-MS of sample from Stage 2A mineralization of the Otani mine. Euhedral pyrite appeared very neatly, while Sn gave a clear image of the stannite. Arsenic appeared more intensely at the edges of stannite and pyrite, and in an unidentified non-sulfidic phase (lower right).

Fig. 4.14 - $\delta^{34}S$ of sulfides from marine sedimentary sulfides (-40 to -10‰), Japan sedimentary and pelitic metamorphic rocks (-21 to -9‰), Japan Paleozoic/Mesozoic stratiform Cu deposits (0 to +5‰

), Japan ilmenite series granitoids (-9 to -2‰), Otani (-10.5 to -8.6‰), Tada (-3.5 to -1.7‰), Akenobe (-3.5 to +0.8‰) and Ikuno (-0.2 to +0.9‰) ore-deposits, and ①Todoromi sulfides, ② quartzite rocks sulfides, ⑤Fushio sulfides. Data from 1: Miyoshi et al. (1988), 2: Ishihara and Sasaki (1992), 3: Sato and Kase (1996), 4: Canfield (2004).

Fig. 4.15 - Mineralization system (represented by thick lines) of the Tada ore-deposits. The vein system of the Tada Mine (9) is called the Ginzan vein family (mainly Cu-Pb-Ag, left of the map). Other vein families (mainly Cu) are called Hayama (including Shichiboh and Kimyozan, center, and Takayama, lower left). Numbers in circles as in Fig.3.3. After the Permanent Memorial of the Tada Ginzan.

Fig.4.16 - Ni/Fe vs Co/Fe in pyrite, pyrrhotite, marcasite (and sulpharsenide, upper right outliers) of studied samples. Solid line represents the 1:1 ratio.

Fig. 4.17 - Distributions of Si, Al, Fe, K, Na, Ca, Mg, Ti, Mn, Ba, Rb, Sr, Zn, V, Cr, Cu, Ce, Y, La, Nd, Co, Ni and Pb in riverbed sediments of the Hokusetsu area.

Fig. 4.18 - Biplot of the loadings on PC1 and PC2 of studied elements, As excluded

Fig. 4.19 - Biplot of the loadings on PC1 and PC2 of studied elements, As included (bold).

Fig. 4.20 - Distributions of K, Na, Ca, Mg, Al, Fe, Sr, Ba, Mn, Ti, Cu, V, Rb, Ni, Cr, Pb, Co, Cd, Ce, La, Y and Nd in river waters in the Hokusetsu area.

Fig. 4.21 – Qualitative repartition of elements in river waters according to their distribution in igneous or sedimentary formations, and their high concentrations being restrained to spring area or along the river courses

Fig. 4.22 - Distribution of Dissolved Transport Index (DTI) for Fe, Al, Mn and As. Most of DTIAs range between 70 and 100, while DTI_{Fe}, DTI_{Al} and DTI_{Mn} range mostly below 40. Fe n=107; Al n=56; Mn n=104; As n=66. DTI = Dissolved (< 0.45μm) conc. / Total conc. x 100.

Fig. 4.23 - Biplot of DTI_{Fe} and DTI_{As}. Most of DTI_{As} plot between 70 and 100, meaning that As is mainly present as a dissolved phase in water. For DTIAs < 50, DTI_{Fe} and DTI_{As} behave together, showing that for low As concentrations (<1 ppb, samples from Ibaraki River), most of the element is absorbed on Fe particles

Fig. 4.24 - DTI classification of Martin in Meybeck (1979). From Foster and Charlesworth (1996)

Fig. 4.25 - Biplot of DTI of Fe/Co and Fe/Pb. The correlated plot of DIT of Co and Pb with DTI of Fe tended to highlight the non-conservative behavior of these elements, likely in a metal-Fe-bearing phase condition.

Fig. 4.26 - Biplots of total and dissolved organic carbon (TOC/DOC) (a, b, c; the line represents the 1:1 ratio), DOC and dissolved As (d, e, f) and DOC vs dissolved Cu (g, h, i) in Yono, Minoh and Ibaraki Rivers, respectively.

LIST OF TABLES

1. INTRODUCTION

1.1 General overview of arsenic in rivers

Arsenic (As) is a minor but ubiquitous metalloid in the shallow crust of the Earth and its hydrosphere. But when ingested, this is a hazardous element that causes organ dysfunction, skin cancers and other severe health afflictions. The World Health Organization (WHO) set a guideline value of As in drinking water to 10µg/L (= 10ppb; the parts-per (pp-) notation will be preferentially used in this study) (WHO, 1993).

Numerous studies on the natural As contamination of groundwater in aquifers have been published because of the critical role of these reservoirs for the supply of drinking water and agricultural usage, and the gigantic scale of affected populations (Fendorf et al., 2010; Smedley and Kinniburgh, 2002). On the other hand, studies on the behavior of As in surface waters are comparably limited, with the exception of biogeochemical studies. Typical studies refer to severe contamination of river systems by geogenic arsenic (Baker et al., 1998; BGS&DPHE, 2001), inflow of As-contaminated hydrothermal waters (Nimick et al., 1998; Timperley and Huser, 1996), As behavior in association with planktonic activities in lakes (Andersen and Bruland, 1991; Sohrin et al., 1997), drainage of mining site (Beauchemin and Kwong, 2006), and pollution by anthropogenic releases like sewage or industrial effluents (Baeyens et al., 2007; Woitke et al., 2003).

Studies on the transportation process of As from the source area to the contaminated aquifers and the distribution of background concentrations in surface waters are important to document the As cycle in the shallow crust and the hydrosphere. However, the whole picture comprising all stages of the geochemical cycle of the element has still some lacks since previous reports usually focus on large streams, deposition in estuarine environment (e.g., Cenci and Martin, 2004; Webster, 2010) or pollution from hydrothermal sources and mining areas (e.,g., Robinson et al., 2015; Wilkie and Hering, 1998)

Very few papers (e.g., Pokrovsky et al., 2006) have been published about the origin and transportation of As in small rivers, within natural conditions that allow the monitoring of base-flow contributions and chemical interactions between the local geology and meteoric waters. Indeed, the geochemical conditions of small streams in mountainous area differ from large rivers because of their discharge size and hydraulic characteristics. Arsenic is an element highly sensitive to the redox

conditions. Because these conditions are susceptible to change along the stream course either spatially or temporally (e.g., at springs or during rain events), the behavior of As between the inorganic and organic compounds of water and the host rocks/sediments changes consequently, and thus its distribution in the different compartments of the rivers. Generally, fresh waters contain As at low levels (<1ppb; Smedley and Kinniburgh, 2002), although in areas where geogenic As is concentrated in the environment (e.g., mineralized or volcanogenic areas), concentrations above 10 ppb could be easily exceeded, e.g., Elqui river basin in northern Chile (Oyarzun et al., 2006) and the Pecora River Valley (Costagliola et al., 2004).

The prediction of natural As-contaminated areas is a key to prevent further large poisoning as observed in South-East Asia and other affected areas. Thus, broad geochemical surveys in relatively natural conditions are useful to fill in the gaps in our understanding of the behavior of As and its geochemical cycle.

1.2 Arsenic occurrence and its associated elements in Japan

As-related health problems have also happened in Japan. These problems were caused by man-made pollutions and the natural occurrence of the element in the environment.

First issues of arsenic poisoning in Japan arose during the 20th century when cases of poisoning through the refining activities (1920 to 1941 and 1954 to 1962) of a As mine were recognized in Toroku village, Miyazaki Prefecture. Arsenicosis also occurred in Nakajo village of Niigata Prefecture from the consumption of well waters contaminated by the nearby arsenic factory in the 1950s (Nakadaira et al., 1995), and in the Sasagadani valley in Shimane Prefecture from the smelting activities of a copper/arsenic mine (Tsuchiya, 1977). Other problems occurred from the wastewaters from a geothermal power plant in South Japan because contaminated waters were drained into the nearby streams, increasing the natural background level of As of the rivers downstream (Nakahara et al., 1978).

In 1993, the Japanese government adopted the WHO standard value of 10 ppb As as the MCL (maximum contaminant level) of environmental waters, including drinking water. As a result of lowering the MCL from 50 ppb to 10 ppb, many supplied waters (mostly groundwaters in coastal plains) of Japan exceeded the limit. The largest contamination was found in Fukuoka and Kumamoto

Prefectures, without related disease being reported (Shimada, 1996). Later in 2003, arsenicosis was diagnosed in Kamisu, Ibaraki Prefecture, on residents who consumed groundwater polluted from the dump of concrete block sealing that was leaking diphenylarsenic acid (Ministry of the Environment, 2008).

A nationwide assessment of the As distribution (among other elements) on the ground surface was achieved through the geochemical mapping of riverbed sediments by Imai et al. (2003) (Fig.1.1). The work enlightened the occurrence of high As levels in sparse but well-defined geological zones of Japan. Riverbed sediments with As>50 ppm were mainly observed along the volcanic fronts in Kyushu, and Northeast Japan from the Itoigawa-Shizuoka Tectonic Line along the subduction of the Philippine Sea and Pacific plates. In the Inner Zone of Southwest Japan, As seemed to be associated with the Cretaceous-Paleogene magmatic activities that produced hydrothermal vein- and skarn-type ore deposits (Ishihara, 1978). Because As tends to be concentrated in sulfide mineral ore deposits, it results in the natural contamination of riverbed sediments in the mines surroundings (Ohta et al., 2005).

The present study is focused on the Hokusetsu region among the Hyogo, Kyoto and Osaka Prefectures (Fig.1.2). In this area, high concentrations of As affecting waters were first reported in 1994 (Shimada, 1996) in Takatsuki City, in 300m-deep wells drilled into the Quaternary sedimentary formations (Osaka Group) that mostly consist of sand and clay layers. The sediments of the marine clays from the Ma 5 layer contained up to 400 ppm As, as measured by Tonokai and Mitamura (1998). The authors suggested that the source of As could possibly be the mineral(s) derived from the hydrothermal ore deposits, occasionally found in the hinterland. In 1995, high As concentrations up to 42 ppb in the main stream and up to 620 ppb in saline spring waters were reported in the Ina River system (flowing in the western part of the Hokusetsu area). These considerably high As levels in the saline waters were likely triggered by the Hanshin (Kobe) Earthquake that changed the pathways of groundwater flow through the mineralized region (Ogoshi et al., 1996; Wada and Fukushima, 1997).

Masuda et al. (1999) documented As contaminated spring waters (~30 ppb) along 2 tributaries of the Yono River in Todoromi village of Minoh City. The authors presumed that the dissolution of sulfide minerals in the Paleozoic/Mesozoic sedimentary rocks was the source of dissolved As. Indeed, Ito et al. (2003) reported the whole rock at the spring site to contain As (4.2 to 16.4 ppm), and the pyrite in these host-rocks contained up to 0.73wt% of As.

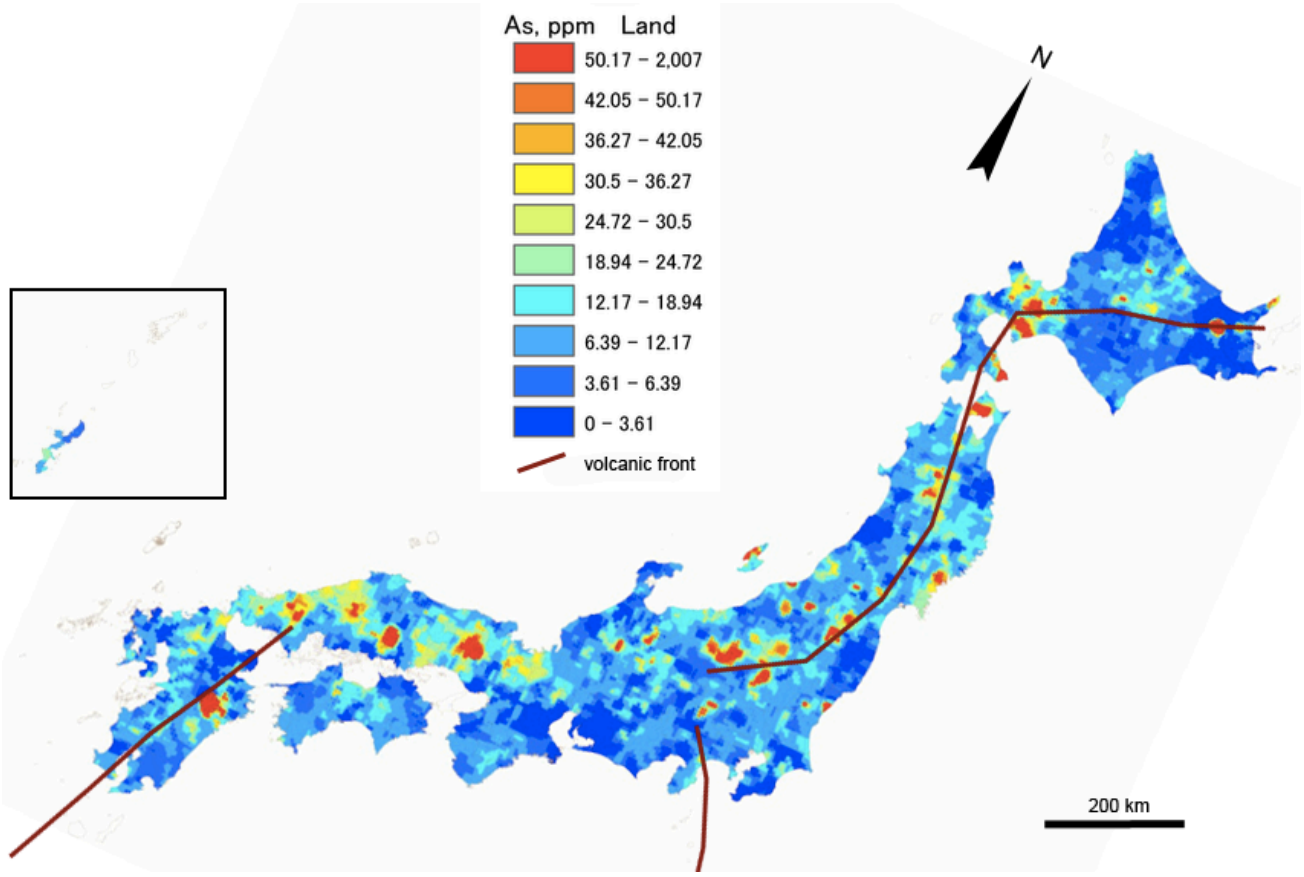

Fig.1.1 - Distribution map of As in riverbed sediments of Japan. The red line represents the volcanic front. After Imai et al. (2004).

Fig.1.2 - Context map of the Hokusetsu region in Japan. Modified from ja.wikipedia.com

In 2003 during the excavation works for a highways tunnel in these same sedimentary formations, As concentrations in Minoh and Senri Rivers increased three times the WHO standard likely due to the inflow of contaminated waters from the tunnel (Osaka Prefecture Government, 2016).

Japan is a country with a long mining history and thus bears about 5000 mining sites, although most of them have closed since the 1980s (JOGMEC, 2013). This rich mining history witnesses the natural occurrence of numerous ore deposits throughout the Japan territory. Unfortunately, along with As, sulfide deposits bear a batch of commodities that usually comprises harmful heavy metals like Ni, Co, Pb or Cd that would pose a threat to the environment including the biosphere and the public safety. One of the largest cases of poisoning caused by the mining activity occurred at the Kamioka mine that exploits a Pb-Zn skarn-deposit in Gifu Prefecture. Sphalerite (ZnS) is a common mineral of the skarn deposits, and the chief ore of cadmium (Cd) (Cook et al., 2009). The mining operations at Kamioka caused a Cd contamination that spread via atmospheric deposition and throughout the Jinzu River system down to the Toyama Prefecture. The large contamination resulted in the Itai-itai disease as people were consuming contaminated river water and agricultural products (mostly rice) (Kobayashi et al., 1970).

The more recent study of Kamiga and Tagiri (2003) showed that the environment around the important Ashio and Hitachi Copper Mines were still affected by the past mining operations that ended in 1973 and 1981, respectively. In addition to As, Ni, Pb, Cd and others trace elements emitted from smelting smokes and wastes were recorded at levels exceeding the national recommended standard and increased the background values. High levels of these elements in smelting slags disposed along the streams were still released into the surrounding riverbed sediments and soils. Therefore, the monitoring of the aforementioned trace elements should complement any geochemical investigation of As when it is believed to originate from sulfides ores, as suspected for the Hokusetsu area.

1.3 Purposes of the present study

The occurrence of high concentrations of As in spring waters of the Todoromi villages and in the Ina River waters after the Hanshin Earthquake had shed light on a possible contamination of rivers via the As-bearing sulfides or fossil ore-fluid hosted in the local Tamba formations. However, it was not clear how wide the contaminated area was.

Also, the question remained of why the pyrite in the Todoromi sedimentary rocks contained such a high amount of As. The origin of this pyrite was unknown but it occurred in a heavily mineralized area, and this lead to suspect a magmatic origin of the pyrite rather than a diagenetic origin. As explained in Section 1.2, mineral deposits from such magmatic sources may also contain harmful trace element besides As, and their release into the environment would constitute an additional source of contaminants that adds up to the As threat.

Additionally, while the chemistry of trace metals of river waters is primarily controlled by that of base flow interacting with host-rocks, it is secondary influenced by adsorption-desorption onto the suspended particles. The sorption exchange between the solid and dissolved fractions in the water column governs the element transportation process in surface water. Depending on the conservative or adsorptive affinity in the water column of As and other hazardous elements, the contamination may extend over the local river basins or be constrained to the source-rock area. It was thus a concern to understand how As and trace elements are transported along the river course.

To answer these questions, the objectives of the present study were threefold. From the Todoromi villages where the As-bearing pyrite was reported, the monitored area was widened to the rivers within the Hokusetsu region to assess the As contamination in relation with the surface geology. Then, the possible link between the As-bearing pyrite in source-rocks and the ore-deposits in the Hokusetsu area was investigated to determine the origin and concentration mechanism of As in rocks. For this purpose, geochemical composition of sulfide deposits, including other trace metals Ni, Co, Pb, were also analyzed. Finally, the influence of surface geology as a source of trace elements, and the fate of As and other elements in regard of the complexation with the ligands present in the river water were discussed.

The documented scenario will be valuable to explain the As cycle at the Earth's surface, especially in the shallow crust and hydrosphere, where water-rock interaction largely affects the water chemistry.

2. GEOLOGY OF THE STUDY AREA

2.1 General geological outlying

The study area is located in the Hokusetsu area, the ancient name of the region that comprises the northern part of Osaka Prefecture, the southwestern part of Kyoto Prefecture including Kameoka, and the southeastern part of Hyogo Prefecture including Inagawa. The study extends over an area of 25km x 19km (475km^2) mainly in the northern part of Osaka Prefecture. The surface geology is depicted in Fig.2.1.

The basement rocks of the study area are mostly sedimentary formations belonging to the Paleozoic and Mesozoic Tamba Belt. The studied formations of the Tamba Belt are divided into the Mesozoic Tamba Terrane in the north of the study site, and the Paleozoic-to-Mesozoic (Permian and Triassic) Ultra-Tamba Terrane in the central part that lies unconformably over the Tamba Terrane. The Terranes are part of ancient complexes composed of pelagic and terrigenous materials that accreted during the Late Triassic to the Jurassic (Sakaguchi 1961; Nakae 1993; Miyachi et al. 2005; Sugamori 2006).

The sedimentary complexes of the Tamba Terrane are mainly composed of sandstone with interbedded sandstone and shale, and shale with sandstone lenses. Triassic to Jurassic slabs of chert and bedded chert frequently occur in the northern part of Tamba Terrane in the Tamba district (north of the Hokusetsu region). Greenstone (as meta-basalt) and limestone are also commonly observed; these rocks formed complexes likely underlying the Tamba Terrane and are thought to be Carbo-Permian seamounts (Sano and Tazaki, 1989).

The Ultra-Tamba Terrane of the study area comprises two formations: the Takatsuki and Yamashita formations. The Takatsuki formation is composed of dark grey to dark green fine to coarse-grained or light grey siliceous sandstone, dark grey to black and locally red shale, and interbedded sandstone and shale. The Yamashita formation is mostly composed of dark gray-bedded shale with fine-grained sandstone laminae, and interbedded shale with sandstone. Ishiga (1990) has described the sandstone of the Ultra-Tamba Terrane to be greenish cataclastic and lithic wacke. Greenstone and chert are rare in the Ultra-Tamba Terrane.

In some places, these sedimentary rocks have been metamorphosed into hornfels and quartzite by contact with intrusive rocks (Matsuura et al., 1995; Miyachi et al., 2005; Miyamura et al., 1972).

Several plutons intruded into the Tamba Belt during the late Cretaceous (Ishizaka, 1971). The main granitic bodies found in the study area are the Ibaraki and the Mikusayama granitic complexes that intruded at the same time (90-80 Ma; Tainosho et al., 1977). The Ibaraki complex, which mainly intruded in the Ultra-Tamba Terrane, is divided into the northern felsic granite Myoken pluton, and the southern Nose pluton. Tainosho (1971) has described the Nose pluton as being formed through the sequential intrusions of the same dioritic magma with differential crystallizations from intermediate quartz-diorite to felsic granodiorite and to granite toward the inner part. The Mikusayama complex, which intruded mainly in the Tamba Terrane, is composed of pyroxene quartz-gabbro, granodiorite and granophyre (Tainosho et al., 1977). The Ibaraki and Mikusayama complexes were derived from a dioritic or tholleiitic magma of the same series of Late Cretaceous magmatism (Tainosho et al., 1977). The chemical and modal compositions of the granitic complexes are very similar, although the Ibaraki quartz-diorite seems richer in biotite than the Mikusayama quartz-gabbro. Numerous granitic porphyry dikes that intruded during the late Cretaceous as well mostly in a south-north direction, but are likely posterior to the granitic intrusions of the study area (Matsuura et al., 1995; Miyachi et al., 2005).

The Tamba Belt formations are overlaid in the south by the Quaternary Osaka Group, which is composed of unconsolidated gravel, sand, clays and ash layers, and Pleistocene terrace deposits. In the west, the formations are overlaid by the Late Cretaceous volcanogenic rocks of the Arima group composed of several rhyolitic lavas and tuffaceous formations (Kasama and Yoshida, 1976).

There are numbers of fault and lineament in the study area (Okada and Togo, 2000) (Fig.2.1). A, D, E, and H in the figure are inferred active faults. B is a fault that has not been active during the Quaternary. C, F, and G are sharp lineaments, which would be fossil faults. Tainosho (1971) and Matsuura et al. (1995) reported a fault (I) running in the northeastern part of the Nose pluton that could be a continuation of the Satsukiyama fault (B), although it was not described in the inventory report by Okada and Togo (2000). While most of the faults are not active, they constitute potential pathways for the infiltration of meteoritic waters and the circulation of groundwater within the rocks.

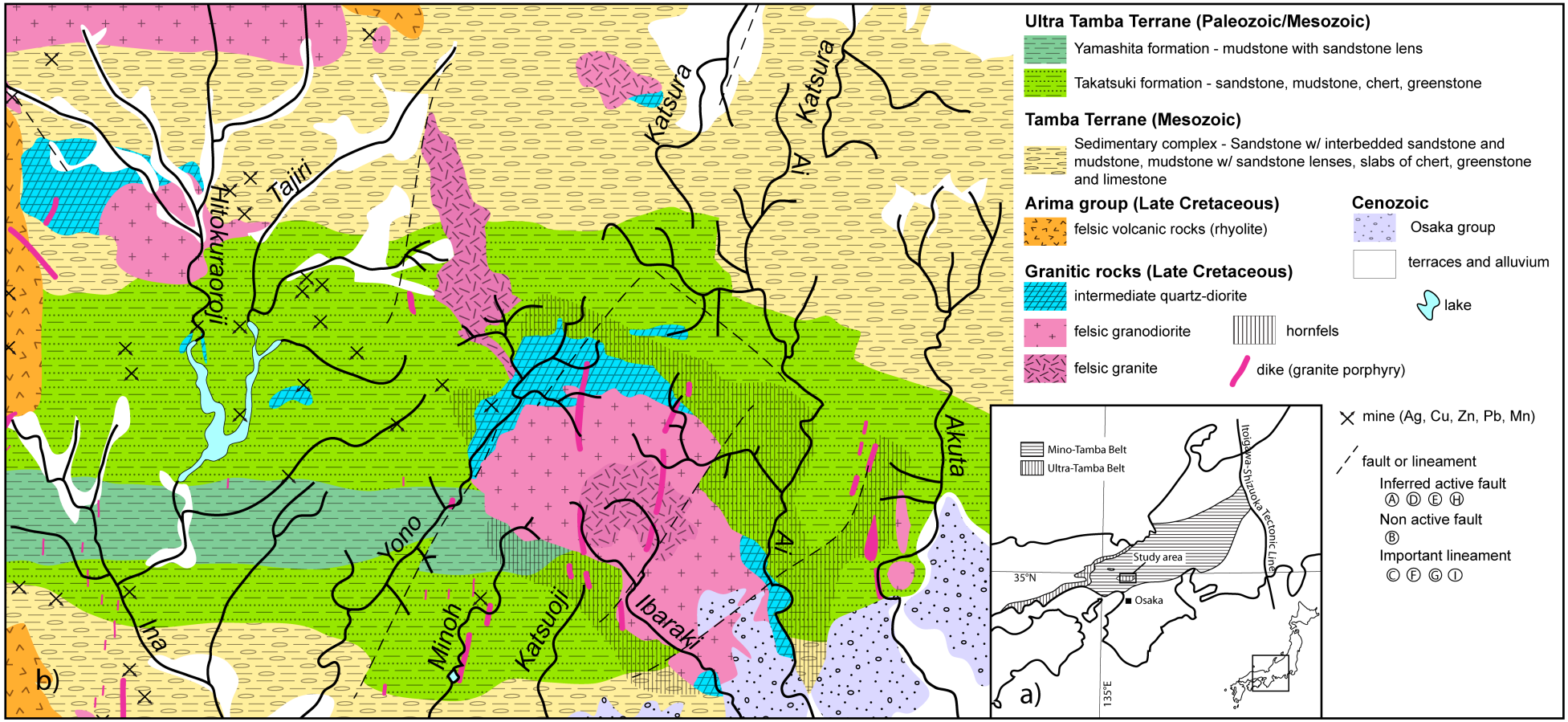

Fig.2.1 - Context map of the study area (a) and its surface geology (b). Most of the geology is composed of sedimentary rocks from Paleozoic/Mesozoic, intruded by felsic and intermediate igneous rocks during Late Cretaceous. Hornfels were found around the Ibaraki Granitic Complex, but it is possible that their occurrence extends over the shaded area on b). Mines of small hydrothermal veins and skarn are indicated. Several active (A, D, E, H) and non-active (B) faults, and lineaments (C, F, G, I) are also reported. (After Miyamura et al., 1972; Matsuura et al., 1995; Okada and Togo, 2000; Miyachi et al., 2005

The investigated rivers are the Ai, Akuta, Hitokuraooroji, Ibaraki, Katsuoji, Katsura, Minoh and Yono Rivers. They are tributaries of the Yodo and Ina River systems in the Osaka and Hyogo Prefectures, respectively. The studied streams flow in the eastern part of the low Hokusetsu Mountains through forest and rural landscapes (usually rice paddy fields), within their natural riverbed. The magnitude of the discharge of the studied streams varies from river spring (<1 L/s) to large stream (>1.5 m3/s) (MLIT, 2013).

2.2 Background on the mineralization of the Hokusetsu region

The mineralization of the Inner Zone of Southwest Japan comprises several types of ore-deposits that formed during the different mineralizing epochs related to the tectonics of the Japan Islands tectonics (Nakamura, 1990; Nakamura et al., 1987; Tatsumi et al., 1970; Watanabe et al., 2016). These are 1) the Late Paleozoic-Early Mesozoic kieslager-type Cu-deposits from submarine volcanism (although the typical deposits are found in the Sanbagawa Belt of the Outer Zone) and the stratabound syngenetic Mn-deposits, 2) the Ni-Co-Cr ore deposits hosted in Jurassic ultramafic formations in Sangun Belt, 3) the Sanyo W-Sn-Cu and Sanin Mo (-Pb-Zn) deposits generated from the Cretaceous-Paleogene magmatism that also produced numerous batholiths, 4) the polymetallic and precious ore deposits, also called subvolcanic vein deposits, from the Late Cretaceous Paleogene igneous episode, and 5) the Neogene felsic volcanism in the Southwest Japan back-arc that produced the volcanic massive Kuroko-type deposits. Additionally, some of the pre-Cretaceous deposits have been altered by the continuous tectonics of the Japan Islands (Takimoto, 1973). The occurrence of As in ore-deposits has been usually reported under the form of arsenopyrite, especially in the Late-Cretaceous/Early Paleogene vein-type deposits.

In regards to the aforementioned types of deposits, the following mineralizations are recognized in the Hokusetsu region. Many pre-Cretaceous strata-bound (i.e., chert-hosted) bedded Mn deposits were accreted in the present Mino-Tamba belt, and widely distribute at the north of the Hokusetsu area (Fig.2.2) (Sato and Kase, 1996; Tatsumi et al., 1970). These deposits formed on deep-sea floor from the diagenesis of Mn hydroxides in a submarine anoxic environment, and in the Tamba area, the ore is essentially rhodochrosite associated with grey to dark gray bedded and massive cherts (Nakamura, 1990). Kieslager-type cupriferous iron sulfide deposits that also formed from submarine volcanism are usually associated with the mineralization epochs of the Mn-deposits

(Kanehira and Tatsumi, 1970; Nakamura, 1990). Although none have been reported in the Hokusetsu region, a few deposits (Fig.2.2) are located in non-metamorphosed terrains of the Tamba Belt (Funaoka and Tsuchikura deposits of mid-oceanic ridge volcanism Besshi-type) and in weakly metamorphosed areas of the Maizuru Belt (Maizuru and Yanahara deposit of back-arc volcanism Hitachi-type) (Sato and Kase, 1996).

The second type of mineralization in Hokusetsu is associated with the igneous activities, which generated the volcanic rocks of the Arima Group and the plutons described in Section 2.1. The Tamba Belt is part of the W-Sn-Cu metallogenic Province (Fig. 2.3) that was formed from the intrusion of the felsic granitoids belonging to the ilmenite (magnetite-free) series of the Sanyo Belt (Ishihara and Sasaki, 1991). W and Sn ore-deposits usually occur as quartz-veins nearby or within rocks of granodiorite and granite (Ishihara, 1978). In the Hokusetsu area, the most important of these deposits is the Sn-W pegmatite-veins of the Otani mine formed from the intrusion of the Gyojayama granodiorite, east of Kameoka (Kyoto Prefecture). Skarn-type deposits producing Cu-Zn-Pb ores also appeared during this mineralization time, when the granitoids were in contact with the few limestone of the Hokusetsu region. The Hatano mine, south of the study area, is one of these skarn-type deposits.

Following the Late Cretaceous plutonism, numerous vein-deposits containing polymetallic Cu-Pb-Zn and precious Au-Ag ores were generated by the Early Paleogene intrusive-dikes. In the Hokusetsu region, the most important Cu-Au-Ag deposit is the Tada mine located in the west of the study area. The Tada ore-deposits are believed to being generated from the intrusion of granite porphyry dikes into the volcanogenic rocks of the Arima Group (Imai et al., 1975). Many other small to intermediate Cu-Zn-Pb vein-deposits were also mined, and all of them were closed during the 1980's. These small vein deposits did not occur nearby plutons but they are reported almost exclusively in the western half of the study area, where the presence of multiple granite porphyry dikes denotes the occurrence of hidden igneous bodies. The locations of these mines are important indicators of mineralization that may bear As.

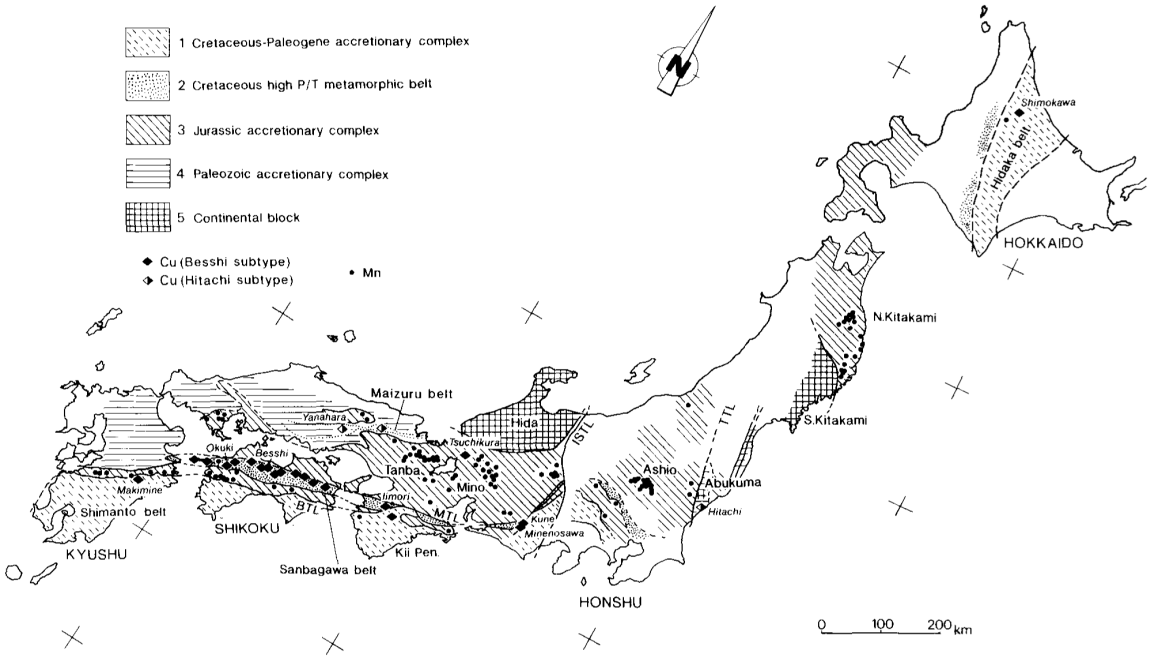

Fig. 2.2 Distribution of the Cu massive sulfide deposits and chert-hosted stratabound Mn deposits in Japan. From Sato and Kase, 1996

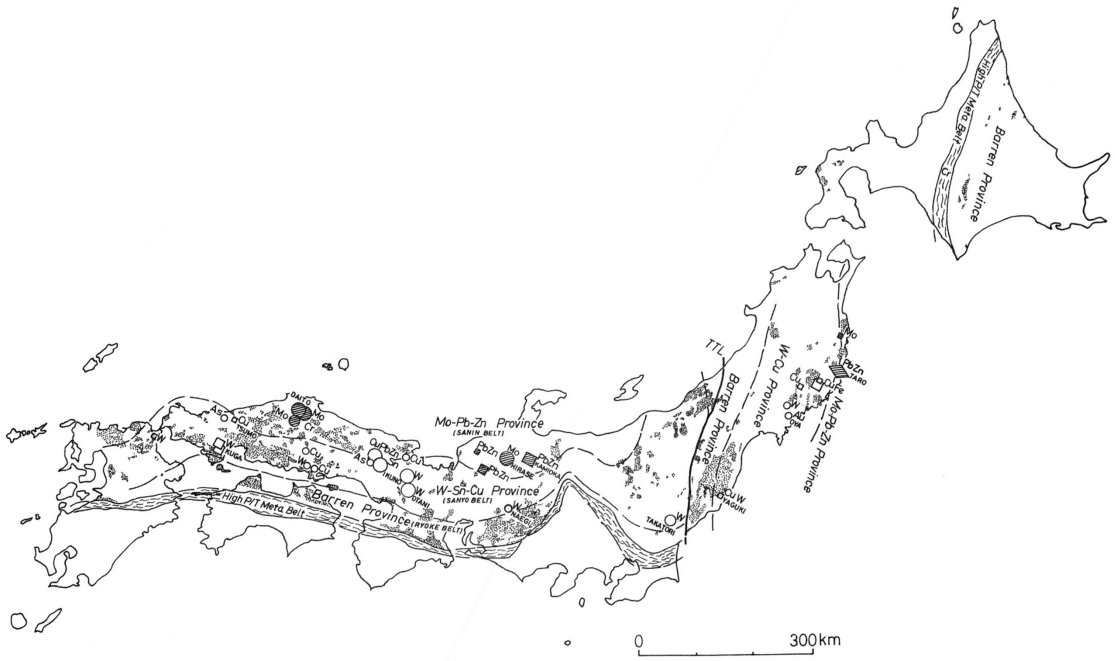

Fig. 2.3 Geotectonic divisions of the Cretaceous to Paleogene granitoids and the distribution of related ore deposits. Types of ore deposits as follow: circles = vein, square = skarn, diamond = stratabound. For size class, see Ishihara (1978). From Ishihara (1978).

3. METHODOLOGY

3.1 Methodological references and approaches

First, the As distribution in the river waters and riverbed sediments were mapped to document the extension of the As affected area and the background level of this element. Because riverbed sediments can be used as a proxy to elucidate the regional element distribution in surface geology (Salminen et al., 1998; Halamić et al., 2001; Imai et al., 2004; Ohta et al., 2005), this medium was used to reveal if specific geological formations contained As or if the As distribution was more diffused. Then, the As-release mechanism into river waters were discussed in relation to the sulfide dissolution into the local hydrosphere, since the sulfide minerals are believed to control the distribution of As in the studied rivers. Ito et al. (2003) had previously used the isotopic ratio of sulfur to specify the source of dissolved sulfates in contaminated spring waters, because sulfur isotopes are useful tools for distinguishing the sources of sulfates in an aquatic environment (Yang et al., 1996; Nordstrom and Wright, 2007). Thus, this methodology was also applied during the present study at sampling locations with high As concentrations.

Second, the isotopic and elemental geochemistry of several sulfides collected in the study area were investigated to confirm that these minerals were responsible for the As contamination of surface waters. Again, the isotopic approach was used as a general method to define the origin of sulfides in rocks and metal deposits (Field, 1966; Seal, 2006). In the Inner Zone of Southwest Japan, many papers have reported the isotopic signatures of the various sulfur reservoirs (rocks, minerals, soil, waters, air, etc.) (Miyoshi et al., 1988; Mizota and Sasaki, 1996; Sasaki and Ishihara, 1979; Sato and Kase, 1996; Shimazaki, 1985; Yamamoto, 1974). The comparison of sulfides sampled from rocks and mines of the area helped understanding the cause of As occurrence in the Hokusetsu region, long known for being a zone with multiple ore-deposits. Other trace elements were also used to test the genetic relationship between the As-bearing pyrite previously studied and other ore-deposits of the study area. E.g., Ni and Co can be used to distinguish between sedimentary, magmatic and hydrothermal origin of pyrite (Bralia et al., 1979; Nishiyama and Ito, 2012), while W and Sn are viewed as elements specific of the Inner Zone plutonism (Ishihara, 1978).

Third, the behavior, i.e. transportation process, of As and other trace elements was studied through the analysis of their concentrations in the total and dissolved phases of the river

waters. The transportation process of the trace metals is governed by their adsorption onto ligands like organic matter, clay particles, iron oxy-hydroxides and manganese/aluminum hydrous oxides (Foster and Charlesworth, 1996; Tessier et al., 1985). Especially, the prominent binding abilities of Fe-, Mn- and Al-hydrous oxides have been demonstrated and modeled in various conditions of pH and solution composition (Benjamin and Leckie, 1981; Dzombak and Morel, 1990; Farley et al., 1985). The reference work of Dixit and Hering (2003) also demonstrated the influence of pH and redox conditions on the ability or inability of Fe oxides to adsorb As. The partitioning in river waters of As and Fe, Mn and Al as its main carriers, and other elements was evaluated via the dissolved transport index (DTI) defined by Martin and Meybeck (1979) using the total (unfiltered) and dissolved (<0.45μm-filtered) concentrations for each element. The DTI indicates the percentage of an element present as a dissolved species, and is calculated as follows:

$$DTI = \text{dissolved concentration} / \text{total concentration} \times 100 \quad \text{(Eq. 1)}$$

In addition to the elements behavior, the influence of the surface geology and factors causing enrichment of sediment geochemistry was assessed with the statistic tool of principal component analysis (PCA). Multivariate statistic analysis are widely used to identify the underlying factors responsible for element distribution in geochemical studies (Borůvka et al., 2005; Halamić et al., 2001; Ohta et al., 2005). The Principal Components Analysis is a statistical tool used to decompose and reduce the variation of a dataset of n-dimensions into p-dimensions, with hopefully $p<<n$. Those p-dimensions are called the principal components. They have the role of reflecting the common variations observed among the data. The utility of PCA resides in the interpretation of those principal components, as it will point at common factors or sources that "explain" the variations.

3. 2 Sample collection

3.2.1. Waters samples

A total of 163 water samples were collected from the Ai, Akuta, Hitokuraooroji, Ibaraki, Katsuoji, Katsura, Minoh and Yono Rivers between 2011 and 2015. The waters were sampled from the middle of the stream whenever possible. Because all rivers were small enough for the bottom and surface waters to be well mixed, the sampling depth was not considered for the water chemistry. At each sampling station, a set of water samples was collected as follows: samples for major anion analysis were filtered with 0.45 μm glass filters and not acidified, and samples for major cations, As

and trace element analysis were preserved with 1:2 (v/v) HNO_3. Among them, samples for analysis of the dissolved concentrations were filtered with 0.45 μm glass filters, whereas those for total concentrations were directly sampled from the stream. All water samples were collected with as little dead space as possible in polyethylene bottles soaked overnight in HNO_3 and rinsed 3 times with ultrapure water. The physico-chemical parameters of the river waters were measured *in situ* during the sampling with adequate probes plunged into the stream for temperature, pH, electrical conductivity (EC), oxidation-reduction potential (ORP), and dissolved oxygen (DO).

3.2.2 Sediments samples

During the water sampling, riverbed sediments were also collected at 84 of the 163 locations on the aforementioned rivers. The sediments were collected from the riverbed with a scoop and stored in zipped bags until arrival at the laboratory on the evening of the sampling day.

3.2.3. Sulfur isotopes samples

In December 2014, river waters for sulfur isotope analysis were sampled from selected points to evaluate the origin of sulfates in As-contaminated rivers. At each location, 1 L of river water was collected. A rock sample of quartzite with large pyrite grains (~1 mm) was also collected at the location where the As concentration of sediment was the highest (the upper reach of the Yono River).

3.2.4 Sulfides minerals

The sulfide minerals in the host rocks and ore-deposits of the study area were analyzed to specify the source(s) of As and associated toxic elements, and their release mechanism into the hydrosphere. The sampling locations are indicated on Fig.3.1. The following rocks were sampled: (1) sandstone and grey shale in Todoromi area, (2) sulfides-disseminated quartzite near the contact of sandstone with the quartz-diorite intrusion, north of the Nose pluton, (3) ores from the W-Sn pegmatite-type Otani mine in Kyoto prefecture, (4) ores from the Cu-Ag Kawaura mine in Minoh, (5) gouge material containing sulfides from the Satsukiyama fault in Fushio area, (6) ores from the hydrothermal-type Hirao mine in Minoh, (7) hornfels with bedded-rhodochrosite ore nearby the Osugahara mine (the mine was not found during field sampling), (8) ores from the skarn-type Hatano mine in Ikeda, (9) ores from the xenothermal-type Tada mine in Hyogo Prefecture. Samples (1) (2) (5) and (7) are host rocks exposed in the flowing area of As contaminated riverwater, and the others are sulfide ores from abandoned mines.

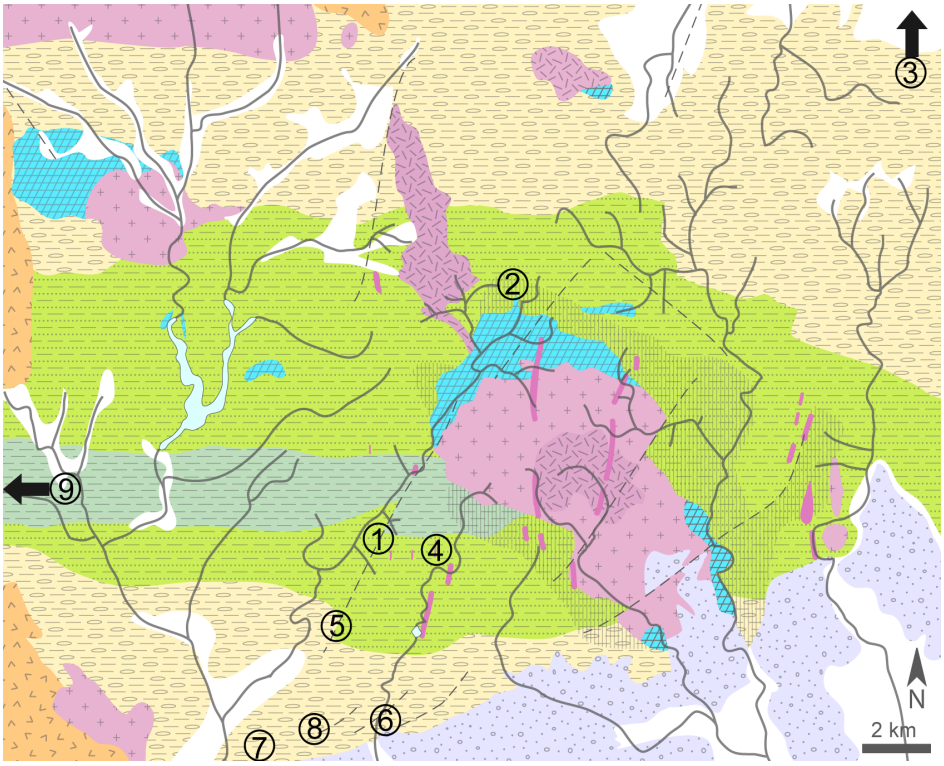

Fig.3.1 - Locations of the analyzed sulfides samples: (1) Todoromi sandstone and shale, (2) Quartzite, (3) Otani W-Sn pegmatite mine in Kyoto Prefecture, (4) Kawaura Cu-Ag mine, (5) Satsukiyama fault in Fushio, (6) Hirao Cu-Pb hydrothermal mine in Minoh, (7) Osugahara Mn mine in Ikeda, (8) Hatano Pb-Zn skarn mine in Ikeda, (9) Tada Cu-Ag xenothermal mine in Hyogo Prefecture. Color code of surface geology as in Fig. 2.1

3.3 Analytical methods

3.3.1 Water samples

The water samples were analyzed for alkalinity as HCO_3^- by HCl titration on the day of sampling, for major anions (F^-, Br^-, Cl^-, NO_3^-, PO_4^{3-}, SO_4^{2-}) by Ion Chromatogaphy (IC Dionex 120) and major cations (Na^+, K^+, Ca^{2+}, Mg^{2+}) by Atomic Adsorption Spectrometry (AAS630 Shimadzu). The AAS analysis of Ca^{2+} and Mg^{2+} was enhanced with the addition of LaCl to suppress interferences with other elements (Al, Si, SO_4) according to Koga et al. (2004). The concentrations of As and trace elements in the unfiltered and 0.45-µm-filtered samples of riverwaters were analyzed by inductive coupled plasma-mass spectrometry (ICP-MS SPQ9700 Hitachi).

3.3.2 Sediments samples

Upon arrival at the laboratory, sediments ranging from fine fractions to coarse sand grains were frozen and vacuum-dried to prevent the alteration of redox sensitive minerals (e.g., sulfide

minerals) from chemical alterations. A dried aliquot was sieved (#80 mesh, 250 μm, Nichika) and milled to a very fine powder with an automatic agate mortar.

The As content of the sediments was determined after digestion by alkali fusion. Briefly, the powdered samples were fused with granular Na_2CO_3 at a 1:10 (w/w) ratio and at 900°C for 45 min. The fused material was dissolved with 1:1 (v/v) HNO_3 and ultra-pure water, brought to 100ml completion, and stored until analysis (Seddique et al., 2008). The obtained solutions were diluted to 1:50 and analyzed by ICP-MS (SPQ9700 Hitachi) in a Collision-Reaction Interface cell with H_2 gas. For checking the accuracy of the fusion and the analysis, the Standard Reference Materials (SRMs) of riverbed sediments JSd-1 and JSd-2, as well as slate JSl-1 (Geological Survey of Japan), were processed in the same manner together with the sediment samples. The measured As concentrations from these duplicate or triplicate SRMs were commonly within 8% error, whereas the maximum error was approximately 21% when the As concentration was low (e.g., JSd-1, 2.42 ppm As) (Table 1).

Besides As, the remaining geochemistry of the riverbed sediments was measured by XRF analysis (RIX2100 Rigaku). As for As, a dried aliquot was sieved (#80 mesh, 250 μm, Nichika) and milled to a very fine powder with an automatic agate mortar. The samples were then baked at 900°C (2h) for loss on ignition (LOI). Then for each sample, 1.8000g of the powder was fused with lithium borate ($LiBO_4$) to make glass beads for XRF analysis.

Table 1
Arsenic concentrations in standard reference materials (SRMs) used during alkali fusion

SRM	Measured (ppm As)	Recommended value (ppm As)	Difference (%)
JSd-1	1.59	2.42	-21
JSd-1	1.63	2.42	-20
JSd-1	1.63	2.42	-19
JSd-1	1.66	2.42	-19
JSd-1	1.74	2.42	-16
JSd-1	1.77	2.42	-16
JSd-1	1.81	2.42	-14
JSd-1	2.61	2.42	4
JSl-1	12.61	14.9	-8
JSl-1	13.00	14.9	-7
JSl-1	13.91	14.9	-3
JSd-2	33.81	38.6	-7
JSd-2	33.98	38.6	-6

3.3.3 Sulfur isotopes

The river waters sampled for S isotopes were filtered at the laboratory just after coming back from the field, then they were processed according to Yanagisawa and Sakai (1983). As for the quartzite, small pieces of the rock were crushed and milled manually into fine powder in a tungsten

carbide mortar. Pyrite in the powder was oxidized with H_2O_2 (30%, Wako Ind. Japan) until bubbling ceased, acidified with 10 ml of 10% (v/v) HCl, and left on a hot plate for 2 h. The obtained solution was filtered to retain the non-oxidized matrix and 10% (v/v) HNO_3 was added to dissolve the remaining iron oxides.

For both the river waters and the quartzite dissolved solution, 0.5 M $BaCl_2$ was added to the obtained solutions, which were put on a hot plate overnight to let the $BaSO_4$ precipitates mature. For each sample, $BaSO_4$ was individually collected on a 0.45 μm cellulose filter and dried at 60°C. The isotopic ratio of sulfur of the precipitates was analyzed after decomposition to release SO_2 using an Element Analyzer (IsoPrime EA, Micromass) coupled to a Gas-Mass Spectrometer (GV Instrument, Ltd) at the Graduate School of Natural Science and Technology of Okayama University.

3.3.4 Sulfide minerals composition

Thick sections of the rock and ore samples were polished to 1μm and prepared for microscope observation, energy-dispersive X-ray spectroscopy (EDS), electron probe micro-analysis (EPMA) and laser ablation-inductively coupled mass spectrometry (LA-ICP-MS).

Sulfides were identified under reflected light with an optical microscope, and by the semi-quantitative EDS analysis of As, Fe, S, Cu, Pb, Zn, Ni and Co. This standardless prospective quantification was performed with EDAX SDD Apollo XP detector (Ametek, USA), at an accelerated voltage of 20kV and MnKα resolution of 125.9eV, coupled to SEM (JEOL JSM-5500, Japan). Concentrations were calculated with the EDAX Genesis Spectrum Viewer software using the ZAF correction method. The analytical conditions and X-ray lines used for target elements are summarized in Table 2.

The same major and trace elements were quantified by wavelength dispersive spectrometry (WDS) with a JEOL JXA-8800K electron probe micro-analyzer (EPMA). The beam was accelerated at 15kV, used at a current of 20 nA, and focused at 3 μm (the analyzed sulfides were mostly < 20 μm). The background counting was ± 10s. The EPMA calibration was carried out with pyrite for Fe and S, chalcopyrite for Cu, nickeline for Ni and As, sphalerite for Zn, galena for Pb, and CoAsS for Co. The ZAF correction method was employed to calculate each element concentration. The analytical conditions are summarized in Table 3.

Table 2

EDS analytical conditions

Microscope		SEM JEOL JSM-5500	
Detector		EDAX SDD Apollo XP detector	
Accelerated voltage		20 kV	
Background counting		45s	
MnKα resolution		125.49 eV	
Element and Line used			
As K	Pb M	Fe K	Ni K
S K	Mn K	Co K	Cu K

Table 3

WDS Electron-Micro-Probe analytical conditions

Microscope		JEOL JXA-8800K	
Accelerated voltage		15kV	
Beam current and Focus		20nA	
Probe Diameter		3μm	
Background counting		10s	
Element and WDS crystal			
S - PET	Fe – LiF	Cu - LiF	As - TAP
Ni - LiF	Co – LiF	Zn - LiF	Pb - PET

The distribution of major and trace elements (^{7}Li, ^{11}B, ^{13}C, ^{23}Na, ^{24}Mg, ^{27}Al, ^{29}Si, ^{35}Cl, ^{39}K, ^{44}Ca, ^{32}S, ^{48}Ti ^{52}Cr, ^{55}Mn, ^{57}Fe, ^{59}Co, ^{60}Ni, ^{63}Cu, ^{66}Zn, ^{71}Ga, ^{73}Ge, ^{75}As, ^{95}Mo, ^{107}Ag, ^{111}Cd, ^{115}In, ^{118}Sn, ^{121}Sb, ^{182}W, ^{185}Re, ^{189}Os, ^{197}Au, ^{202}Hg, ^{205}Tl, ^{208}Pb, ^{232}Th, ^{238}U) in sulfides and matrix was mapped or analyzed along a single ablation line, by LA-ICP-MS on a NWR193 Excimer laser ablation system (New Wave Research, USA) and a quadrupole iCAP Q ICP-MS (Thermo Scientific, Germany) at the Geochemistry and Cosmochemistry laboratory of the Kyoto University. The analytical conditions for LA-ICP-MS are summarized in Table 4. The elemental mapping by laser-ablation was visualized with the software iQuant2 (Suzuki et al., 2015).

Table 4
Laser-Ablation and ICP-MS analysis conditions

Laser	NWR Excimer laser
Wavelength	193 nm
Fluence (J/cm^2)	6.7
Repetition rate (Hz)	10 Hz
Scan speed (µm/s)	1-5
Spot size (µm)	10, 35, 70
Warm up time (s)	10
Wash out time (s)	20
ICP-QMS	
Model	Thermo iCAP-Q
Carrier Ar	0.80 l/min
Carrier He	0.71 l/min
Data acquisition parameters	
Data acquisition protocol	Time resolved analysis

Element	**Dwell time (s)**	**Elem.**	**Dwell t. (s)**	**Elem.**	**Dwell t. (s)**	**Elem.**	**Dwell t. (s)**
^{7}Li	0.01	^{44}Ca	0.01	^{73}Ge	0.01	^{182}W	0.01
^{11}B	0.01	^{48}Ti	0.01	^{75}As	0.01-0.02	^{185}Re	0.01
^{13}C	0.01	^{52}Cr	0.01	^{88}Sr	0.01	^{189}Os	0.01
^{23}Na	0.01	^{55}Mn	0.001	^{95}Mo	0.01	^{197}Au	0.01
^{24}Mg	0.01	^{57}Fe	0.001-0.01	^{107}Ag	0.01	^{122}Hg	0.01
^{27}Al	0.01	^{59}Co	0.01	^{111}Cd	0.01	^{205}Tl	0.01
^{29}Si	0.01	^{60}Ni	0.01	^{115}In	0.01	^{208}Pb	0.001-0.01
^{32}S	0.001	^{63}Cu	0.01	^{118}Sn	0.01	^{232}Th	0.01
^{35}Cl	0.01	^{66}Zn	0.01	^{121}Sb	0.01	^{238}U	0.01
^{39}K	0.01	^{71}Ga	0.01	^{137}Ba	0.01		

3.3.5 Principal Components Analysis PCA

In this study, the geochemistry of riverbed sediments was hypothesized to vary mainly according to the surface geology, i.e., the concentrations of two elements originated from the same lithology will linearly change together (=common variation). The core tool of PCA is the correlation coefficient (Pearson's moment correlation coefficient) based on the covariance of the chemical composition of the sediments, i.e., each coefficient signifies the degree of similarity among the concentration variations for element pairs. The PCA results can be used to distinguish the common sources of analyzed elements, especially the lithological (or else) sources. The PCA calculations were executed with Matlab R2009b software on datasets of 1) XRF data, and 2) XRF data with As, which was quantified from after alkali-fused sediments (cf. Section 3.3.2).

4. RESULTS AND DISCUSSION

4.1 ARSENIC DISTRIBUTION IN RIVERWATERS AND BED SEDIMENTS OF THE HOKUSETSU AREA

4.1.2 Results

The geochemistry of river water and riverbed sediments was extensively analyzed. Only the As concentrations and its related components of interest are discussed in this chapter, and the remaining geochemistry is discussed in Section 4.3. These results are grouped by rivers and summarized in Table 5 (complete data sets are in Annex 2). The spatial distributions of As of riverwaters and riverbed sediments are shown in Figs. 4.1 and 4.2, respectively.

Arsenic in river waters

The As was maldistributed in rivers of the study area. Notably, concentrations >5 ppb appeared around the Ibaraki Granitic Complex, especially at the quartz-diorite margins, in contrast with waters sampled in sedimentary rocks far from the plutons. However, similar distributions of high As concentrations were not observed around the Mikusayama granitic complex, despite the occurrence in this complex of pyroxene quartz-gabbro with chemical compositions similar to those of Ibaraki quartz-diorite.

Concentrations of As were <1 ppb in river waters originating from or flowing through the felsic parts of the Ibaraki Granitic Complex in both the Nose and Myoken plutons, except for a spring water sample (5.9 ppb) on the upper reach of the Ibaraki River. The As concentrations of water were also low in rivers flowing in the northern and eastern parts of the sedimentary formations. In these areas, concentrations consistently remained <3 ppb, which would be the background concentration of arsenic in rivers flowing through sedimentary formations of the Hokusetsu area.

Six water samples exceeded the WHO standard of 10 ppb As, and four of them were from the Yono River. Among those, the most contaminated waters (38.3 and 34.1 ppb) were taken in the source area of two small Yono tributaries, in the Todoromi village, where Masuda et al. (1999) had previously reported the As contamination of the local spring waters (i.e., resurging groundwater) along these tributaries. In the present study, a large increase in As concentrations (from 1.2 to 34.1

ppb) was observed in the tributary waters, in association with an increase of water temperature (from 6.7 to 12.1°C), EC (from 24 to 58 μS/cm), HCO_3^- (from 15 to 47 ppm) and SO_4^{2-} (from 4.6 to 9.3 ppm). Those correlated increases indicated the mixing of the young river waters with the inflow of a more mineralized water that obviously created the As contamination. The other waters with As concentrations >10 ppb were found on the upper reach of the Yono River (10.7 ppb), the lower reach of the Ai River (10.9 ppb), and the lower reach of the Minoh River (11.5 ppb) where local increases of As, EC, and SO_4^{2-} were also observed.

Overall, the waters containing >5 ppb As were observed in relation to the following geology; (1) waters from the upper reach of the Yono River (5.0–10.7 ppb) flowing in areas of hornfels and quartzite near the quartz-diorite intrusion; (2) waters from the middle reach tributary (8.4 ppb) and the lower reach (10.9 ppb) of the Ai River located at the margin and in the vicinity of the quartz-diorite intrusion, respectively; and (3) waters from the lower reach of the Minoh River (11.5 ppb) located in an area marked by magmatic intrusion. In addition, highly As-contaminated river waters were commonly found near faults and lineaments. The anomalous increase of As concentrations at Todoromi appeared where the Satsukiyama non-active fault (B in Fig. 2.1) was running across the tributaries. On the Ai River, the high As concentrations appeared where the I and G faults crossed the stream course. This implies that these fracture zones are pathways of As-containing groundwaters.

As in riverbed sediments

The As concentration of riverbed sediments ranged from <1 to 55.2 ppm with an average concentration of 10.3 ppm, which is consistent with the typical average As concentration of 5 to 10 ppm of sedimentary rocks (Smedley and Kinninburgh, 2002), and concordant with that of riverbed sediments from Central Japan (8 ppm) (Ohta et al., 2005). The highest As concentrations (39.4 to 55.2 ppm) were observed in the sediments derived from hornfels and quartzite at the upper reach of the Yono River. The quartzite was heavily disseminated with pyrite, but the river waters taken from the same location had As <10 ppb. On the other hand, no such elevated As contents were measured in bed sediments (11 ppm) near the Mikusayama complex with the quartz-gabbro intrusion in contact with sedimentary rocks (Tainosho et al., 1977) or nearby small hydrothermal Cu veins.

At the Todoromi tributaries, the As concentrations of the sediments derived from sandstone and mudstone averaged 24.8 ppm. This was higher than the concentration of whole rocks containing pyrite (4–16 ppm As) measured by Ito et al. (2003). At the location of As >10ppb on the Minoh River, sediments had 20.8 ppm As, whereas As concentrations of sediments taken upstream

Table 5

Chemical and isotopic composition of river water and riverbed sediments of small streams in the Hokusetsu area

River		Temperature (°C)			pH			EC at 25°C (μS/cm)			SO_4^{2-} (ppm)			As (ppb)			As in sediments (ppm)				$\delta^{34}S$ (%CDT)			
		Min	Max	Med	Min	Max	Med	Min	Max	Med	Min	Max	Med	Min	Max	Med		Min	Max	Med	Water			Rock
Ai R.	(n=38)	11,5	28,2	17,1	5,2	9,1	8,1	37	462	130	1,6	43,5	5,7	0,2	**10,9**	1,0	(n=6)	6,1	19,9	9,2				
Akuta R.	(n=17)	13,1	22,0	17,0	7,1	8,8	8,4	74	200	149	1,6	33,5	7,1	0,6	3,4	1,0	(n=6)	1,0	14,6	12,2				
Ibaraki R.	(n=25)	7,9	15,9	12,1	6,9	8,1	7,8	43	172	96	2,6	13,3	6,9	0,1	5,9	0,5	(n=12)	1,0	13,5	2,1	+3,9			
Ina R.	(n=13)	13,3	18,2	16,4	7,3	8,7	8,3	48	163	85	3,0	10,1	5,6	0,5	1,0	0,6	(n=12)	4,9	11,2	7,2				
Katsuoji R.	(n=2)	12,4	14,1	13,3	7,7	7,9	7,8	111	496	303	4,9	170,9	87,9	2,0	4,6	3,3								
Katsura R.	(n=12)	12,4	20,5	17,4	4,3	8,8	8,1	49	205	130	1,9	23,8	7,5	0,3	1,6	0,7	(n=5)	5,8	13,5	7,1				
Minoh R.	(n=18)	8,6	13,6	12	7,2	8,1	7,7	64	151	112	3,4	10,9	7,4	0,2	**11,5**	1,5	(n=11)	2,8	20,8	8,1	+8,9	+5,0	+3,7	
Yono R.	(n=42)	6,7	26,1	12,1	6,9	8,9	7,8	22	238	65	1,0	31,7	6,6	n.d.	**38,3**	2,0	(n=12)	2,6	55,2	8,1	+2,6	+6,8	+6,4	-8,8

Bold numbers indicate As concentrations above the WHO limit (10ppb)

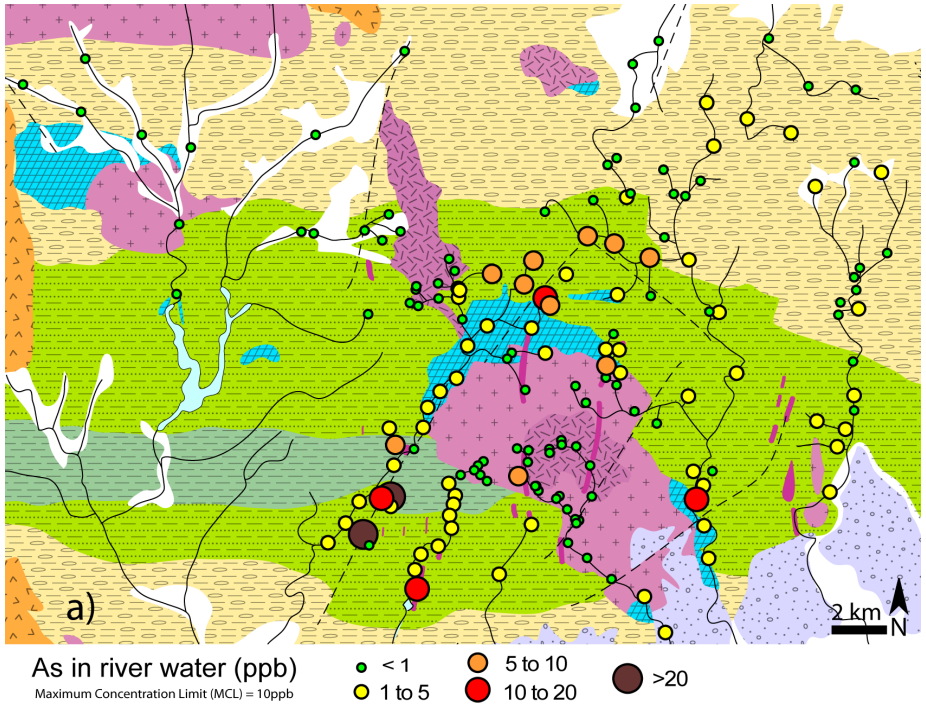

Fig. 4.1 Distribution of arsenic concentrations of riverwaters in Hokusetsu area.

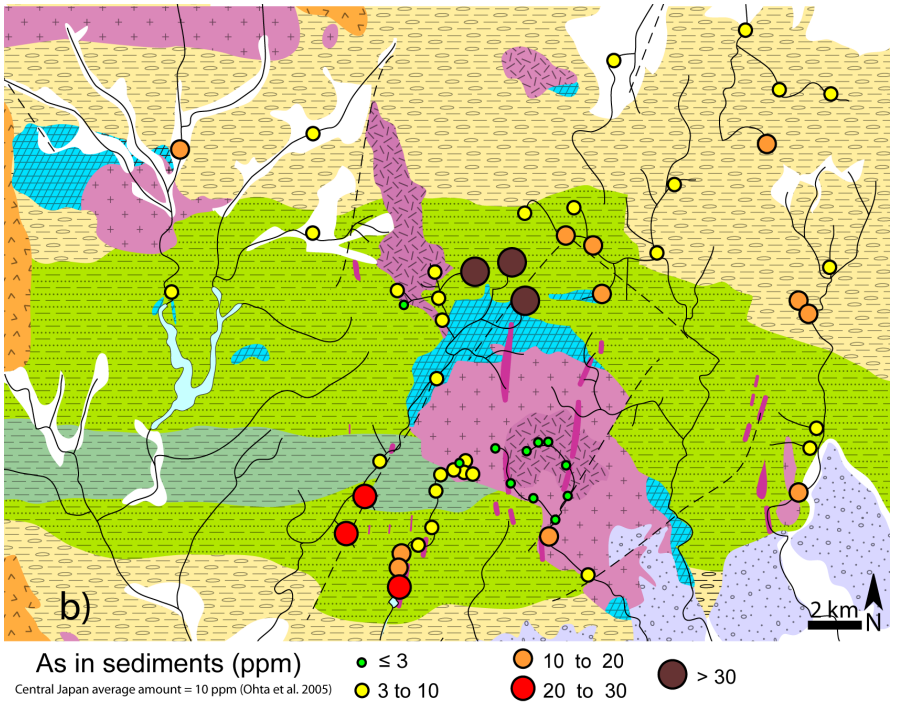

Fig. 4.2 Distribution of As concentrations of riverbed sediments in Hokusetsu area.

remained <11 ppm. There, contact-metamorphosed rocks and large dikes were observed, and a small, now closed, mine of hydrothermal Cu vein was also reported upstream. Thus, the As occurrence may be related to the mineralization induced by the local magmatism.

Excluding the high As-bearing samples, which were suspected ore mineralization, riverbed sediments derived from the sedimentary rocks of the Tamba Belt commonly had a median As content of 8.4 ppm (n=33), in accord with the median concentration (8 ppm As) of sediments derived from the accretionary complex in Central Japan, as reported by Ohta et al. (2005). Bed sediments of the Ibaraki River taken from the center of the Nose granitic pluton were depleted in As, with concentrations <3 ppm. A sediment sample containing 13.5 ppm As was taken in the granodiorite area, although the As concentration of water from the same location was low (0.7 ppb).

The relationship between the As concentrations of river waters and riverbed sediments (Fig. 4.3) generally showed a positive correlation. The correlation was especially noticeable for waters with As concentrations >5 ppb in the Ai, Minoh, and Yono Rivers taken from the sedimentary formations. The outlying group (circled in Fig. 4.3) of low As concentrations in water associated with As-rich sediments (>40 ppm As) corresponded to the samples from the area of hornfels and quartzite disseminated with pyrite.

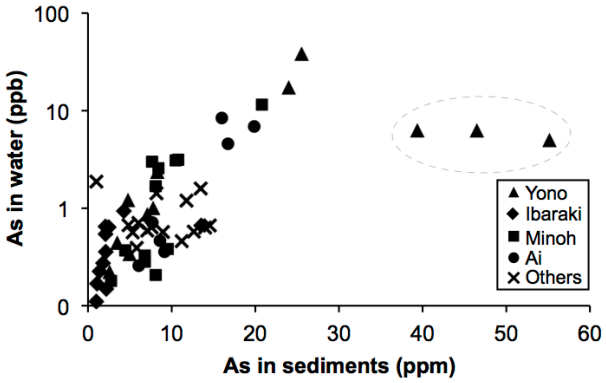

Fig. 4.3 As concentrations in bed sediments and riverwaters. Samples with water concentrations >3 ppb As correlated positively, except for Yono River samples from the hornfels area (triangles on the right). Samples with water concentrations <3 ppb As showed a more scattered behavior. Circle emphasized outlying samples (refer to text for explanation). Others rivers are: Akuta, Hitokuraooroji, Katsuoji, Katsura and Tajiri Rivers

Dissolved sulfates in river waters

The As concentrations of river waters were high in areas where sulfide mineralization was suspected (e.g., a mine near the Minoh river or sulfides in the Todoromi sandstone and greenstone). It was previously hypothesized that the As-contaminated water formed via dissolution of pyrite, which contained up to 0.73 wt% As (Ito et al., 2003). Thus, the concentrations of As and dissolved

SO_4^{2-} in river water, as well as the sulfur isotope ratio of those SO_4^{2-}, were examined to evaluate the effect of pyrite oxidation as a common source of As in the rivers of this study area.

The relationship between the dissolved SO_4^{2-} and As concentrations is shown in Fig.4.4. The plot comprises samples of river waters collected during this study (black and grey symbols) and spring waters reported by Ito et al. (2003) (open symbols). The plots show two distinctive groups (A and B in the figure) and an intersecting one (C).

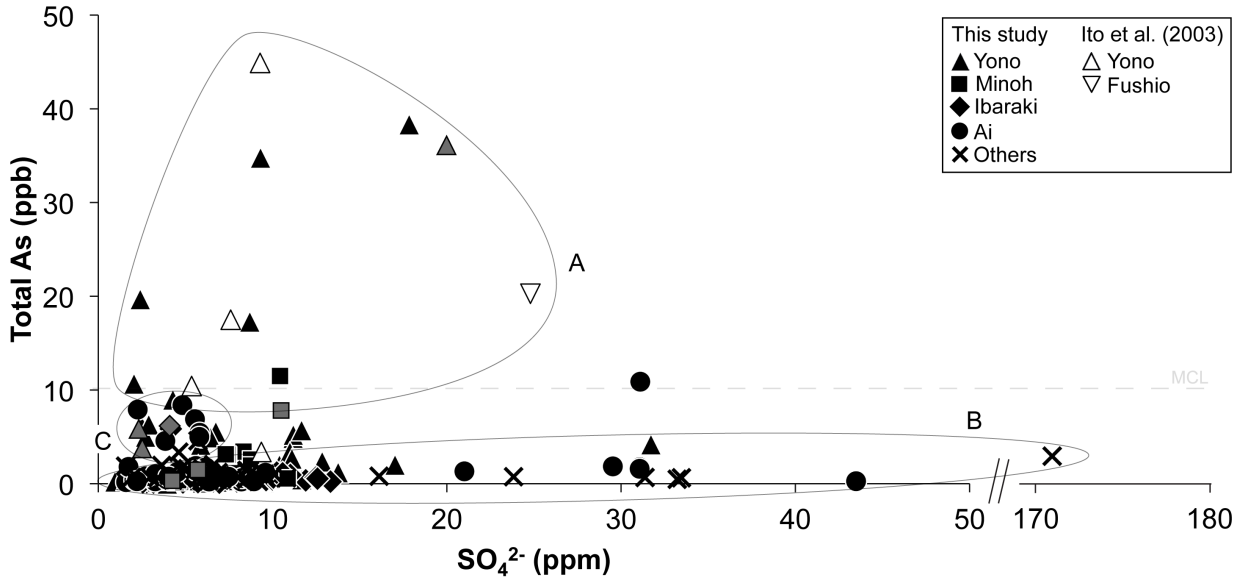

Fig. 4.4 Dissolved SO_4 and As concentrations in riverwaters. Data include riverwater samples from this study (black symbols), samples for sulfur isotopes analysis from this study (grey symbols) and Ito et al. (2003) (open symbols). Others rivers are: Akuta, Hitokuraoroji, Katsuoji, Katsura and Tajiri Rivers. For the enclosed areas A, B and C, see in the text.

Group A comprises the As-contaminated waters with low dissolved sulfate concentrations (<25 ppm), with the exception of a sample from the Ai River (10.9 ppb As; 31 ppm SO_4^{2-}). Samples containing As concentrations >10 ppb exhibited a positive correlation between As and SO_4^{2-}, implying pyrite dissolution, as suggested by Ito et al. (2003). However, once entering the river streams, the As-contaminated spring waters were diluted with ambient meteoric water containing SO_4^{2-} derived from different sources, and the relationship of these two components became ambiguous.

Group B shows low concentrations of As irrelative to the SO_4^{2-} concentrations. Most of the samples collected far from the plutonic intrusion belong to this group and have SO_4^{2-} that clustered between 0 and 15 ppm. The waters with elevated concentrations of SO_4^{2-} were sampled near anthropogenic activities such as a stone quarry, a waste treatment plant (171 ppm SO_4^{2-}), a landfill, fish farming, highway works, and household wastewaters. The effluents from those activities were almost free of As, and anthropogenic inputs of this element could be excluded from the studied rivers. The concentrations of As <3 ppb were then due to mineral dissolution, as the surrounding geological formations still contain small amounts of As (Ohta et al., 2005).

Group C is at the intersection of the contaminated waters of group A and the low-As waters of group B. The samples of this group were without serious anthropogenic SO_4^{2-} inputs and exhibited a mild As contamination.

Sulfur isotopic ratios

Fig. 4.5 shows the map of the $\delta^{34}S$ values (as $‰_{CDT}$) of dissolved SO_4^{2-} in selected river waters and the $\delta^{34}S$ values of rock sulfides. Fig.4.6 plots the relationship between $\delta^{34}S$ and its related SO_4^{2-} concentrations, showing a decreasing trend in $\delta^{34}S$ with increasing SO_4^{2-} concentration, plausibly due to the increasing contribution of pyrite dissolution. The $\delta^{34}S$ values of SO_4^{2-} ranged from +2.6 to +8.9 ‰, which corresponds to the $\delta^{34}S$ ranges for sulfide-sulfur in Paleozoic stratiform deposits (0 to +5.0‰) (Sato and Kase, 1996) and the sulfate-sulfur in native inland Japanese soils (+1.7 to +8.9‰) (Mizota and Sasaki, 1996).

The $\delta^{34}S$ value (-8.8‰) of the pyrite in quartzite was much lower than those of the sedimentary rocks analyzed by Ito et al. (2003), and in the range of igneous sulfides. The waters from the quartzite area had sulfate-$\delta^{34}S$ values of +6.8‰ and +6.4‰, which are much higher than the $\delta^{34}S$ of pyrite in this rock. The waters from the uppermost reaches of rivers yielded $\delta^{34}S$ values greater than +5‰, and they contained very low concentrations of SO_4^{2-} and As (Fig.4.4), suggesting a small contribution to the water chemistry of anthropogenic SO_4^{2-} or SO_4^{2-} and As originating from pyrite dissolution. Thus, the $\delta^{34}S$ of these young waters must be that of the background sulfates, i.e., those of inland soils.

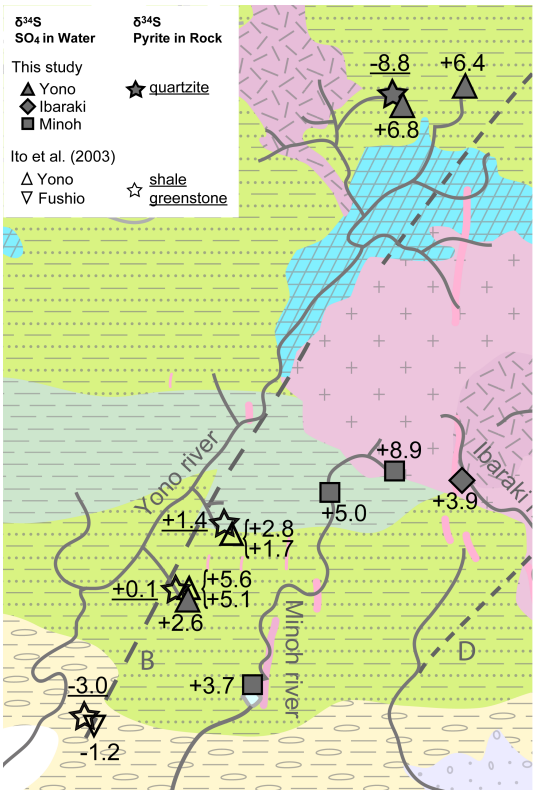

Fig. 4.5 Mapping of $\delta^{34}S$ isotopic ratio from pyrite in rocks of the study area (star and underlined figures) and dissolved sulfates in water (other symbols). Black symbols: data from this study. Open symbols: data from Ito et al., 2003.

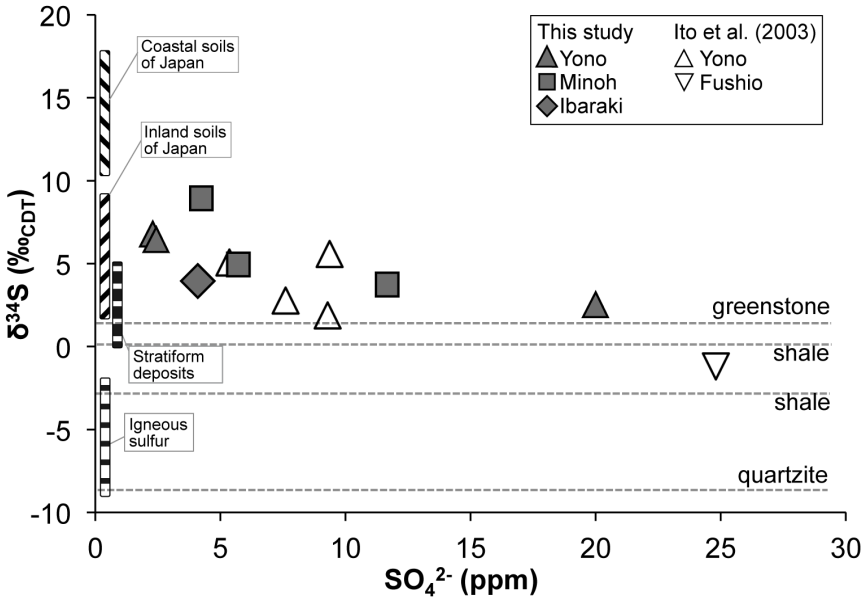

Fig. 4.6 Biplot of SO_4 concentrations of riverwater and their corresponding $\delta^{34}S$ isotopic ratio. Dashed lines represent the $\delta^{34}S$ isotopic ratio of pyrite from rocks of the study area. Data show a general mixing process between high $\delta^{34}S$ (>+5‰) from young waters impacted by sulfur soil infiltrations to $\delta^{34}S$ (< 0‰) from pyrite in rocks. After Mizota & Sasaki, 1996 (soil data), Sato & Kase, 1996 (stratiform deposits) and Ishihara and Sasaki, 1991 (igneous sulfur).

The $\delta^{34}S$ of the other river waters and the contaminated spring waters reported by Ito et al. (2003) plotted within the range of $\delta^{34}S$ of stratiform deposits, although it overlapped with the $\delta^{34}S$ of inland soils. Data for water containing As concentrations >10ppb (Group A on Fig.4.4) have $\delta^{34}S$ closer to that of stratiform deposits. One spring water, with 19 ppb As, 8 ppm SO_4^{2-} and $\delta^{34}S$ +2.8 ‰, was clearly caused by pyrite dissolution, as this water issued directly from the basement rock (Ito et al., 2003). Thus, the $\delta^{34}S$ values <+2.8 ‰ of As-contaminated waters must be explained by the large contributions of dissolved pyrite and/or other sulfide minerals in the host-rocks.

4.1.2 Discussion

Role of the geology in arsenic distribution

The distribution of As in river waters is concordant with the distribution of the surface geology and consequently with that of riverbed sediments derived from surface regolith (Fig. 4.3). This means that the water chemistry is mainly controlled by the baseflow chemistry via water-rock interactions. In the study area, the background As concentration of river waters flowing in the sedimentary rock areas is less than 3 ppb (#1 on Fig.4.7), while river waters flowing through As-depleted granitic rocks had consequently the lowest As concentrations (#2 on Fig.4.7).

Most of the high As concentrations in river water appear in a halo around the Ibaraki Granitic complex, implying that the As contamination is related to the magmatic intrusion (#3 on Fig.4.7). However, As is scarce in river waters and bed sediments near the Mikusayama complex, despite both complexes having a similar magmatic origin. This can be explained by the following three possibilities: 1) a lack of contact-metamorphosed sedimentary rocks containing disseminated As-bearing pyrite, 2) a discharge (> 0.5 m^3/s (MLIT, 2013)) large enough to dilute inflow of As-contaminated groundwater (measured at approximately 0.6 l/s near the Ibaraki complex), and 3) no prominent fault or lineament to work as an infiltration path for oxic groundwater. Among those possibilities, and regarding the size of the river streams of the area, the rapid mitigation of As in the large-discharge rivers around the Mikusayama complex is more likely. This has already been observed by Ashida et al. (2001), when As concentrations of several hundred ppb in spring water decreased to few tens of ppb in the Ina River tributaries of size similar to the studied rivers.

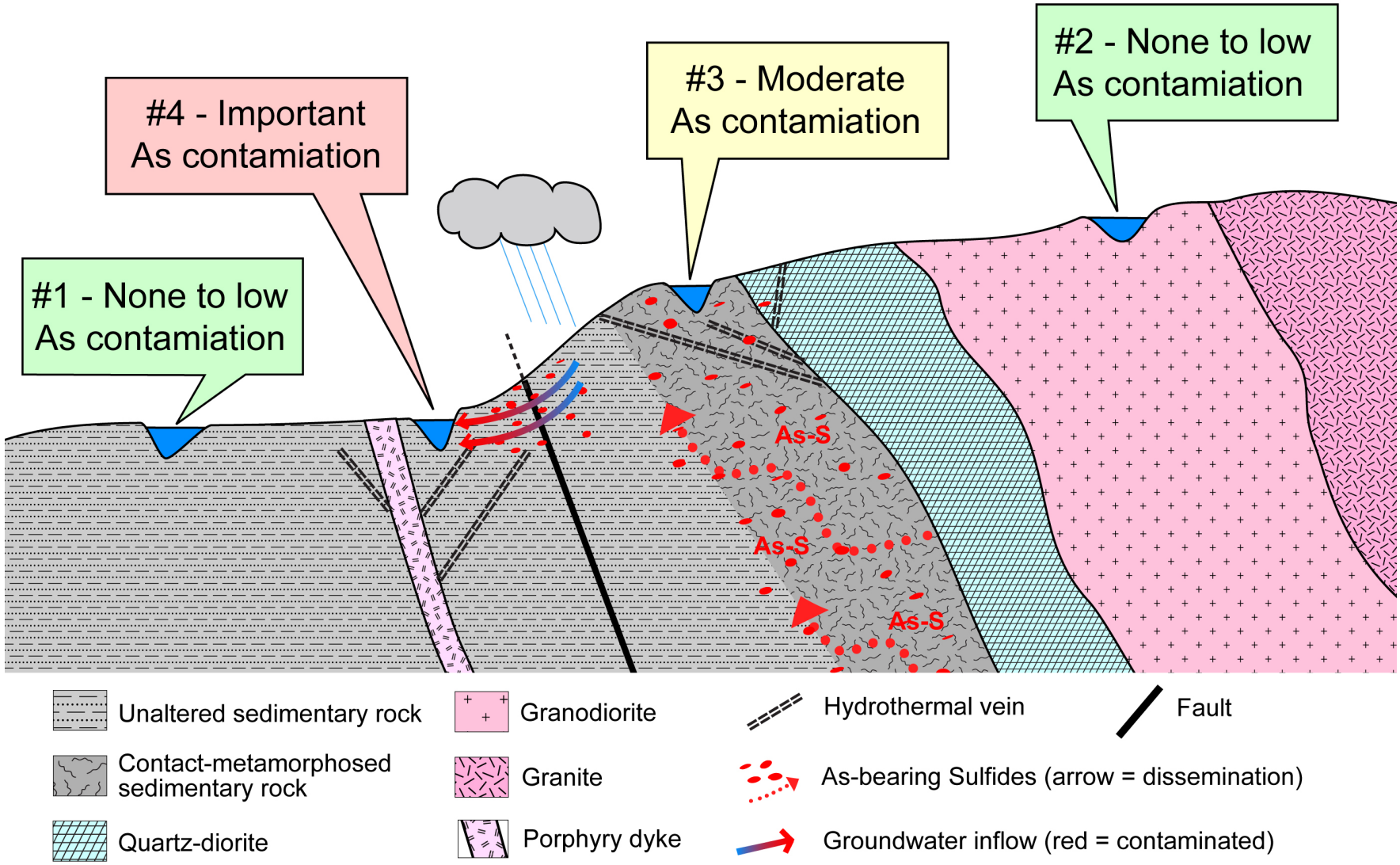

Fig. 4.7 - Summary model of As contamination in the study area, in relation with the geological settings. Highest contamination appears in zone of rocks disseminated with As-bearing sulfides and fractured by fault.

The high (>10 ppb) As concentrations of river water are not solely due to the presence of mineralization. For example, the sediments derived from the quartzite heavily disseminated with sulfides had a high As level (55 ppm), which indicates an enrichment of this element at the time of the contact-metamorphism, although the As concentrations of river waters at this location were <10 ppb. Arsenic would not be easily mobilized because of the induration of the quartzite matrix compared with the non-metamorphosed sedimentary rocks of the study area. The As contamination is more apparent at locations where a deeper contaminated groundwater flows into rivers of small discharge and in the area of non-metamorphosed rocks, in which the pyrite oxidation-dissolution would occur, but still in the vicinity of the plutonic intrusion. Faults play an important role in the oxidation of pyrite, as seen with the Satsukiyama fault, because they promote the percolation of oxygenated meteoric waters through the sheared sedimentary formations that have a higher specific surface contact area (#4 on Fig.4.7). The reaction of pyrite dissolution is then enhanced, and the release of As loads becomes higher than in unfractured host-rocks.

Role of sulfide dissolution in arsenic contamination

The $\delta^{34}S$ values of sulfides reported for the geologic terrain including the study area can be grouped into two different ranges, according to the type of sulfide deposit. The sulfur isotopes of sulfides largely fractionate in the sediments due to the variable redox conditions and the associated biological activities. But the sulfur isotope ratio of sedimentary sulfides fixed in oceanic crust also changed with geological settings and time; the $\delta^{34}S$ of those from the Permian to the Jurassic were -10 to -30‰ on average (Canfield, 2004), whereas sulfide minerals found in massive subseafloor sulfide deposits during the same period were within 0 to +8‰ (Seal, 2006). The Mino-Tamba sedimentary formations, to which the study area belongs, were accreted from the Permian to the Jurassic (Charvet, 2013; Isozaki, 1997) and host some of these massive stratiform Cu deposits, with $\delta^{34}S$ of sulfides ranging from 0 to +5‰ (Sato and Kase, 1996). From Ito et al. (2003), two of the $\delta^{34}S$ values of sulfides from the Paleozoic/Mesozoic greenstone and shale (+0.1 and +1.4 ‰, respectively) are in this range, suggesting the sulfides are classified as this type of deposit.

The Hokusetsu area belongs to the Tertiary W-Sn-Cu mineralized province of Japan (Ishihara, 1978) and bears many hydrothermal polymetallic veins enriched with chalcopyrite and pyrite. The ore deposits were induced by the late Cretaceous/Paleogene intrusion of granites and have a range of $\delta^{34}S$ for sulfide of -9‰ to -2‰ (Ishihara and Sasaki, 1991). The sulfides in quartzite and the pyrite in the Fushio shale had negative $\delta^{34}S$ (−8.8‰ (this study) and −3.0‰ (Ito et al., 2003),

respectively) in the range of igneous $\delta^{34}S$, but still in contrast with one another. Based on the ranges of sulfur isotopic compositions of sulfide minerals from important mines in Southwest Japan, Miyoshi et al. (1988) established a distinction between the ore deposits of subvolcanic origin (e.g., Tada Mine in the study area, with $\delta^{34}S$ ranging from -3.5 to -2.2‰) and of plutonic origin (e.g., Ohtani Mine, with $\delta^{34}S$ ranging from -10.5 to -8.6‰). The quartzite around the Nose pluton was formed by contact metamorphism with the granitic intrusion. Its S isotopic ratio is concordant with those of the Ohtani ore minerals, which clearly shows that the sulfides were disseminated in relation to the intrusion of the pluton. As noted above, sulfides in the quartzite did not considerably increase the level of As in the surrounding water, suggesting that the type of mineralization and its degree of crystallization play an important role in determining the As levels of the studied river waters.

SO_4^{2-} is a product of the oxidation-dissolution of As-bearing pyrite, which occurs in oxic aquatic environments as follows:

$$4FeAsS + 13O_2 + 6H_2O \rightarrow 4Fe^{2+} + 4SO_4^{2-} + 4HAsO_4^{2-} + 8H^+ \quad \text{(Eq. 2)}$$

Ito et al. (2003) confirmed this reaction based on a positive correlation between the SO_4^{2-} and As concentrations in spring waters in the Todoromi area. In this study, the behavior between the dissolved sulfates and As could not be established through a simple stoichiometry due to the dilution of the As load in all rivers and the mixing of SO_4^{2-} derived from different sources.

In this study, Fushio sample excluded, the river water with the highest As concentrations had the lowest $\delta^{34}S$ values (+2.6‰; Fig. 4.8) similar to the $\delta^{34}S$ of pyrite in the greenstone (+1.4‰) and shale (+0.1‰).

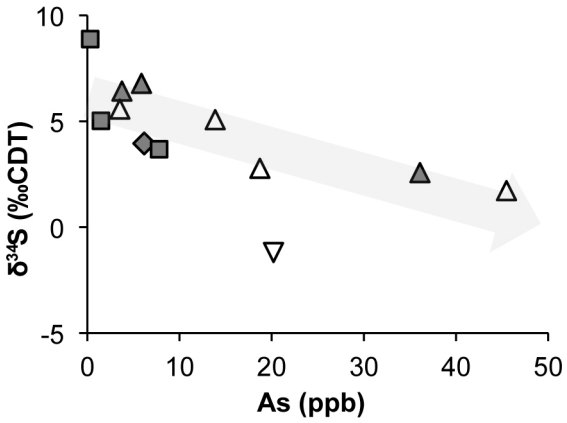

Fig. 4.8 –Arsenic concentrations and isotopic sulfur ratio of river waters from the present study (gray symbols) and Ito et al. (2003) (open symbols). The general evolution shows a decrease of the isotopic signal with the increase of As concentrations.

The least deviance of the isotopic ratio between rock and water was observed at Fushio with the sulfates of spring waters (-1.2‰) and the ambient shale (-3.0‰) by Ito et al. (2003). Field (1966),

confirmed later by Toran and Harris (1989), emphasized that a small degree of fractionation leading to ^{34}S depletion of a few ‰ in waters occurs during sulfide oxidation. This would explain the discrepancy between the ratios of the host-rocks and the lighter ratios in waters. Therefore, in the present study, waters with As concentrations >10 ppb have low $\delta^{34}S$ affected by the sulfates derived from the oxidation of pyrite and other sulfides in the ore-deposits described above.

In the study area, the highest concentrations appeared essentially around the Ibaraki granitic intrusion, and in areas where sulfide mineralization have been observed. Indeed, the sulfide isotopic ratio pointed at the possible magmatic origin of those sulfides that contain As. Still, two types of sulfide deposits have been distinguished from the isotopic data. The source of those sulfides and the reason why they contain such amount of As have yet to be cleared. To answer those questions, it is required to compare the sulfides responsible for As contamination and those from the ore-deposits found throughout the study area. This is the focus of the second part of the present study.

4. 2 ARSENIC IN SULFIDES FROM ORE DEPOSITS OF THE HOKUSETSU AREA

4.2.1 Results

The analyzed sulfides are described in the following. Their quantitative geochemistry, including As concentrations, is summarized in Table 6.

Todoromi sandstone and shale ((1) on Fig. 3.1)

Sandstone - The As contamination of spring waters at Todoromi villages (Fig. 4.1 in Section 4.1.2) was believed to occur because of the dissolution of As-bearing sulfides hosted in sedimentary rocks (Ito et al., 2003). The wacke sandstone sampled at this location was stained with red minerals (Fig. 4.9). The red minerals were mainly observed along micro-fractures within the rock and on the surface of macro-fractures, the both fracture types being filled with calcium. Minerals at the center of the red stains were chalcopyrite ($CuFeS_2$) and magnetite (Fe_3O_4) with a colloform texture (Fig.4.10a&b). The red stains were Fe oxides, likely hematite, a common alteration product of magnetite (Craig and Vaughan, 1994). In the colloform assemblages, As was higher in the magnetite (up to 0.20wt%) than in the chalcopyrite. The assemblages also contained Pb measured up to 1.70wt%, Zn 0.42wt%, Ni 0.59wt% and Co 0.26wt% (Table 6). Molybdum (Mo) and Au were also detected by LA -ICP-MS (Fig.4.11a). EDS and EPMA analyses also revealed that the rock was dotted with magnetites that were not altered (i.e., there was no red halo around the grains). In these magnetites, As reached 0.35wt%. In a small fracture, a grain of pyrrhotite ($Fe_{1-x}S$) and another of magnetite/pyrrhotite with a lamellae texture and a rusted halo (Fig.4.10c) were identified. As in this magnetite was variable (0 to 0.31wt%) and very low in pyrrhotite (<0.02wt%).

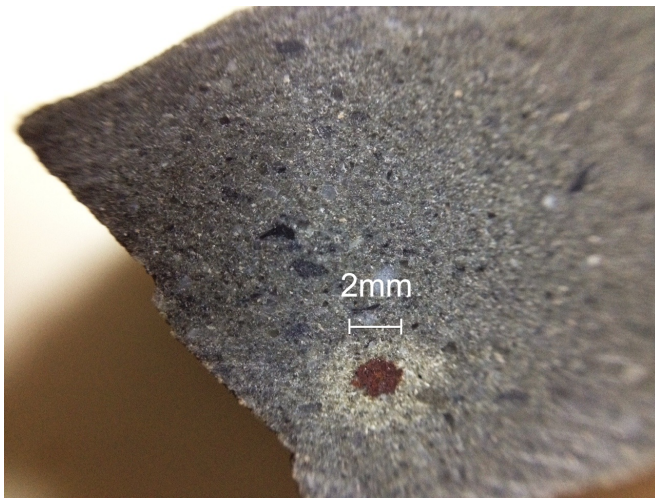

Fig.4.9 Altered colloform assemblage of magnetite/ chalcopyrite in the wacke sandstone of Todoromi area.

Table 6

Results of Electro Probe micro analysis (EPMA) on samples collected in the Hokusetsu area (unit: wt%; bold figures indicate highest wt% As in the sample)

Location	Mineral	S	Fe	As	Cu	Zn	Pb	Co	Ni	Total
Sandstone (Todoromi)	mag	0.187	49.995	n.d.	0.188	0.13	1.365	0.198	0.315	52.378†
	mag	0.047	46.714	0.307	0.909	0.423	1.692	0.086	0.246	50.424†
	mag	0.133	49.57	n.d.	0.117	0.364	0.893	0.161	0.451	51.689†
	po	39.026	58.741	0.023	0.057	0.036	n.d.	0.16	0.286	98.329
	po	39.498	59.247	n.d.	0.076	0.056	n.d.	0.16	0.276	99.313
	po	39.19	58.732	n.d.	0.045	0.061	n.d.	0.162	0.11	98.30
	mag	0.073	47.057	0.051	0.865	0.232	0.681	0.258	0.589	49.806
	mag	0.042	47.44	0.21	0.994	0.192	0.961	0.227	0.462	50.528†
	mag	0.047	49.848	0.23	1.368	0.225	0.149	0.253	0.521	52.641†
	mag	0.049	43.33	**0.35**	0.818	0.129	0.857	0.087	0.163	45.783†
	collo. mag.	0.057	48.082	0.197	0.073	0.005	0.055	0.047	n.d.	48.516†
	collo. mag.	0.038	45.512	0.019	n.d.	0.05	0.027	0.066	n.d.	45.712†
	collo. mag.	0.038	46.799	0.016	n.d.	0.017	n.d.	0.077	0.006	46.953†
	collo. mag.	0.119	51.306	0.085	0.046	n.d.	0.208	0.057	0.033	51.854†
Shale (Todoromi)	sulfars.	19.886	6.603	38.180	n.d.	n.d.	0.096	13.346	8.128	86.239
	sulfars.	18.324	4.427	34.805	n.d.	0.032	18.887	9.145	10.915	96.535
	sulfars.	20.141	4.333	**41.198**	1.263	0.035	n.d.	11.903	13.11	91.983
	mrc	53.60	45.307	n.d.	n.d.	0.026	0.078	0.087	0.026	99.124
	mrc	52.586	44.895	0.089	n.d.	n.d.	n.d.	0.057	0.017	97.644
	mrc	46.969	40.953	0.045	0.063	0.049	0.021	0.078	0.027	88.205
	py	53.133	44.907	0.408	0.018	n.d.	n.d.	0.051	0.004	98.521
	py	52.533	43.53	0.413	0.004	0.022	n.d.	0.045	0.017	96.564
	py	53.387	45.912	0.416	n.d.	n.d.	n.d.	0.062	n.d.	99.777
	gl	13.408	0.363	n.d.	0.058	n.d.	78.065	0.09	0.044	92.028
	sp	34.05	5.391	n.d.	0.142	66.761	n.d.	0.038	0.004	106.386
Quartzite	po	35.755	49.109	n.d.	0.021	n.d.	0.011	0.103	0.092	85.091
	po	36.208	48.742	0.006	n.d.	0.043	n.d.	0.097	0.094	85.19
	po	36.046	48.785	0.016	n.d.	0.016	0.016	0.094	0.121	85.094
	po	36.073	48.948	**0.050**	n.d.	0.022	n.d.	0.086	0.07	85.249
	po	36.028	48.798	0.002	n.d.	0.043	n.d.	0.062	0.105	85.038
	po	36.003	47.803	n.d.	0.016	0.056	n.d.	0.087	0.05	84.015
	cp	31.768	24.779	0.018	25.907	0.085	n.d.	0.021	n.d.	82.578
	cp	32.126	23.895	0.005	25.618	n.d.	n.d.	0.027	n.d.	81.671
	sp	31.119	7.548	n.d.	0.042	46.236	n.d.	0.026	0.015	84.986
Otani mine	py	47.752	35.002	n.d.	0.110	0.004	n.d.	0.039	0.01	82.917
	py	46.917	34.905	0.001	0.002	0.209	0.077	0.033	n.d.	82.144
	st	31.325	22.962	n.d.	23.959	0.264	0.054	0.047	n.d.	78.611
	st	28.661	9.88	n.d.	23.676	2.190	n.d.	0.014	0.021	64.442
	st	30.867	22.801	n.d.	23.427	0.067	n.d.	0.018	n.d.	77.18
	st	26.048	7.554	n.d.	16.988	2.244	n.d.	n.d.	0.018	52.852
	cp	27.446	18.511	n.d.	17.131	0.052	n.d.	0.017	0.015	63.172
	sp	29.626	6.546	**0.002**	0.037	40.337	n.d.	0.015	0.006	76.569
	sp	30.542	6.925	n.d.	0.106	46.633	n.d.	0.035	n.d.	84.241

† the total was not recalculated to oxide to emphasize the presence of S. n.d. : not detected

Table 6 (cont.)

Location	Mineral	S	Fe	As	Cu	Zn	Pb	Co	Ni	Total
Kawaura mine	py	53.108	45.854	0.497	0.251	0.145	0.057	0.085	0.056	100.053
	py	52.711	44.573	0.788	0.011	0.044	0.047	0.065	0.016	98.255
	py	53.273	45.551	0.085	0.052	n.d.	n.d.	0.089	n.d.	99.050
	py	53.455	45.185	0.234	0.132	0.004	n.d.	0.067	n.d.	99.077
	py	52.176	44.122	**0.815**	0.027	0.046	0.109	0.053	n.d.	97.348
	py	52.712	43.665	0.354	0.268	0.062	0.052	0.055	0.445	97.613
	py	52.352	43.75	0.583	0.008	0.531	n.d.	0.146	0.157	97.527
	py	51.494	43.108	0.529	0.403	1.108	n.d.	0.096	0.436	97.174
	cp	34.592	29.299	n.d.	33.544	0.218	0.093	0.039	0.019	97.804
	cp	34.67	28.943	0.006	33.041	0.993	0.077	0.038	n.d.	97.768
	cp	34.532	29.376	n.d.	33.585	n.d.	n.d.	0.029	n.d.	97.522
	sp	33.501	4.996	n.d.	1.642	64.116	n.d.	0,00	n.d.	104.255
	sp	33.203	5.309	0.012	1.291	65.877	n.d.	0.017	n.d.	105.709
	sp	33.897	5.4	n.d.	1.735	63.248	n.d.	0.002	n.d.	104.282
Fushio (Satsukiyama flt.)	py	53.907	44.996	0.019	0.051	0.029	0.005	0.564	n.d.	99.571
	py	42.115	40.923	0.001	0.039	0.004	n.d.	0.115	0.119	83.316
	py	53.494	45.584	n.d.	0.026	0.106	n.d.	0.098	0.024	99.332
	py	53.242	45.852	n.d.	n.d.	0.020	n.d.	0.047	0.214	99.375
	py	51.254	45.307	n.d.	0.016	n.d.	n.d.	0.064	0.062	96.703
	py	51.390	42.992	0.019	n.d.	n.d.	n.d.	0.07	0.171	94.642
	py	52.662	44.598	n.d.	0.012	n.d.	n.d.	0.061	n.d.	97.333
	py	53.338	45.818	n.d.	0.014	n.d.	n.d.	0.075	n.d.	99.245
	py	51.486	44.725	**0.088**	n.d.	n.d.	n.d.	0.05	n.d.	96.349
	py	54.080	45.189	0.002	n.d.	n.d.	n.d.	0.067	n.d.	99.338
Hirao mine (hornfels)	py	48.523	37.216	n.d.	0.003	0.044	n.d.	0.050	0.071	85.907
	py	48.274	37.184	n.d.	0.036	n.d.	0.005	0.072	0.095	85.666
	py	46.672	32.424	n.d.	n.d.	n.d.	n.d.	0.309	1.343	80.748
	py	47.203	34.871	n.d.	n.d.	n.d.	n.d.	0.075	0.664	82.813
	py	35.379	47.468	**0.006**	n.d.	0.067	n.d.	0.069	0.210	83.199
Hirao mine (ore deposit)	py	48.915	40.464	n.d.	n.d.	0.02	n.d.	0.085	0.068	89.552
	py	48.951	39.904	n.d.	0.133	0.029	n.d.	0.082	0.066	89.165
	py	49.659	39.193	n.d.	n.d.	n.d.	0.031	0.062	0.034	88.979
	cp	33.184	26.509	**0.008**	28.737	0.049	0.038	0.029	0.041	88.595
	cp	32.665	26.275	n.d.	28.197	0.041	0.076	0.018	0.004	87.276
	cp	34.677	29.344	n.d.	33.132	0.153	0.011	0.029	0.002	97.348
	cp	32.819	25.775	n.d.	27.628	0.102	0.027	0.026	n.d.	86.377
	sp ?	23.194	2.851	n.d.	0.015	15.609	0.077	0.025	n.d.	41.771
	gl	11.271	0.038	n.d.	n.d.	0.472	67.291	n.d.	0.015	79.087

† the total was not recalculated to oxide to emphasize the presence of S. n.d.: not detected

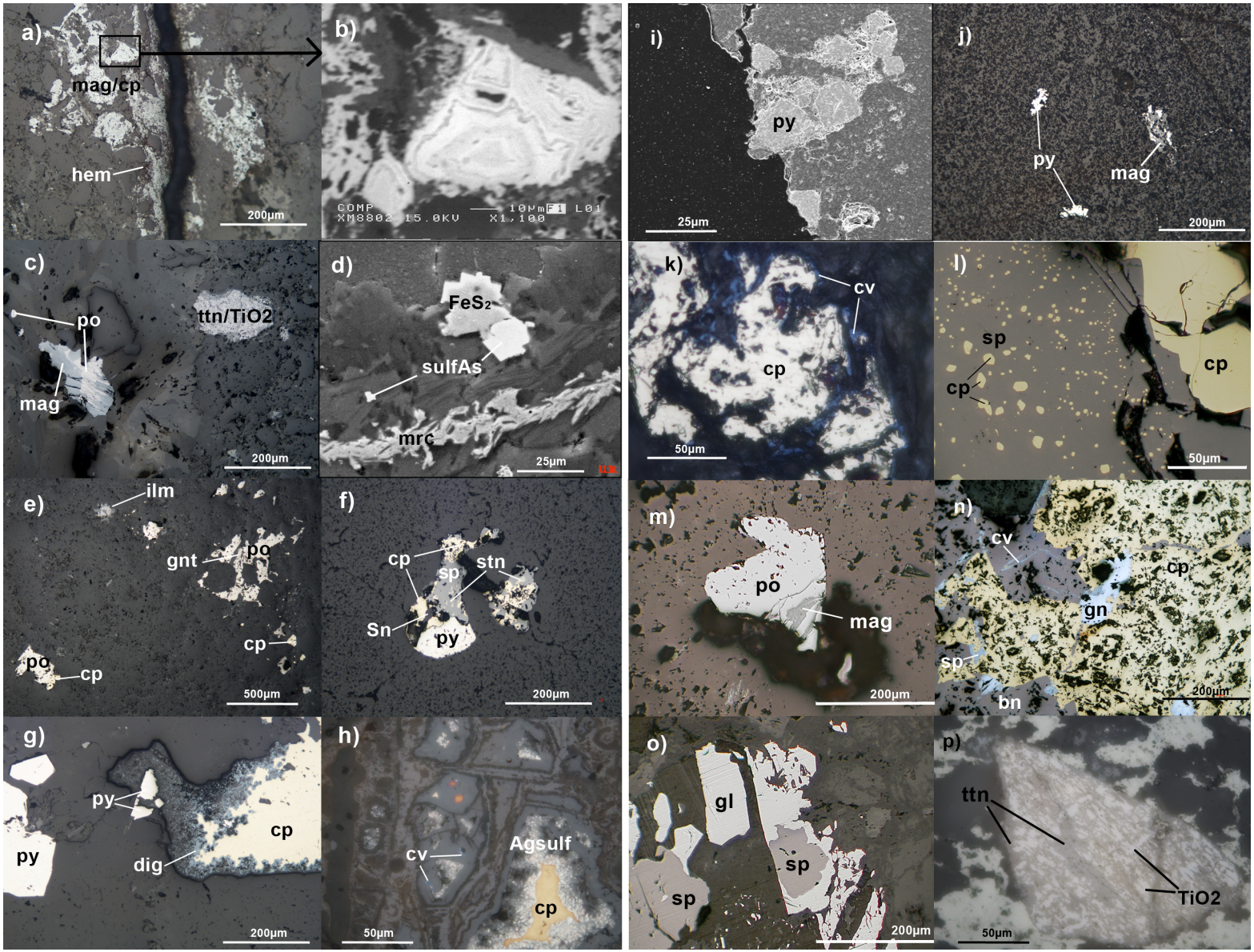

Fig. 4.10 Photomicrographs in reflected light of **a**) magnetite (mag) and chalcopyrite (cp), and hematite (brown red) in Todoromi sandstone, **b**) back-scatter electron (BSE) detail image of the magnetite/chalcopyrite assemblage with colloform texture, **c**) Todoromi sandstone with magnetite (mag) and pyrrhotite (po), and titanite (ttn) with Ti oxide (TiO_2), **d**) scanned electron image (SEI) of Todoromi shale with headspear-shape marcasite (mrc) and sulfarsenide (sulfAs) of gersdorffite-cobaltite solid solution. Photomicrographs in reflected light **e**) in quartzite of pyrrhotite (po), chalcopyrite (cp), ilmenite (ilm) and garnet (gnt), (**f**) Otani Mine assemblage with stannite (stn), native Sn (Sn), sphalerite (sp), pyrite (py) and chalcopyrite (cp), Kawaura mine sulfides with (**g**) pyrite, chalcopyrite (cp) rimed with digenite (dg) and (**h**) chalcopyrite surrounded by Ag-sulfides (Ag sulf), and covellite (cv, blue). (**i**) Scanned electron image (SEI) of pyrite (py) in shale gauge (dark grey) of Satsukiyama fault (Fushio). Photo-micrographs in reflected light of (**j**) deformed pyrite (py; white) and magnetite (mag; grey) in hornfels nearby Hirao mine, (**k**) assemblage of chalcopyrite (cp) rimed with covellite (cv, blue) from Hirao hydrothermal ore deposit, (**l**) assemblage of chalcopyrite (cp) and sphalerite (cp) with chalcopyrite disease (cp blebs in sp) at Hirao mine, (**m**) pyrrhotite (po) and magnetite (mag) in hornfels near Osugahara mine, and (**n**) Tada mine massive sulfide of chalcopyrite (cp), bornite (bn), sphalerite (sp), galena (gl) and covellite (cv, blue), **o**) sphalerite (sp) and galena (gl) in Hatano skarn deposit, **p**) authigenic TiO_2 mineral (rutile, bright areas) overgrown by titanite (ttn, gray areas).

.

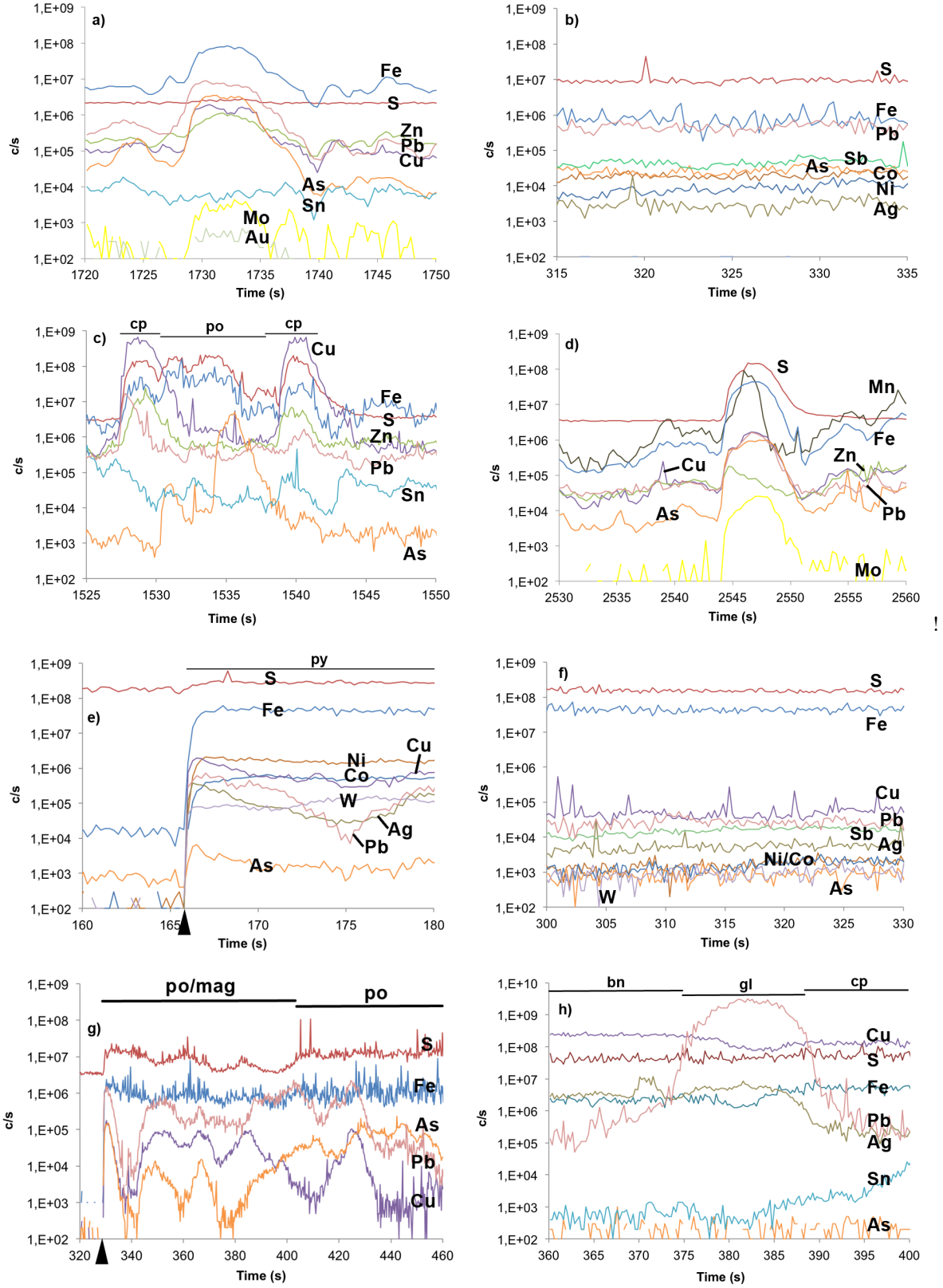

Fig. 4.11 - Time resolved ablation line **a**) across a weathered chalcopyrite/magnetite assemblage in Todoromi sandstone, b) of marcasite sulfide in Todoromi shale, **c**) across a sulfides assemblage of chalcopyrite (cp) and pyrrhotite (po) in contact-meta- morphosed quartzite sample, **d**) across a pyrite in hornfels rocks nearby Hirao mine, **e**) across massive pyrite from Hirao hydrothermal deposit (the black arrow marks the firing of the laser), **f**) of a veinlet of fine-grained pyrite in massive pyrite from the Hirao hydrothermal deposit, **g**) across of a pyrrhotite with magnetite exsolution in hornfels rocks near Osugahara Mn mine (the black arrow marks the firing of the laser), and h) in sulfide assemblage of bornite (bn), galena (gl) and chalcopyrite (cp) of the Tada xenothermal ore-deposit.

The rock was also disseminated with Ti oxide minerals that were overgrown by titanite (sphene, $CaTiSiO_5$) along their rims and their inside cracks (Fig. 4.10p). Arsenic was very low (<0.05wt%) in these Ti minerals. LA-ICP-MS revealed that some of the Ti-minerals contained some Sn, while Sn was not detected in the colloform assemblage or the magnetite/pyrrhotite assemblages. From the microscope observations, it was noticed that the rock had a granoblastic deformation, likely from the Late Cretaceous contact-metamorphism.

Shale - The shale contained very small (<10 μm) disseminated subhedral grains of pyrite (FeS_2). Arsenic in pyrite grains large enough to be probed reached 0.42wt%. An elongated crystal of FeS_2 with a spearhead shape was observed (Fig. 4.10d). The peculiar shape suggested this sulfide was marcasite, a dimorph of pyrite that formed in acidic (pH<4-6) environment and low temperature hydrothermalism, and is usually found in ancient marine sedimentary rocks (Schieber, 2004, 2011). The As, Ni and Co in the marcasite were below <0.1wt%. LA-ICP-MS analysis revealed important levels of Pb, as well as the occurrence of Sb and Ag (Fig. 4.11b), which would evidence the low temperature formation of the marcasite (Yamaoka, 1958).

Next to the elongated marcasite, a sulpharsenide (Fig.4.10d) was observed; it had an average composition of 11.98wt% Co, 11.23wt% Ni, 5.67wt% Fe and As:S ratio of 0.84:1. The Co:Ni and As:S ratio resembled to either a solid solution between cobaltite (CoAsS) and gersdorffite (NiAsS) (Fanlo et al., 2004; Fukuoka and Hirowatari, 1980; Ixer et al., 1979) or a Ni-rich alloclasite. The gersdorffite-cobaltite solid solution had been identified by Fanlo et al. (2004) in the highest temperature (>600°C) phase of the paragenesis of the San Juan de Plan ore-deposit (Spain). This would be in contradiction with the low temperature conditions suggested by the marcasite. It was likely that the sulpharsenide and the marcasite were deposited at different times. Crystallography analyses are required to confirm the true nature and the formation environment of this sulpharsenide.

Quartzite rock (2)

In the quartzite, pyrrhotite was the most abundant sulfide mineral. It had a median Fe/S=0.87 (i.e., x=0.13 in $Fe_{(1-x)}S$), corresponding to the monoclinic form Fe_7S_8. Galena was detected as impurity in pyrrhotite but was rare. Other minor sulfides were chalcopyrite and sphalerite ((Zn, Fe)S) (Fig.4.10e). The sphalerite contained appreciable amounts of Fe (7.55wt%) and Ca. Ilmenite ($FeTiO_3$) were also observed, as well as Ca/Ti-rich garnet that was identified as andradite ($Ca_3(Fe^{3+},Ti)_2Si_3O_{12}$) (Fe was only a minor element in this mineral). The element mapping by LA-

ICP-MS showed that As was concentrated in small phases (Fig.4.12), and EPMA only measured As up to 0.05wt% in pyrrhotite, which also contained Co and Ni, up to 0.10wt% and 0.12wt%, respectively.

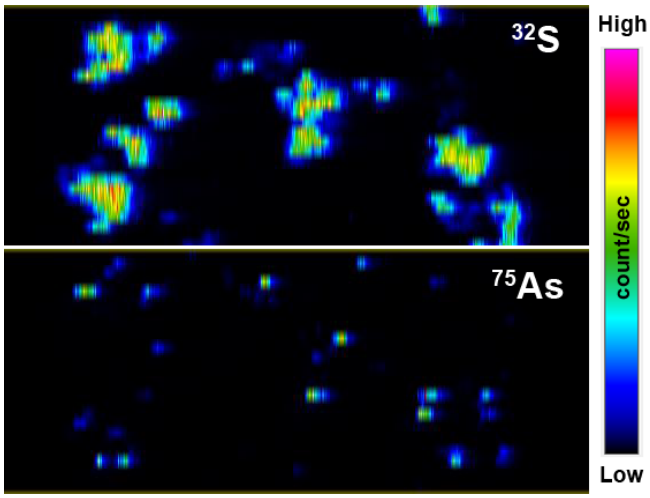

Fig.4.12 Element mapping of ^{32}S and ^{75}As by LA-ICP-MS of the quartzite sample. The mapping of sulfur delimited well the sulfide minerals of the sample. Arsenic appeared in minute places scattered all over the sulfides, mainly in pyrrhotite.

W-Sn Otani Mine (3)

The Otani Mine is a pegmatite-vein deposit that formed from the intrusion of the Gyojayama granodiorite. In the studied sample, LA-ICP-MS revealed that As was mainly distributed on the rim of stannite (Cu_2FeSnS_4) and in an unknown none-sulfide phase, and less in the pyrite (Fig. 4.13). The As was barely detected (<0.002wt%) by EPMA in any sulfides (Table 6). Native Sn was detected during the EDS analysis. The stannite and chalcopyrite replaced and was exsolved from the sphalerite, respectively (Fig. 4.10f). Kelly and Turneaure (1970) interpreted this replacement due to a Cu/Fe-bearing solution, posterior to the sphalerite precipitation. Similar to the sulfides in quartzite, LA-ICP-MS showed that the sphalerite contained 6.74wt% Fe. From the observation of abundant amounts of stannite, native Sn and the presence of pyrite, it was inferred that the studied sample was mineralized at Stage IIA of the mineralization sequence of the deposit, with temperatures between 272°C and 194°C (Nakamura and Kim, 1982).

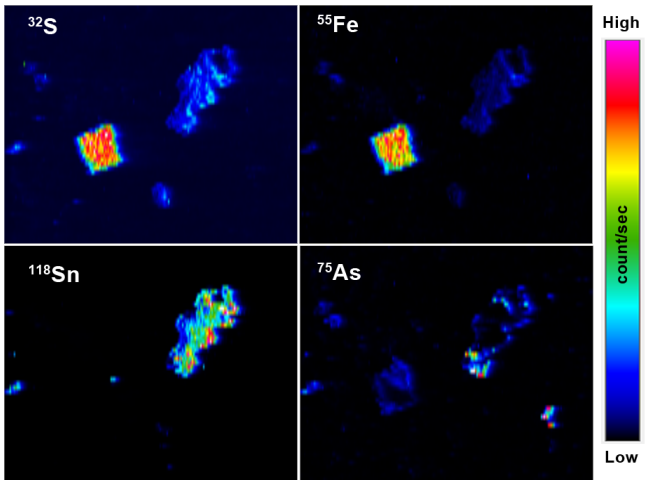

Fig.4.13 Element mapping of ^{32}S, ^{55}Fe, ^{118}Sn and ^{75}As by LA-ICP-MS of sample from Stage 2A mineralization of the Otani mine. Euhedral pyrite appeared very neatly, while Sn gave a clear image of the stannite. Arsenic appeared more intensely at the edges of stannite and pyrite, and in an unidentified non-sulfidic phase (lower right)

Kawaura Mine (4)

The Kawaura Mine is located upstream of the lower-reach of Minoh River, of which water was contaminated by As, in a zone of granite porphyry dikes within the Ultra-Tamba belt. It is a hydrothermal deposit that was mined for Cu and Ag (Osaka Mining Supervisory Bureau, 1933). The analyzed sulfides were subhedral pyrite with occasional sphalerite exsolution, and chalcopyrite with replacement of digenite (calculated as $Cu_{10}S_6$) along its rims (Fig. 4.10g). Arsenic concentrated up to 0.82wt% mainly in pyrite, which also contained Ni up to 0.44wt%, Co up to 0.15wt% and Pb up to 0.11wt%. As levels in chalcopyrite and sphalerite were low (>0.02wt% As). It is suspected that the As levels in sphalerite, also Fe-rich (5.3wt%), were slightly higher because of its emplacement within As-rich pyrite. In another sample within quartz gangue, chalcopyrite was rimed by Ag-sulfides and covellite (CuS), identified by SEM-EDS analysis (Fig. 4.10h). The emplacement of digenite, covellite and Ag-sulfides riming chalcopyrite indicated that these minerals precipitated after the deposition of chalcopyrite. The digenite and covellite were likely the alteration products of or overgrowth on the chalcopyrite, formed from an ore-fluid inflow subsequent to the chalcopyrite precipitation. The sulfide assemblages observed in the Kawaura samples were very similar to those of Tada Mine described in Imai et al. (1975), in which the Ag-sulfide and digenite appeared in the late stages of the mineralization with the decreasing temperatures and sulfur fugacity of the ore fluids.

Satsukiyama fault at Fushio (5)

At Fushio, where the As concentrations in spring waters reached 20.3 ppb (Ito et al., 2003), sulfide minerals were found in the gouge of the Satsukiyama fault. The sulfides were chiefly euhedral and subhedral pyrite (Fig. 4.10i). Pyrite contained low As (only up to 0.09wt%) but higher levels of Co and Ni (up to 0.56wt% and 0.21wt%, respectively). Ag was detected in pyrite by EDS analysis. Chalcopyrite and sphalerite were also observed, as individual grain rather than in assemblages but no As was detected in these sulfides.

Hirao Mine (6)

Ore deposits – The Hirao Mine is a Cu-Zn hydrothermal ore-deposit in the Tamba formations in Minoh city, south of the study area. Sulfides were sampled from two different veins of the deposit. Massive porous pyrite sampled from one of those veins (first vein) was depleted in As, while appreciable levels of Cu, Co and Ni (although < 0.1wt% in most analyzed spots), Pb, W and Ag were detected by LA-ICP-MS (Fig. 4.9e). Microscope observations showed another type of a small pyrite, brighter than the surrounding massive pyrite. From LA-ICP-MS, this pyrite was depleted in As, Ni, Co but Pb, Ag and Sb were detected (Fig. 4.11f). Also, abundant chalcopyrite (with As <0.01wt%) coexisted with the massive pyrite. The chalcopyrite was usually rimed with blue copper mineral that resembled Fe-rich covellite (Fig. 4.10k) with an average formula of $Cu_{17}FeS_{20}$. Major minerals from another vein (second vein) in Tamba shale chloritized by hydrothermal fluids, were Ag-rich galena, Mn-rich sphalerite with chalcopyrite disease, and Sn-rich chalcopyrite (Fig. 4.10l). These minerals did not contain As.

Hornfels - In hornfels found at the site of the second vein of Hirao mine, pyrite was the dominant sulfide mineral, occurring as very small (<10μm) disseminated euhedral grains. The pyrite was sometimes occurring with magnetite in a skeletal texture and altered shape (Fig. 4.10j). Pyrrhotite (as $Fe_{0.83}S$) was also identified with EDS. Pyrite contained elevated Ni and Co (up to 1.34wt% and 0.31wt%, respectively), but virtually no As (<0.01wt%) was detected by EPMA, although As appeared clearly within the pyrite probed by LA-ICP-MS (Fig. 4.11d). LA-ICP-MS also showed that Mo and Mn, but not Sn, have accumulated in some of the sulfides.

Hornfels nearby Osugahara mine (7)

Osugahara mine was a Cu-Ag ore deposit located at the east of Hirano mine, however, the exact location was not found during the field survey. From the river sediments around the presumed mine location, fresh samples of bedded rhodochrosite ($MnCO_3$) ore hosted in dark grey chert were collected. In these samples, sulfides were rarely observed and only one small sulfide was analyzed. It was pyrrhotite and magnetite (Fig. 4.10m), similar to the minerals observed in Todoromi sandstone. Arsenic was detected in the pyrrhotite with LA-ICP-MS (Fig. 4.11g). The rhodochrosite also contained non-sulfidic W/Sn minerals with usually low As and Pb.

Hatano mine (8)

The Hatano mine located in the vicinity of the Hirao and Osugahara mines was a skarn-type deposit, from which Zn and Pb minerals were mined. Mn/Fe-rich sphalerite and Ag-rich galena were observed (Fig. 4.10o), and barely contained As.

Tada mine (9)

The Tada mine, located at the west of the study site, is a historical important xenothermal deposit that was exploited for Ag, Cu, Pb and Zn. The LA-ICP-MS analysis of massive Ag-rich minerals of bornite/chalcopyrite/galena (Fig. 4.10n) showed that As was almost inexistent (Fig. 4.11h).

4.2.2 Discussion

Types of ore deposits of the study area

Some of the sulfur isotopic results have been discussed in Section 4.1.2. Here, the isotopic ratios of the studied sulfides are reconsidered in regard to the ore mineralization recognized in the Inner Zone of Southwest Japan, and grouped into 3 types (Fig 4.14): 1) the Paleozoic/Mesozoic kieslager-type cupriferous stratiform deposit from submarine volcanism, 2) the Cretaceous to Paleogene plutonic and 3) subvolcanic deposits mentioned in Section 2.2. The kieslager-type deposits are occasionally found in the Maizuru-Tamba Terranes, and characterized by pyrite-chalcopyrite-sphalerite assemblages with colloform texture; pyrrhotite may also be present. These

deposits usually laid within definite stratigraphic horizons in volcanogenic-sedimentary formations (Nakamura, 1990).

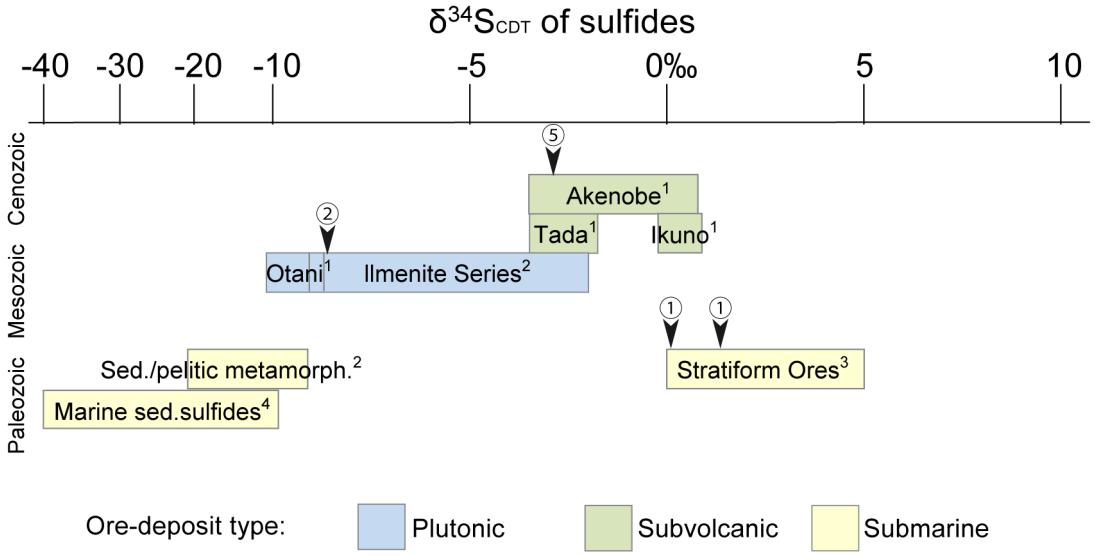

Fig. 4.14 $\delta^{34}S$ of sulfides from marine sedimentary sulfides (-40 to -10‰), Japan sedimentary and pelitic metamorphic rocks (-21 to -9‰), Japan Paleozoic/Mesozoic stratiform Cu deposits (0 to +5‰), Japan ilmenite series granitoids (-9 to -2‰), Otani (-10.5 to -8.6‰), Tada (-3.5 to -1.7‰), Akenobe (-3.5 to +0.8‰) and Ikuno (-0.2 to +0.9‰) ore-deposits, and ①Todoromi sulfides, ②quartzite rocks sulfides, ⑤Fushio sulfides. Data from 1: Miyoshi et al. (1988), 2: Ishihara and Sasaki (1992), 3: Sato and Kase (1996), 4: Canfield (2004).

The plutonic- and subvolcanic-type deposits in Southwest Japan are found in association with the Late Cretaceous to the Early Paleogene magmatic activities (Takimoto, 1973). The plutonic-vein and subvolcanic-vein type ore mineralizations can be distinguished by the depth of the deposits, i.e., the subvolcanic deposit are formed at the shallower depths (from subsurface to 2km-deep) than the plutonic deposit (>2 km-deep) (Laznicka, 1985). The emplacement of the plutonic vein deposits is directly related to the granitoid intrusions of Late Cretaceous, while the subvolcanic deposits are usually associated with underneath granitic cupolas and granite porphyry dikes (Nakamura et al., 1987). The origin of the sulfides from the three aforementioned types of deposits is discussed in details below.

Paleozoic/Mesozoic submarine type deposits of the study area – The $\delta^{34}S$ of the sulfides in the greenstone and shale of the Todoromi area were consistent with the isotopic ratios of sulfides from Paleozoic/Mesozoic stratiform cupriferous deposits of Japan (Sato and Kase, 1996). Some of these deposits are found in the unmetamorphosed or weakly metamorphosed Pre-Cretaceous Terranes of Southwest Japan, and believed to form syngenetically with submarine volcanic activities because of

the constant association of the cupriferous ores with greenstone and bedded chert (Watanabe, 1957). The $\delta^{34}S$ of shale in Todoromi (+0.1%) was lower than $\delta^{34}S$ of greenstone (+1.4%), but still in the range of the isotopic ratio of Paleozoic/Mesozoic sulfides. The lower ratio may reflect the influence of sulfur sourced from the Late-Cretaceous Early Paleogene magmatism that is characterized by much lower $\delta^{34}S$ (cf. the *Plutonic type* Section below). In the present study, the ore mineral assemblages hosted in the weakly metamorphosed Todoromi sandstone were magnetite/chalcopyrite with a colloform texture and magnetite/pyrrhotite. These assemblages were similar to those of the Yanahara deposit (Kanehira and Tatsumi, 1970), and the colloform texture of this deposit was interpreted by Mitsuno (1988) as the relics of pyrite and chalcopyrite that were desulfurized into magnetite, and sometimes pyrrhotite, by the Late Cretaceous contact-metamorphism. The submarine volcano-sedimentary nature of the Todoromi formations was further advocated by the occurrence of greenstone (meta-basalt). Although the present analyzed ore minerals in Todoromi sandstone were not found as a massive ore typical of other stratiform Cu ore-deposits in the Pre-Cretaceous Terranes, the sulfur isotopic ratio, mineralogy and geological environment of these minerals strongly supported their Paleozoic/Mesozoic submarine origin.

Pyrite, marcasite, sulpharsenides were observed in the grey shale. Most of these mineral grains were small in size (<10μm) and disseminated in altered matrix of the shale, suggesting they formed via external supply of the elements. The occurrences of marcasite and gersdorffite-cobaltite solid solution indicated contradictive temperature conditions. The solid solution mineral of gersdorffite-cobaltite is usually found associated with granitic intrusion (Fanlo et al., 2004; Fukuoka and Hirowatari, 1980; Hem et al., 2001; White et al., 2014) only at temperature >500°C (Klemm, 1965), whereas the marcasite forms at much lower temperatures; e. g., Yamaoka (1959) observed that pyrite and marcasite occurred in the later stage of the mineralization of the Toroku xenothermal deposit (Miyazaki Prefecture).

While the origin of the aforementioned sulfides remained uncertain, magmatic origin is probable for the occurrence of chalcopyrite, sphalerite, and galena in the shale. During the field survey, considerable amounts of granite porphyry rocks were found from excavation of the Minoh toll road tunnel at Todoromi running within sedimentary rocks, suggesting that the hydrothermal alteration of the sedimentary formations from the igneous intrusion occurred in this area. Therefore some of the sulfides in the shale may be related to this magmatic activity. The influence of the Cretaceous igneous activities was also evidenced onto the older ore deposits by the occurrences of

W/Sn minerals in the rhodochrosite of the Mesozoic bedded Mn deposits, collected near the Osugahara Mine.

Plutonic type deposits of the study area – In the Inner Zone of Southwest Japan, sulfides of the plutonic type are characterized by low $\delta^{34}S$ in the range of -10% to -2%. The studied sulfides, mainly pyrrhotite, in the quartzite had an average $\delta^{34}S$ value of -8.8%, typical of the plutonic type and similar to those of the Otani mine (Miyoshi et al., 1988). Pyrrhotite is indeed recognized as the major sulfide phase in granitic-induced ore deposits (Ishihara and Sasaki, 2002). Andradite and ilmenite were both present in the quartzite. Andradite is a garnet mineral that formed via contact-metamorphism (Deer et al., 2012), and ilmenite is rare but a characteristic magmatic minerals associated with the Late Cretaceous granitoids (Ishihara, 1970, 1977). Additionally, sphalerite in the quartzite had levels of Fe similar to those from Otani Mine, indicating this mineral formed in association with granitic intrusion (Tsukimura et al., 1987) and in equilibrium with pyrrhotite (Vaughan and Craig, 1997). Those evidences strongly supported that the sulfides in the quartzite have deposited in relation to the quartz-diorite intrusion, and thus classified as a plutonic-type ore.

Tainosho (1971) concluded that the parental dioritic magma of the Ibaraki granitic complex was generated in the lower crust or the upper mantle. Upon ascension to shallower depths, quartz-diorite started crystallization at depth below 7km and temperature around 870°C, deeper and hotter than the final molten that produced the center part of granite (adamellite), which crystallized at about 2km-deep and 780°C. The studied quartzite had an indurated matrix with disseminated sulfides, and no hydrothermal deposits have been reported in the immediate surroundings of the quartzite. Thus, the sulfides were plausibly deposited from volatiles of the early dioritic magma in a pneumatolytic process, in which the infiltration of hot magma gas and vapors induced the metamorphism of sandstone into quartzite and the dissemination of sulfides. According to the Lindgren's classification (1933), this type of ore-deposits form at great depth (>4.5km) and under high temperature (likely 500°C to 800°C), which conditions are consistent with those described above by Tainosho (1971).

Subvolcanic type deposits of the study area – The subvolcanic type deposits are characterized by polymetallic ores and often the multiple supplies of ore-fluids from the upheaval and withdrawal of an underneath magma (Miyoshi et al., 1988; Takimoto, 1973). The paragenesis of the Japanese subvolcanic polymetallic ores is structured from early copper sulfides, to Zn-Pb sulfides, to later Ag-bearing minerals sulfides (Imai et al., 1975). This variation of paragenesis has been recognized in the ore of the Tada mine (Cu-Ag-Sn-Zn-Pb), which is also a typical example of the xenothermal (rapid loss of heat/pressure) vein-type deposit (Imai et al., 1975).

The similar mineralization system to that of the Tada mine is thought to spread well outside the mine, with several vein families represented on Fig. 4.15. In the Inagawa and Kawanishi districts (western part of the study area) between the Ibaraki intrusion and the volcanogenic Arima formation, many ore-deposits with the main commodities of Cu-Zn-Pb-Ag were reported, whereas mines with same commodities were almost inexistent in the east of the Ibaraki intrusion (Osaka Mining Supervisory Bureau, 1933; Osaka Mining Supervisory Office, 1911). These deposits included the Akamatsu mesothermal ore-deposits (not sampled during the study) that comprises mainly chalcopyrite, pyrite and pyrrhotite, with minor sphalerite, galena and arsenopyrite (Takimoto, 1973). Imai et al. (1975) made a distinction between the mesothermal Akamatsu and the xenothermal Tada deposits owing to their geological settings, i.e., in sedimentary and volcanogenic formations, respectively. These settings are also remarkably comparable to the Ashio ore-deposit that encompasses a mesothermal model in chert/shale and a xenothermal model in rhyolitic rocks (Imai et al., 1975).

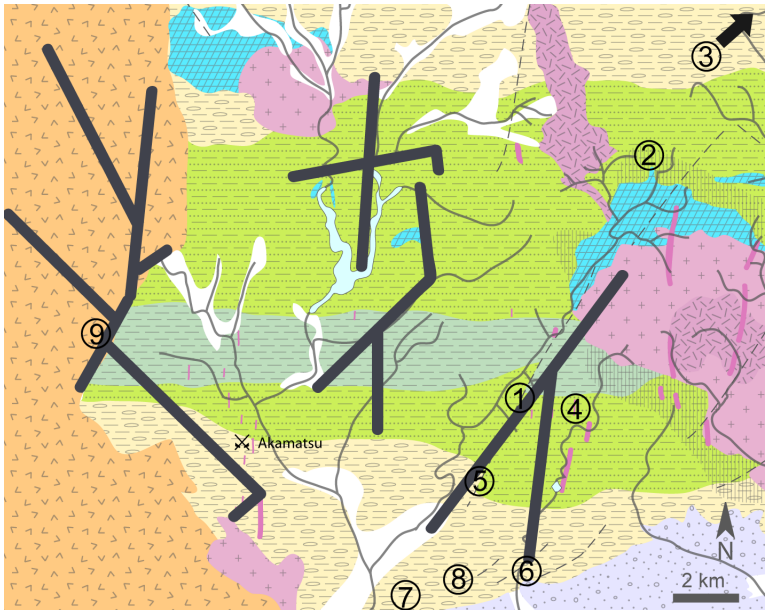

Fig. 4.15 Mineralization system (represented by thick lines) of the Tada ore-deposits. The vein system of the Tada Mine (9) is called the Ginzan vein family (mainly Cu-Pb-Ag, left of the map). Other vein families (mainly Cu) are called Hayama (including Shichiboh and Kimyozan, center, and Takayama, lower left). Numbers in circles as in Fig.3.3. After the Permanent Memorial of the Tada Ginzan.

The hydrothermal veins in Akamatsu mine were believed to form with the intrusion of granite porphyry dikes within the shale, as it is generally described for the subvolcanic-type deposits (Takimoto, 1973). Numerous granite porphyry dikes (Matsuura et al., 1995) and gravimetric data of

the Inagawa and Kawanishi districts (at 2.67g/m^3, GSJ/AIST, 2011) suggested the occurrence of plutonic masses beneath the study area. The presence of mines only between two igneous formations strongly suggests that the mesothermal subvolcanic Cu-ore deposits like Akamatsu were formed in relation to the hydrothermal fluids ascending from the underneath Late Cretaceous magma into the overlying Tamba Terranes.

The Kawaura and Hirao ore-deposits were mined for Cu-Ag and Cu-Pb-Zn, respectively. The both mines shared the same geological settings as those of the Akamatsu and Ashio mesothermal ore-deposits, i.e., they were located in sedimentary formations intruded by granite porphyry dikes. At both the Kawaura and Hirao mines, the sequence of deposition was similar to the paragenesis of the Tada subvolcanic-type deposit. The sulfide assemblage at the Kawaura mine indicated that the Ni/Co-rich pyrite and chalcopyrite crystallized first, and sphalerite was exsolved from pyrite with decreasing temperatures. The fluid circulation in the later stages at decreasing sulfur fugacity subsequently caused the chalcopyrite alteration into digenite. Those fluids also induced the precipitation of Ag sulfides around the chalcopyrite. The Hirao also presented the same sequence of mineralization, with an initial deposition of a Ni/Co-rich pyrite and chalcopyrite that was later altered to covellite by a subsequent ore-fluid circulation. From the consistency of their characteristic paragenesis and their geological settings with others mesothermal subvolcanic deposits, the Kawaura and Hirao hydrothermal mines can thus be classified in the same type.

In Fushio along the Satsukiyama fault, the main sulfides were chiefly euhedral pyrite that was sometimes enriched in Ag, an element commonly found in the subvolcanic deposits of the area. The accessory chalcopyrite did not show signs of alteration by the later fluids. The $\delta^{34}S$ (-3.0‰) (Ito et al., 2003), however, was indicative of the subvolcanic type sulfides. Additionally, the Kawaura, Hirao and Fushio sulfides were all categorized in the same Takayama vein family (Fig. 4.13). These observations suggested that these sulfides at Fushio also belonged to the same mesothermal subvolcanic type ore-deposits.

Co/Fe and Ni/Fe ratio

Co and Ni has been used as a tool to distinguish the origin of sulfides, especially pyrite, in several types of ore deposits and sedimentary formations (Bajwah et al., 1987; Davidson, 1962; Loftus-Hills and Solomon, 1967). Nishiyama and Ito (2012) used the Ni/Fe and Co/Fe ratio to distinguish the felsic and mafic origin of sulfides from Otani and others Japanese deposits (Ashio,

Chichubu, Shimogawa, Taishu and Shakanai). Among those data, only the kieslager-type deposits of Shimogawa was distinct from others with higher Co/Fe ratio, but without further explanations from the authors. The Ni/Fe and Co/Fe ratios of sulfides from this study were plotted in Fig. 4.16. Most of the plots are within the same range although sulfides from a same location occasionally have distinguishable values; e. g., for sulfides from the Todoromi, pyrrhotite in the sandstone had higher Ni/Fe and Co/Fe than pyrite and marcasite in the shale. The pyrrhotite was an alteration product of pyrite by an igneous intrusion, and probably did not preserve the initial value of the primary pyrite. Campbell and Ethier (1984) stated that Ni tends to concentrate in alteration pyrrhotite more than the primary pyrite. The higher Ni/Fe of the pyrrhotite studied here would be an analogue of this case. At the Hirao mine area, the pyrite in hornfels had higher Ni/Fe ratio than those in the ore deposit. They also contained Mn, as well as Mo as similar to the sulfides in the Todoromi sandstone, indicating the same Paleozoic/Mesozoic submarine origin. No distinction was observed among pyrites from Kawaura, Fushio and Hirao hydrothermal deposits. This would suggest the sulfides precipitated from ore-fluids originated from the similar hydrothermal activities, and it is consistent with the fact the deposits could be categorized in the same vein family.

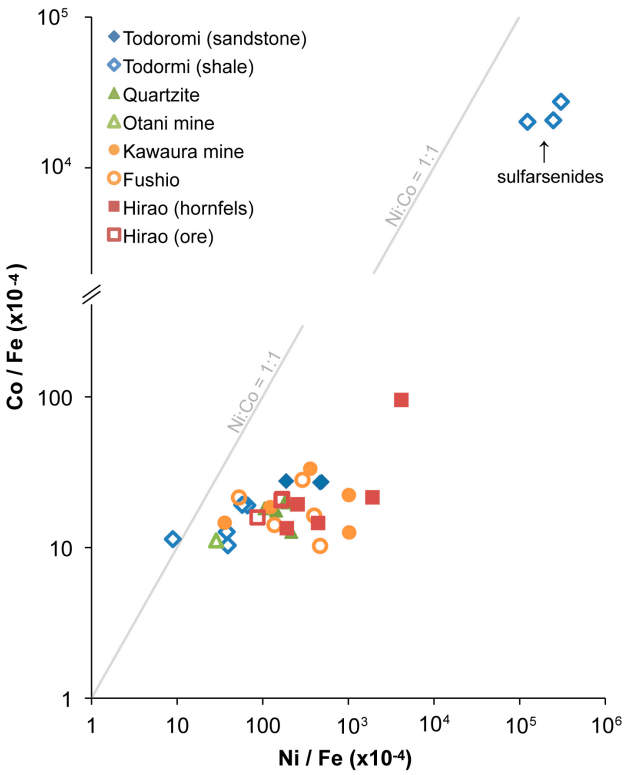

Fig.4.16 Ni/Fe vs Co/Fe in pyrite, pyrrhotite, marcasite (and sulpharsenide, upper right outliers) of studied samples. Solid line represents the 1:1 ratio.

As and trace elements in sulfides of Paleozoic/Mesozoic sedimentary rocks

Arsenic in the sandstone was detected mainly in magnetite rather than in other minerals. The studied colloform assemblages of magnetite/chalcopyrite were similar to those of the Paleozoic/Mesozoic Yanahara ore deposits in the Maizuru belt, which had been contact-metamorphosed by Late Cretaceous intrusion. The occurrence of magnetite and pyrrhotite was interpreted by Mitsuno (1988) as the result of the desulfurization of the primary pyrite by the metamorphism. Indeed, porphyry dikes were observed at the sampling site of Todoromi, and the granoblastic texture of the sandstone suggested that the rock was weakly metamorphosed. The absence of Sn and the presence of Mo and Au in the colloform ore-minerals evidenced that their formation was not related to the Cretaceous reducing felsic magmatism that otherwise supplied Sn to the related plutonic and subvolcanic ore deposits of the Hokusetsu area (e.g., Otani mine), from the melting of crustal rocks (Hedenquist and Lowenstern, 1994). The Mo and Au suggested a more oxidative process of ore mineralization, as seen with the plutonism that induced the Mo(-Pb-Zn) ore deposits and had higher oxygen fugacity than that forming the W-Sn-Cu ore province.

Arsenic was already present in the primary pyrite at the time of its oxidation by the Cretaceous/ Paleogene igneous activities, and remained in the secondary magnetite. The later oxidative Ca-metasomatism evidenced from the rutile/titanite mineral is viewed as the process that chemically altered (possibly martitized; Augustithis, 1995) the magnetite into to hematite (e.g., El-Gemmizi, 1996). Indeed, the hematite halo was observed only around magnetites sited along calcium-filled micro and macro-fractures of the rock. These successive alterations of the primary sulfides likely reorganized their chemical composition and weakened their crystallinity, from which As could easily be released when they got eventually weathered.

Cu, Zn and Pb were also retained with As in the minerals altered to iron oxides. This inefficiency to migrate out of iron oxides was observed by Lu et al. (2005) during pyrite weathering at the Jiguanshan mine (Anhui, China). They observed the immediate washout of S and the belated release of As, Cu and Zn as these elements were kept within alteration oxides layers. This would explain why As, Cu, Zn and Pb, but not S, were detected during LA-ICP-MS in the assemblages. This retardation then induced the ongoing release of As in subsurface waters that are now flushing the sandstone and cause the As contamination of spring waters in the Todoromi area. However, the rare occurrence of Paleozoic/Mesozoic cupriferous ore deposits in the study area may limit this contamination process solely to the Todoromi area.

In the Todoromi shale, As was primarily concentrated in the sulpharsenides and less in pyrite/marcasite. While the origin of the sulpharsenides was not clear, they plausibly contributed to As contamination when exposed to oxidative conditions (e.g., oxidized water circulation, open air exposure, etc.). The sulpharsenides could occur in zones where high-temperature sulfide ore deposits were reported, especially in the west of the study area, between the Arima volcanic formation and the Ibaraki granitic complex.

As and trace elements in sulfides from the granitoids intrusion

The geochemical mapping of As in riverbed sediments (Fig. 4.2) showed that the center part of the Nose pluton was As-poor (<3 ppm As in sediments), while the contact-metamorphosed rocks (e.g., quartzite) were enriched in As. The depletion in As from the most felsic rocks in the Nose pluton was obvious. Essozv et al. (1965) have shown that As tends to be enriched in the more mafic layer of the emblematic Skaergaard layered intrusion (in Greenland), where pyrrhotite and magnetite were the most abundant Fe-minerals (Hunter and Sparks, 1987; Wager et al., 1957). This can be explained by the preferential partitioning of As in the early stages of the magma crystallization.

During the cooling of the ascending dioritic magma, As would have preferentially partitioned in the degassing vapors enriched in sulfur. Keppler et al. (1999) and Beermann et al. (2015) demonstrated that S partitions readily into vapors at oxidizing conditions ($D^{vap/melt}$= 47 ±4 (Keppler et al. (1999); 3 ±1 to 96 ±24 (Beermann et al. (2015)) and even more at reducing conditions ($D^{vap/melt}$= 468 ±32; 164 ±13 to 236 ±26, respectively) of magma at temperatures >750°C and depths >2kbar (about 7km). Using the chemical composition of the biotite in quartz-diorite at 870°C by Tainosho (1971), and the geothermometer equations from Wones and Eugter (1965), the redox state of the early crystallizing magma in the Nose pluton was calculated to be log f_{O2} = -15.4, below the Ni-NiO and the FMQ oxygen buffers. The calculation indicated the reducing conditions of the magma, and thus the presence of S-rich magmatic vapor was highly probable.

Simon et al. (2007) have demonstrated that in a rhyolitic melt, the partitioning of As into the magmatic vapor phase was enhanced by the presence of S in the vapor, after comparing experimental S-free ($D^{vap/melt}$= 1.0 ±0.1) and S-bearing systems ($D^{vap/melt}$= 2.5 ±0.3). A similar partitioning was also unexpectedly observed during the quenching of sulfide melt, by Helmy et al. (2010) who deduced that upon cooling of magma (i.e., ascending magma), As would be incorporated in sulfide melt, and later in hydrothermal fluids. Therefore, the observations of these previous experimental studies and

those inferred from Tainosho's work would explain the preferential partitioning of As in the vapor phase of the early dioritic magma. The vapors later precipitated as As-bearing sulfides disseminated in the contact-metamorphosed quartzite and other sedimentary rocks in contact with the quartz-diorite body.

During crystallization of the magma, residual As in the magma was either incorporated into crystalizing minerals or remained the residual melt. At low S condition (i.e., in the later stage of the dioritic magma), As would remain in the melt rather than in the monosulfide solution (Helmy et al., 2010; Kosyakov and Sinyakova, 2015). Upon the crystallization of major minerals, Ewart and Griffin (1994) showed that As is incorporated in magnetite over other minerals, in several types of melts (basalt to high silica rhyolite). In the case of the Ibaraki complex, the content of magnetite gradually decreased from 4.2wt% in the coarse-grain quartz-diorite to 0.8wt% in the fine-grain porphyritic adamellite (Tainosho, 1971), with a corresponding decrease of an average As concentration from 4.8 ppm in sediments from quartz-diorite regolith to 1.7 ppm in sediments from adamellite. Such synchronous depletions of magnetite and As concentration of whole rock were also explained in the differentiation series of the layered Skaergaard intrusion by Essozv et al. (1965).

In 4.1.2, it was hypothesized that the low As concentrations in stream waters associated with the highest As-contaminated sediments derived from quartzite was due to the high crystallinity of the As-bearing sulfides. The sulfides in quartzite were mostly monoclinic pyrrhotite (Fe_7S_8) (Fe > 46wt%) that is more resistant to oxidation than the hexagonal pyrrhotite. Pyrrhotite dissolution is also impeded by the presence of trace elements (e.g., Ni, Co, Cu) (Janzen et al., 2000), and pyrrhotite dissolves more easily than pyrite (Nicholson and Scharer, 1993), and would release As into water more readily than pyrite. EPMA results showed that the As concentration of pyrrhotite was usually lower than those of pyrite (Table 6). Therefore, an intense dissemination of pyrrhotite would explain the As-enrichment of the whole rock, but comparatively, the low As content of each pyrrhotite grain would explain the low As concentrations of water.

The sulfides in quartzite were deposited via pneumatolytic process, and were strictly related to the intrusion of the dioritic magma. Similar As-bearing ore minerals can be expected in the vicinity of the Mikusayama granitic complex that also crystallized from a dioritic magma. However, the sediments collected in the contact area of the Tamba formation and Mikusayama quartz-gabbro were not significantly enriched with As, of which concentrations were comparable to the average of sediments from accretionary complex (Fig. 4.2 in Section 4.1). As-bearing ore-deposits induced by granitoids intrusion were rare in the study area; the Otani W-Sn ore deposit is the only case of this

type. Although the Otani deposits included arsenopyrite, As in other sulfides was low compared to those from the ore-deposits of the subvolcanic type in this study.

As and trace elements in sulfides of subvolcanic origin

The Tada Mine is classified as a xenothermal vein-deposit, same as the Akenobe and Ikuno Mines in Hyogo Prefecture and the Ashio Mine in Tochigi Prefecture. No As was detected in the bornite/chalcopyrite/galena, which were precipitated at the late stage of the ore mineralization, whereas pyrite (along with chalcopyrite) plausibly containing As was precipitated earlier at higher temperature and sulfur fugacity (Imai et al., 1975). Since the Akenobe and Ikuno xenothermal ore-deposits include arsenopyrite, it is likely this mineral would also occur as a minor phase in the Tada ore-deposits, although Imai et al. (1975) did not report it, and it was not found in the sample analyzed in the present study.

The pyrite of the Kawaura mine was the most As-rich among the studied sulfides. The origin of As in the hydrothermal deposits of the area was barely documented in the previous studies. Arsenopyrite and As-bearing pyrite are common among the ores of the subvolcanic type (Imai et al., 1975), which are found in numbers in the western part of the study area. In the study of Ashida et al. (2001), the As content of Ina River bed sediments was concomitant of Cu, Pb and Zn derived from the subvolcanic ore-deposits of the area. Thus it is likely that the As also originated from these deposits. Similarly, the subvolcanic Kawaura deposit in the vicinity of Minoh River would be a source of the As in bed sediments and the groundwater inflow into the lower reach (Section 4.1) contaminated from the dissolution of these As-bearing sulfides.

Arsenic was not detected in other studied subvolcanic deposits at similar levels observed at the Kawaura mine. At the Fushio, the paragenesis of sulfides was not observed as easily as for that of Kawaura deposit. Sulfides were mainly pyrite in quartz gangue, but the presence of Ag in some of them was indicative of a late stage of the ore mineralization. Thus, the As content lower than that of the Kawaura deposit would be explained by a different stage in the paragenetic sequence. At the Hirao mine, the fingerprint elements of W, Sn and Sb in the sulfides pointed at the Late Cretaceous magmatism and/or country rocks, as explained by Yamaoka (1958), and the As concentration was low in the sulfides from early and later stages. Pyrite disseminated in hornfels nearby the Hirao mine contained Cu, Zn, Pb and Mo, similar to the sulfide minerals from Todoromi, and was altered to magnetite, signifying the impact of a contact-metamorphism by Cretaceous intrusion. The As

detected in these pyrite/magnetite was thus presumed to be originally in the pyrite, as concluded for the As present in the magnetite of Todoromi sandstone. At the Osugahara site, the rhodochrosite in metamorphosed black hornfels contained W/Sn minerals undoubtedly disseminated by the Late Cretaceous felsic intrusion.

The present chapter on the ore-deposits of the Hokusetsu area has emphasized the presence of important levels of As in ore minerals related to the different mineralization episodes of the Hokusetsu area, as well as other trace metals with a hazardous nature (Ni, Co, Pb, Cd, etc.). The dissolution of these minerals caused the As contamination of some river waters. Previous mining-related pollutions have shown that the behavior of trace metals is critical to the spread of contamination, depending on the element-source distribution, the rapid mitigation (usually via adsorption) or the conservation of elemental concentrations in the water column. Therefore, the next chapter focuses on the fate of As, associated trace metals and some others elements upon their release from their source-rock into the water column and along the studied river course, to further complete the As geochemical cycle and that of others related elements in the Hokusetsu rivers.

4.3 DISTRIBUTION AND TRANSPORT OF TRACE METALS IN RIVERS OF THE HOKUSETSU AREA

In this section, the major and minor geochemistry of bed sediments and waters of the Hokusetsu rivers are documented. Geochemical mapping and analysis of fractionation gave insights on the behavior of elements between water and bed sediments, from their source-rock and along the flowing paths.

4.3.1 Results

Major and trace elements in riverbed sediments

The data of the riverbed sediment geochemistry is summarized in Table 7. The location of sampling points and the complete analytical results are given in Annex 3 and 4. The geochemical maps of major (Si, Al, Fe, K, Na, Ca, Mg and Ti) and minor (Mn, Ba, Rb, Sr, Zn, V, Cr, Cu, Co, Ni, Pb and some REYs (La, Ce, Nd and Y)) elements are shown in Fig. 4.17.

The major and trace elements distributed heterogeneously, and the element distribution did not straightforwardly correspond to the surface geology. However, similar to the As distribution described in Section 4.1 (Fig. 4.2), the sediments from the central part of the Ibaraki granitic complex contained element concentrations that highly contrasted with those from surrounding igneous rocks; e.g., sediments from the central part derived from adamellite regolith were depleted in Ca, Mg, Fe and Ti, and enriched in K, compared to those from the quartz-diorite.

The analyzed elements occasionally gave similar distribution patterns; e.g., Rb and K were both very high in the sediments from the central part of the Ibaraki complex but slightly differed in the sedimentary areas. Among the REYs, only Y was concentrated in the sediments from the central part of the Ibaraki complex (except a few samples, for which analytical errors were suspected), while La, Ce and Nd distributions were different from Y; La was slightly concentrated outside the Ibaraki complex, whereas Ce and Nd distributed mostly in the outer part of the Nose pluton (mostly in the quartz-diorite area). Conversely, the Sr distribution was very similar to those of Ca, Mg and Ti. It suggested that these elements were derived from minerals of a same source-rock (likely quartz-diorite) and those minerals had similar stability to the chemical weathering. The distribution of Ba

was concentrated in the adamellite exposing area of the Ibaraki complex, while several samples in the sedimentary Tamba formations were also Ba-rich.

Table 7

Data summary of the geochemistry of riverbed sediments in the study area

Element	Unit	N	Min	Max	Med	Mean
SiO_2	wt%	84	55,95	88,48	70,75	70,83
Al_2O_3	wt%	84	10,08	18,34	14,19	14,10
Tot-Fe_2O_3	wt%	84	1,83	13,27	5,14	5,15
K_2O	wt%	84	1,62	6,83	3,02	3,40
Na_2O	wt%	84	0,68	3,96	1,51	1,57
CaO	wt%	84	0,23	4,77	1,34	1,50
MgO	wt%	84	0,26	3,32	1,36	1,33
TiO_2	wt%	84	0,26	7,56	0,76	1,11
MnO	wt%	84	0,02	0,86	0,14	0,16
As*	ppm	39	n.d.	55,19	7,7	11,06
Ba	ppm	84	28,76	792,83	421,39	420,79
Rb	ppm	84	58,30	340,75	128,93	149,03
Sr	ppm	84	64,21	268,99	129,67	134,89
Zn	ppm	84	8,35	567,57	111,48	128,67
V	ppm	84	n.d.	364,99	114,89	123,48
Cr	ppm	84	5,65	169,78	68,92	68,12
Cu	ppm	84	4,98	263,63	26,40	38,94
Y	ppm	84	15,05	108,64	40,50	46,34
La	ppm	84	n.d.	266,69	28,45	33,27
Ce	ppm	84	4,76	724,10	45,47	61,72
Nd	ppm	84	3,45	49,34	22,75	24,31
Co	ppm	84	2,86	55,79	18,09	23,01
Ni	ppm	84	2,20	96,40	27,51	27,36
Pb	ppm	84	n.d.	299,87	14,38	27,05

*analyzed by ICP-MS after alkali-fusion ; n.d. = not detected

The sediments collected from the Ultra-Tamba Terrane were enriched in V, Cr, Co and Ni compared to those from the Tamba Terrane and igneous rock area. Zn was concentrated more in the western part of the Tamba and Ultra-Tamba Terranes and along Yono River than in the easternmost part of the study area. Similar to the Zn, Cu was also concentrated in the Ultra-Tamba and along the Yono River while depleted in the sediments from the center of Nose granitic rocks.

Pb, Al and Mn had different patterns from the above-mentioned elements and/or the surface geology. Pb distributed fairly homogeneously along the rivers flowing through sedimentary formations and igneous rock bodies, except the sediments on the Yamashita Formation (within the Ultra-Tamba rocks) along the Yono River, in which the high concentrations of Pb were observed.

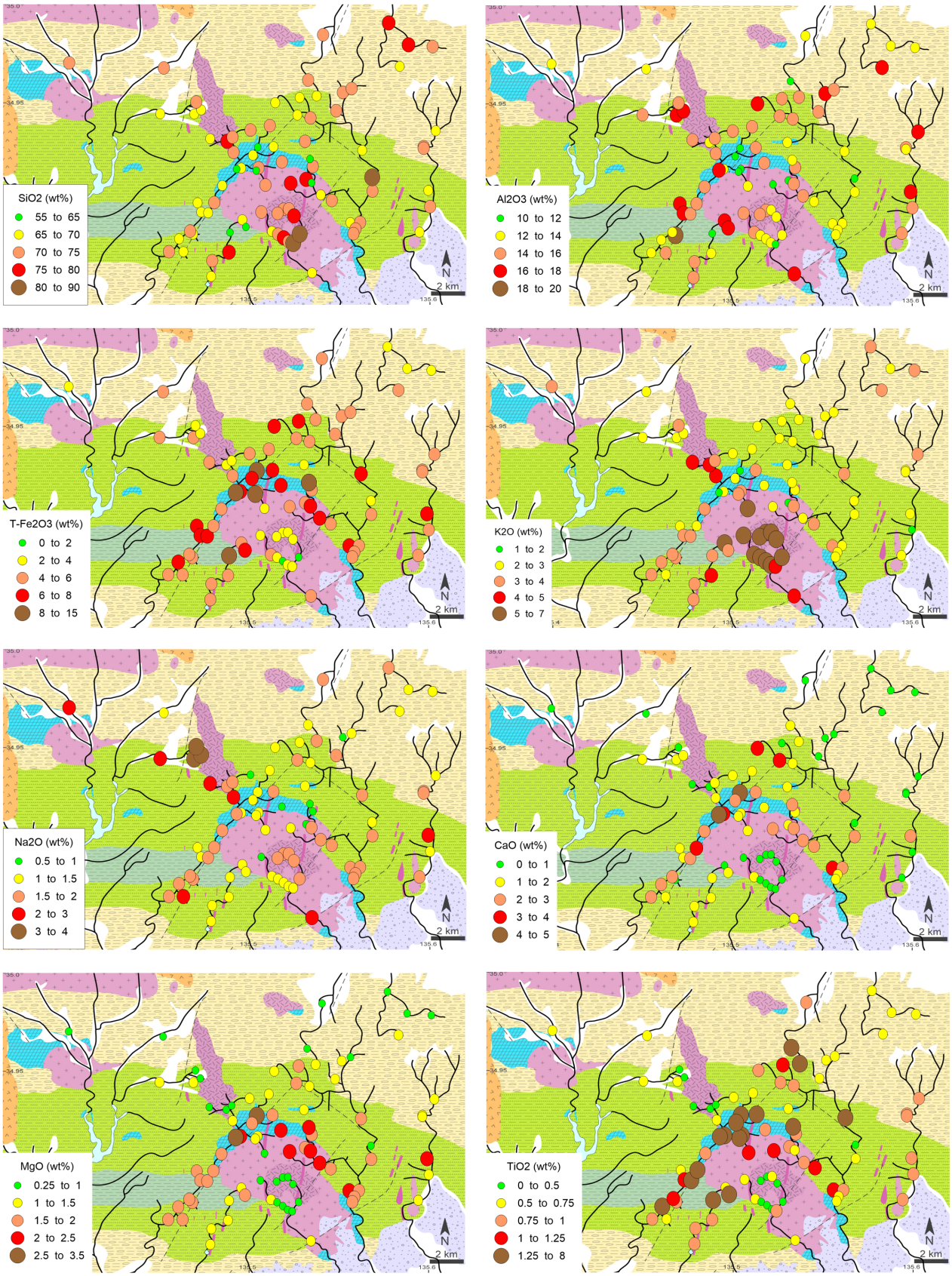

Fig. 4.17 – Distributions of Si, Al, Fe, K, Na, Ca, Mg, Ti, Mn, Ba, Rb, Sr, Zn, V, Cr, Cu, Ce, Y, La, Nd, Co, Ni and Pb in riverbed sediments of the Hokusetsu area.

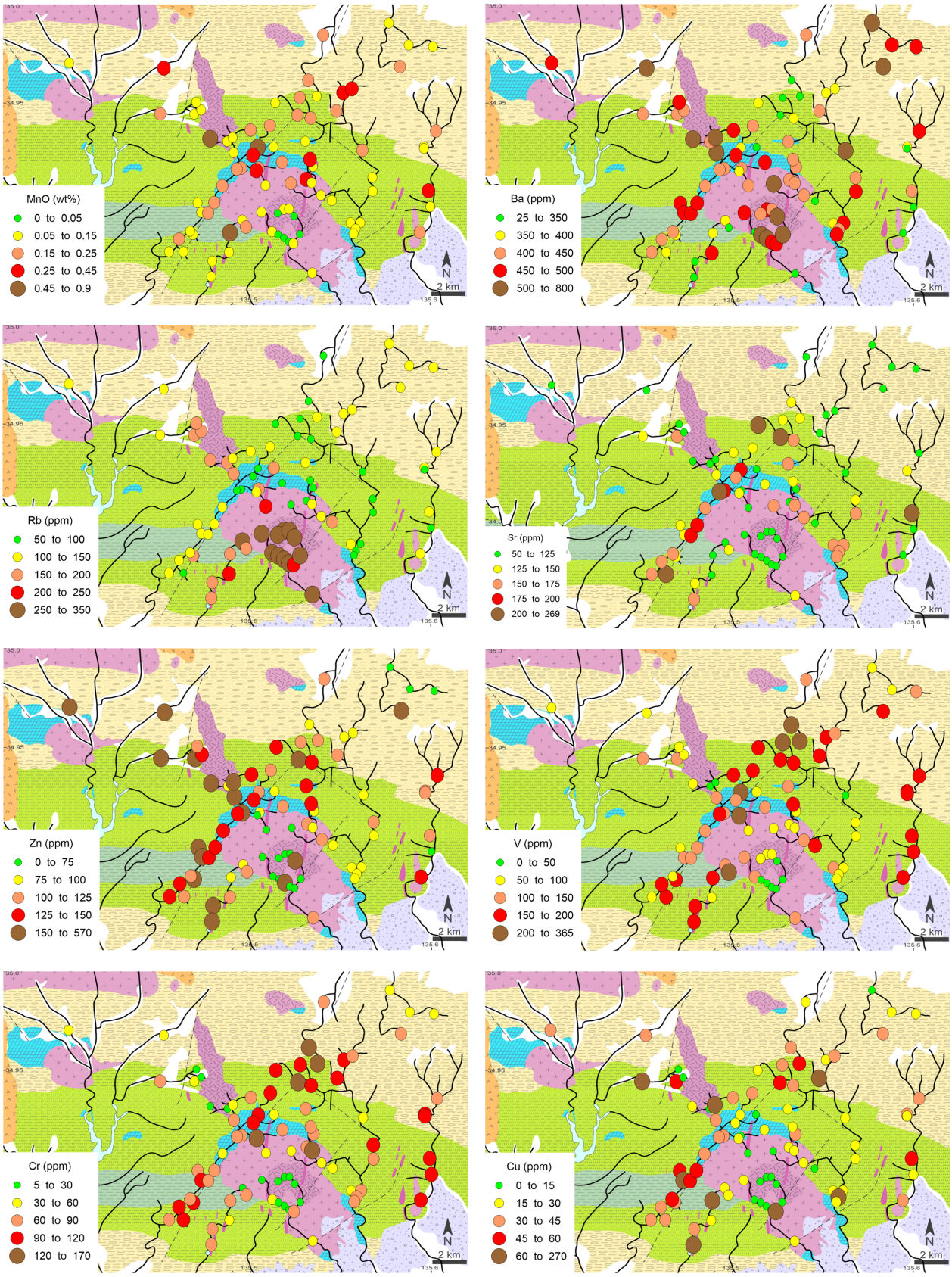

Fig. 4.17 – (continued)

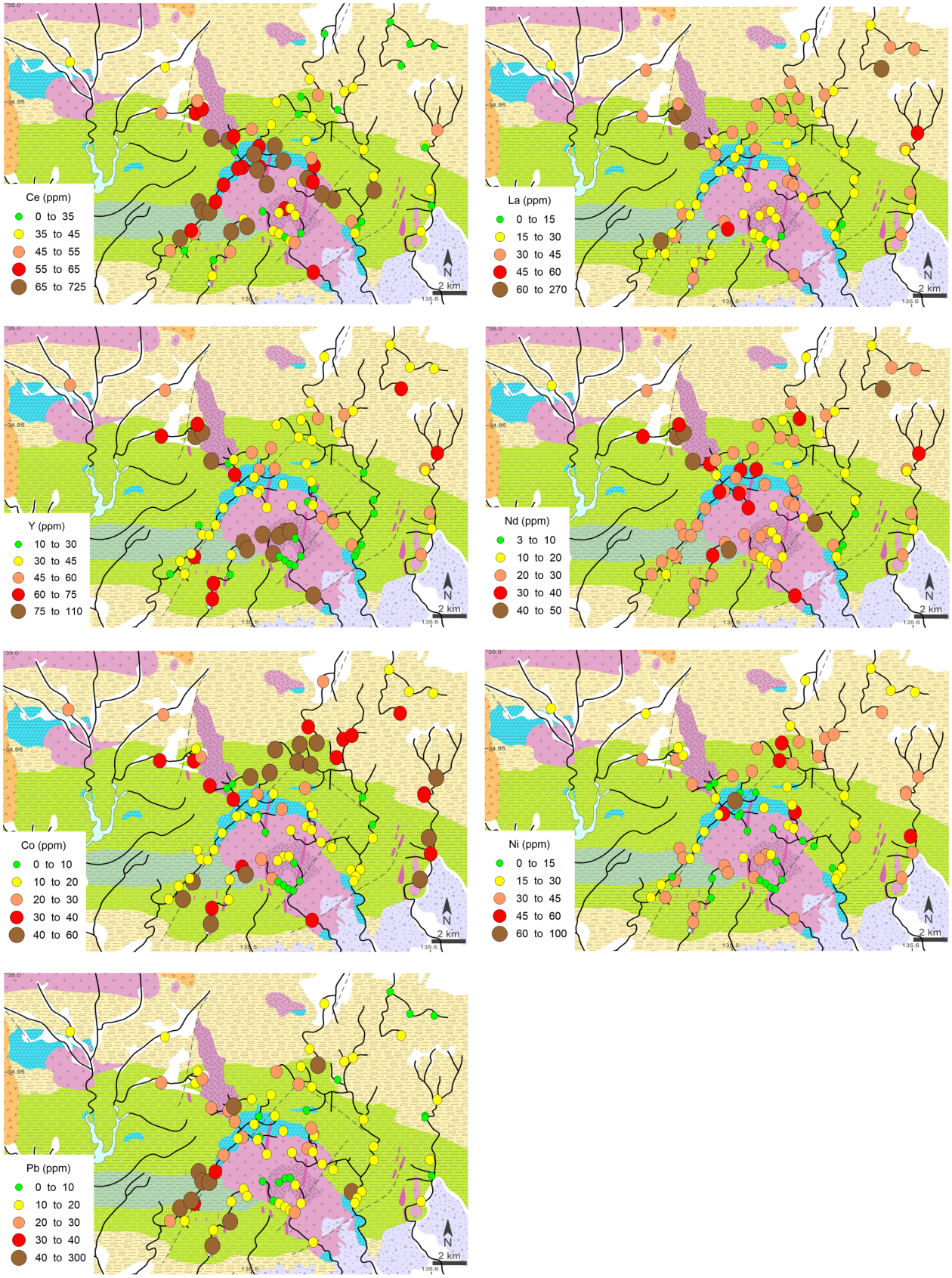

Fig. 4.17 – (continued)

Si, Al and Na concentrations of the sediments did not largely vary throughout the study area and high levels were observed in the sediments from all geology. The distribution pattern of Mn resembled to that of Fe. Mn was also depleted at the Nose pluton granitic center, while highly Mn concentrated sediments were not observed in relation to the geology

The distribution of As in riverbed sediments was explained in Section 4.1 and shown in Fig. 4.2. Because the numbers of As data was smaller than those of elements described here, relationships of As and other elements are occasionally limitedly discussed. Even though, the As clearly showed the similar distribution to those of trace metals, which were depleted in the adamellite exposed area and enriched in Ultra-Tamba formation.

Element association in riverbed sediments

To characterize the relationship of riverbed sediment geochemistry with regoliths on the studied river channels and assess the main source-rock of each element, principal component analysis (PCA) was performed. Because PCA allows reducing the size of data set to common factors (called principal components), it was used to identify similar variations among the distributions of elements having common origins. Two data sets were used to avoid statistical noise caused by the lack of As data; one without As data (n = 84 samples; data set referred as Set_{AsExc}) and one including As (n = 39 samples; data set referred as Set_{AsInc}). Si, Na, and Nd were omitted as their distribution were not linked to any peculiar source-rocks or were redundant with others.

Pearson's moment coefficients - The Pearson's moment coefficients (PMC, r) for the both data sets were computed in the first stage of PCA and tested for p-values. Only values of $r \leq -0.45$ and $r \geq 0.45$ were significant at the $p<0.001$ level. Therefore, the correlations between two elements with $r>\pm0.45$ was only considered here. The Pearson coefficient matrix (CM) for Set_{AsExc} and Set_{AsInc} are shown in Tables 8 and 9, respectively.

Results of the CM confirmed some of similarity of observed distribution patterns observed from the geochemical mapping described above. K and Rb were highly correlated ($r= 0.96$), as they were both sourced from adamellite. Ca, Mg and Fe, as well as Sr, have $r >0.65$ among each other in Set_{AsExc}, denoting positive correlations in their spatial distribution, likely emphasizing the common quartz-dioritic origin. Trace metals V, Cr, Co and Ni had $0.59\leq r \leq 0.83$ in Set_{AsInc} and $0.47\leq r \leq 0.72$ in Set_{AsExc}, denoting similarities in their distributions, especially among the sediments from the

Table 8

Matrix of Pearson's moment correlation coefficients of geochemistry (As excluded) of riverbed sediments

	Mg	Ca	K	Ti	Al	Fe	Mn	V	Cr	Co	Ni	Cu	Zn	Pb	Rb	Sr	Ba	Y	La
Ca	0,79																		
K	-0,59	-0,40																	
Ti	0,42	0,44	-0,24																
Al	0,04	-0,10	0,03	-0,34															
Fe	0,78	0,66	-0,53	0,82	0,00														
Mn	0,26	0,24	-0,29	0,58	-0,04	0,66													
V	0,42	0,22	-0,49	0,42	0,24	0,59	0,34												
Cr	0,50	0,28	-0,69	0,29	0,02	0,50	0,22	0,66											
Co	0,12	-0,12	-0,37	-0,11	0,58	0,20	0,25	0,72	0,47										
Ni	0,16	-0,05	-0,39	-0,13	0,44	0,14	0,15	0,41	0,46	0,68									
Cu	0,14	0,04	-0,16	0,18	0,01	0,21	0,11	0,08	0,18	-0,01	0,07								
Zn	0,02	0,12	-0,03	-0,13	0,28	0,01	0,08	0,00	0,09	0,18	0,17	0,15							
Pb	0,15	0,19	-0,01	0,00	-0,04	0,09	-0,04	-0,07	0,03	-0,16	-0,13	0,17	0,10						
Rb	-0,53	-0,35	0,96	-0,22	0,15	-0,46	-0,32	-0,36	-0,64	-0,27	-0,32	-0,17	-0,04	-0,02					
Sr	0,68	0,79	-0,45	0,19	0,06	0,45	0,10	0,30	0,41	0,15	0,22	0,05	0,19	0,09	-0,39				
Ba	-0,26	-0,14	0,31	-0,20	-0,11	-0,26	0,15	-0,72	-0,48	-0,44	-0,21	0,00	0,13	0,04	0,13	-0,15			
Y	-0,20	-0,12	0,31	-0,11	0,53	-0,04	0,13	0,23	-0,26	0,41	0,26	-0,18	-0,05	-0,13	0,45	-0,15	-0,14		
La	-0,02	0,03	-0,07	0,11	0,17	0,15	0,21	0,20	0,14	0,15	0,10	-0,06	0,08	0,06	-0,03	0,01	-0,01	0,20	
Ce	0,20	0,24	-0,09	0,02	-0,03	0,10	0,00	-0,06	-0,04	-0,16	-0,10	-0,04	-0,04	0,00	-0,08	0,14	0,02	-0,06	0,01

	r ≥0.45
	r ≤-0.45

Table 9

Matrix of Pearson's moment correlation coefficients of geochemistry (As included) of riverbed sediments

	Mg	Ca	K	Ti	Al	Fe	Mn	**As**	V	Cr	Co	Ni	Cu	Zn	Pb	Rb	Sr	Ba	Y	La
Ca	0,59																			
K	-0,59	-0,26																		
Ti	0,65	0,46	-0,38																	
Al	0,40	0,22	0,01	0,13																
Fe	0,85	0,59	-0,55	0,67	0,57															
Mn	0,02	0,08	-0,15	0,00	0,19	0,40														
As	**0,40**	**0,09**	**-0,38**	**0,08**	**0,12**	**0,36**	**0,03**													
V	0,73	0,35	-0,53	0,72	0,52	0,79	0,02	**0,29**												
Cr	0,67	0,33	-0,82	0,37	0,20	0,57	-0,02	**0,43**	0,61											
Co	0,71	0,34	-0,55	0,37	0,68	0,86	0,34	**0,43**	0,83	0,65										
Ni	0,78	0,49	-0,46	0,32	0,64	0,79	0,29	**0,32**	0,59	0,59	0,78									
Cu	0,21	0,13	-0,29	0,26	0,02	0,25	0,06	**0,12**	0,09	0,37	0,15	0,12								
Zn	0,36	0,57	-0,34	0,12	0,26	0,46	0,32	**0,20**	0,26	0,49	0,42	0,47	0,33							
Pb	0,21	0,44	-0,14	0,16	0,28	0,34	0,27	**0,19**	0,08	0,22	0,21	0,24	0,52	0,65						
Rb	-0,47	-0,15	0,96	-0,25	0,08	-0,45	-0,24	**-0,38**	-0,38	-0,76	-0,45	-0,36	-0,28	-0,32	-0,16					
Sr	0,64	0,80	-0,39	0,29	0,23	0,51	0,04	**0,20**	0,35	0,46	0,43	0,53	0,09	0,42	0,34	-0,31				
Ba	-0,51	-0,26	0,32	-0,64	-0,20	-0,39	0,42	**-0,05**	-0,75	-0,46	-0,42	-0,27	-0,08	-0,03	0,10	0,09	-0,23			
Y	-0,21	0,00	0,70	-0,12	0,43	-0,02	0,13	**-0,27**	-0,04	-0,58	0,00	0,10	-0,31	-0,06	-0,05	0,77	-0,18	0,05		
La	-0,01	-0,02	-0,02	0,01	0,55	0,33	0,60	**0,09**	0,15	-0,05	0,36	0,33	0,04	0,23	0,26	-0,07	-0,07	0,29	0,35	
Ce	0,09	0,30	0,23	0,41	0,21	0,31	0,42	**-0,06**	0,12	-0,28	0,06	0,11	0,10	0,09	0,26	0,28	0,06	-0,04	0,44	0,28

r ≥0.45
r ≤-0.45

Ultra-Tamba sedimentary formation area. Y had a higher positive r score with K and Rb in Set_{AsInc} than in Set_{AsExc}, and was completely unrelated to La and Ce.

The CM of both datasets also pointed at new features, but still in accordance with previous descriptions made from the observation of element mapping. Fe was remarkably correlated with Ti and Mn in Set_{AsExc} (r= 0.82 and 0.66 respectively). Fe, Mn and Ti are the main elements that constitute the suspended mineral particles of the river water column and may settle at river bottom, possibly causing a simultaneous enrichment in the sediments. Al, working as a ligand in the forms of hydroxides and/or clay particles in suspended particles, was related to La, Fe, V, Co and Ni in Set_{AsInc}. V, Cr, Co and Ni were negatively correlated with K, Rb and Ba in the both datasets, and positively correlated with Mg and Fe ($r>0.67$ and $r>0.57$, respectively) in Set_{AsInc}. These two facts would denote the depletion of trace metals of the adamellite and a common origin from quartz-diorite, respectively. Pb positively correlated with Zn (r=0.65) in Set_{AsInc}, but not in Set_{AsExc} (r=0.10) that covers more variable geologies.

The distribution of As did not correlate to any other element distributions, i.e., $r <0.45$ for all pairs with the analyzed elements. The highest coefficients were observed with Co and Cr (r=0.43). From the previous observations of the As-depletion in adamellite (Fig. 4.2), it is natural that As was negatively correlated to K and Rb. However, these pairs had weak negative correlations (r=-0.38). The small coefficients of As with the other elements were consistent with the hypothesis of Section 4.1; the As was related to the occurrence of pyritic ores (in which Co is also common), rather than a specific lithology, unlike most of the studied elements.

Principal Components Analysis - The principal components represent factors (or axis) that care the maximum variation of all elemental distributions. Because the studied elements had distributions that varied greatly from one another, it required up to 7 and 5 factors (i.e., PC), on Set_{AsExc} and Set_{AsInc} respectively, to explain at least 80% of the patterns variance; e. g., PC1 explained only 29% of variance of Set_{AsExc} and only 38% of Set_{AsInc}. Such variances suggest the weak correlations, since multivariate analysis would commonly result with 3 to 4 common factors to explain 90% of the variance. However, the groups of elements observed with the PCA underlined some of the observations previously made. Loadings (or scores) of the studied elements on the seven first PCs are shown in Table 10 and 11 for Set_{AsExc} and Set_{AsInc}, respectively. Fig.4.18 and 4.19 represent the plots of loadings on PC1 and PC2 of the studied elements.

Table 10

Matrix of P.C. loadings for studied elements (As excluded) of riverbed sediments

P.C.	1	2	3	4	5	6	7
Mg	0,80	0,28	0,01	0,27	0,20	-0,01	-0,10
Ca	0,64	0,45	-0,11	0,47	0,24	0,02	-0,05
K	-0,81	-0,04	-0,38	0,18	0,08	-0,19	-0,10
Ti	0,55	0,39	-0,60	-0,26	-0,08	-0,10	-0,10
Al	0,07	-0,72	-0,01	0,49	-0,02	-0,03	-0,07
Fe	0,85	0,21	-0,42	0,04	-0,07	-0,03	-0,09
Mn	0,49	0,04	-0,53	-0,07	-0,51	0,27	-0,10
V	0,75	-0,44	-0,20	-0,22	0,17	-0,18	0,03
Cr	0,79	-0,14	0,27	-0,25	-0,02	-0,10	0,14
Co	0,47	-0,82	0,06	-0,04	-0,04	0,04	-0,05
Ni	0,42	-0,63	0,26	0,05	-0,16	0,16	-0,10
Cu	0,21	0,12	0,11	-0,02	-0,45	-0,51	-0,27
Zn	0,10	-0,15	0,22	0,52	-0,45	-0,13	-0,08
Pb	0,06	0,25	0,07	0,31	-0,12	-0,58	0,42
Rb	-0,74	-0,16	-0,44	0,22	0,20	-0,25	-0,10
Sr	0,64	0,18	0,17	0,48	0,22	0,05	-0,09
Ba	-0,45	0,34	0,01	0,29	-0,57	0,38	-0,06
Y	-0,13	-0,65	-0,54	0,24	0,14	0,04	-0,07
La	0,16	-0,22	-0,31	0,11	-0,24	0,09	0,76
Ce	0,09	0,25	0,00	0,28	0,30	0,39	0,15
Eigen value	5,82	3,10	1,83	1,63	1,44	1,18	0,98
Variance %	29	15	9	8	7	6	5
Cum. Var. %	29	45	54	62	69	75	80

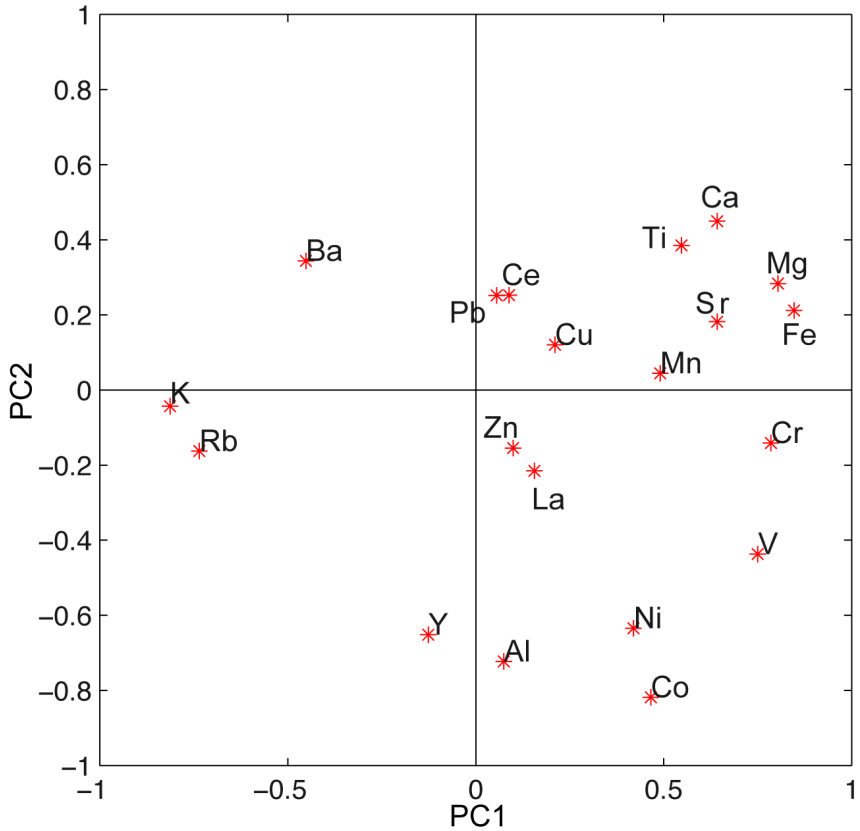

Fig. 4.18 – Biplot of the loadings on PC1 and PC2 of studied elements, As excluded.

Table 11

Matrix of P.C. loadings for studied elements (As included) of riverbed sediments

P.C.	1	2	3	4	5	6	7
Mg	-0,89	-0,05	-0,24	0,05	0,09	0,09	0,12
Ca	-0,62	0,19	-0,07	0,60	0,26	0,26	-0,02
K	0,74	0,53	-0,21	0,17	0,13	-0,15	0,11
Ti	-0,62	0,02	-0,44	0,24	-0,52	0,11	0,02
Al	-0,49	0,62	-0,11	-0,30	0,23	-0,32	-0,10
Fe	-0,92	0,26	-0,06	-0,06	-0,12	0,11	0,04
Mn	-0,24	0,48	0,59	-0,19	-0,27	0,39	-0,08
As	-0,44	-0,17	0,19	-0,22	0,11	-0,13	0,80
V	-0,81	0,05	-0,43	-0,22	-0,16	-0,07	-0,05
Cr	-0,81	-0,45	0,08	-0,09	0,08	-0,15	-0,09
Co	-0,86	0,19	-0,05	-0,37	0,07	-0,08	-0,01
Ni	-0,81	0,26	0,00	-0,18	0,26	0,03	-0,04
Cu	-0,34	-0,13	0,33	0,36	-0,40	-0,54	-0,04
Zn	-0,58	0,16	0,43	0,33	0,21	-0,16	-0,17
Pb	-0,40	0,26	0,49	0,50	-0,02	-0,35	0,05
Rb	0,63	0,56	-0,39	0,20	0,14	-0,19	0,09
Sr	-0,64	-0,02	-0,03	0,40	0,45	0,28	0,01
Ba	0,48	0,18	0,74	-0,05	0,14	0,21	0,11
Y	0,25	0,86	-0,29	-0,06	0,14	-0,08	-0,01
La	-0,21	0,62	0,40	-0,41	-0,15	-0,03	-0,09
Ce	-0,12	0,66	-0,08	0,32	-0,47	0,22	0,23
Eigen value	7,89	3,34	2,39	1,81	1,34	1,09	0,81
Variance %	38	16	11	9	6	5	4
Cum. Var. %	38	53	65	74	80	85	89

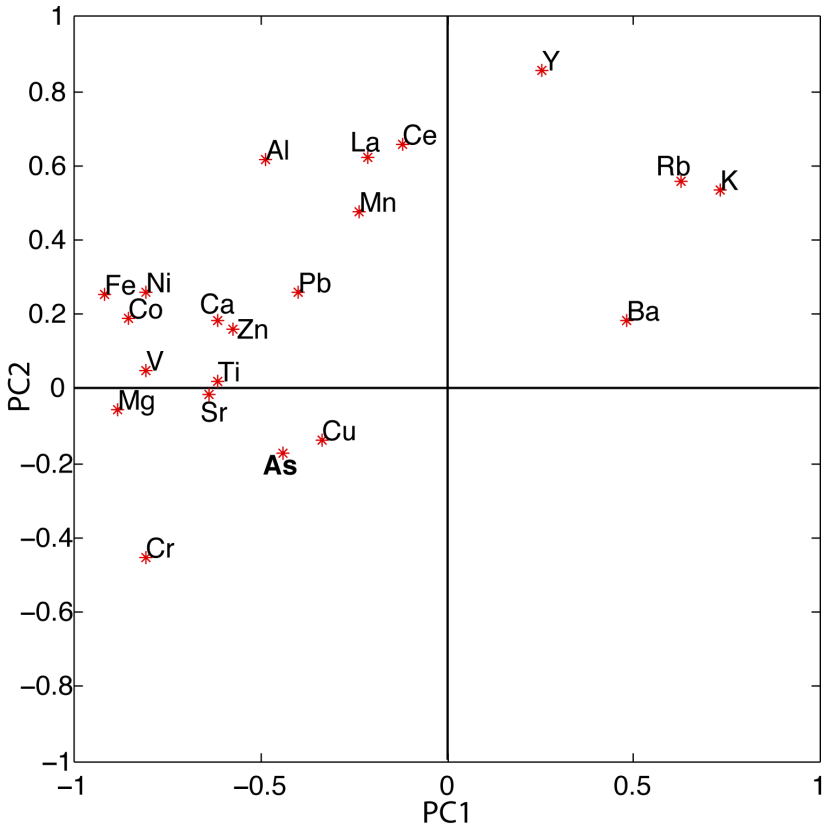

Fig. 4.19 - Biplot of the loadings on PC1 and PC2 of studied elements, As included (bold).

Overall, the results discriminated the sources of trace transition metals; i. e., depleted in felsic granitic rocks compared with the mafic quartz-diorite and the sedimentary rocks, both of which seemed enriched in those. Most of the loadings of Fe/Mg and K/Rb on the two groups documented the prominent influence of chemical composition of differentiated granitic rocks on the elements.

The CM of both datasets also pointed at new features, but still in accordance with previous descriptions made from the observation of element mapping. Fe was remarkably correlated with Ti and Mn in Set_{AsExc} (r= 0.82 and 0.66 respectively). Fe, Mn and Ti are the main elements that constitute the (Fig. 4.19). Thus, the quartz-diorite was more concentrated sources of these elements than the Ultra-Tamba formation.

Y and La were distinct from each other on Set_{AsExc} as they loaded on different PCs (2 and 7, respectively), while in PC2 of Set_{AsInc}, REYs were accompanied with Al, likely because of common variance in concentrations outside the Ibaraki complex. Ba scored distinctively on both sets but always with Mn (PC5 and PC3 on Set_{AsExc} and Set_{AsInc}, respectively). Because of large variations in the distributions, Zn, Cu and Pb were generally under-represented (loading were <0.58). The Zn had its higher loading on PCs different from the Cu and Pb, because of a lack of common source, while the Cu and Pb loaded equally on PC6 of Set_{AsExc} (although the score were poor).

Arsenic did not seem to correlate with any elements. Most importantly, high As load was represented on PC7, showing the singularity of its distribution not related to any particular geology. Even though, the As was plotted close to the Cu in Fig.4.19, suggesting its origin related to ore mineralization.

Major and trace elements in river waters

The total (unfiltered) concentrations of studied element of river waters are summarized in Table 12 and mapped in Fig.4.20.

Concentrations of major elements (Na, Ca, Mg, K) and Sr progressively increased along the flow, irrelatively to host-rock type. This was especially prominent on Ibaraki River. These elements are highly dissociated in aqueous conditions, and their adsorption onto suspended matter and precipitation in riverbed bottom were minimal. Their increasing concentrations would be attributed to the residential time of subsurface water toward downstream before flowing out as baseflow, since the dissolved salt concentrations increased with prolonging the time of water-rock interaction.

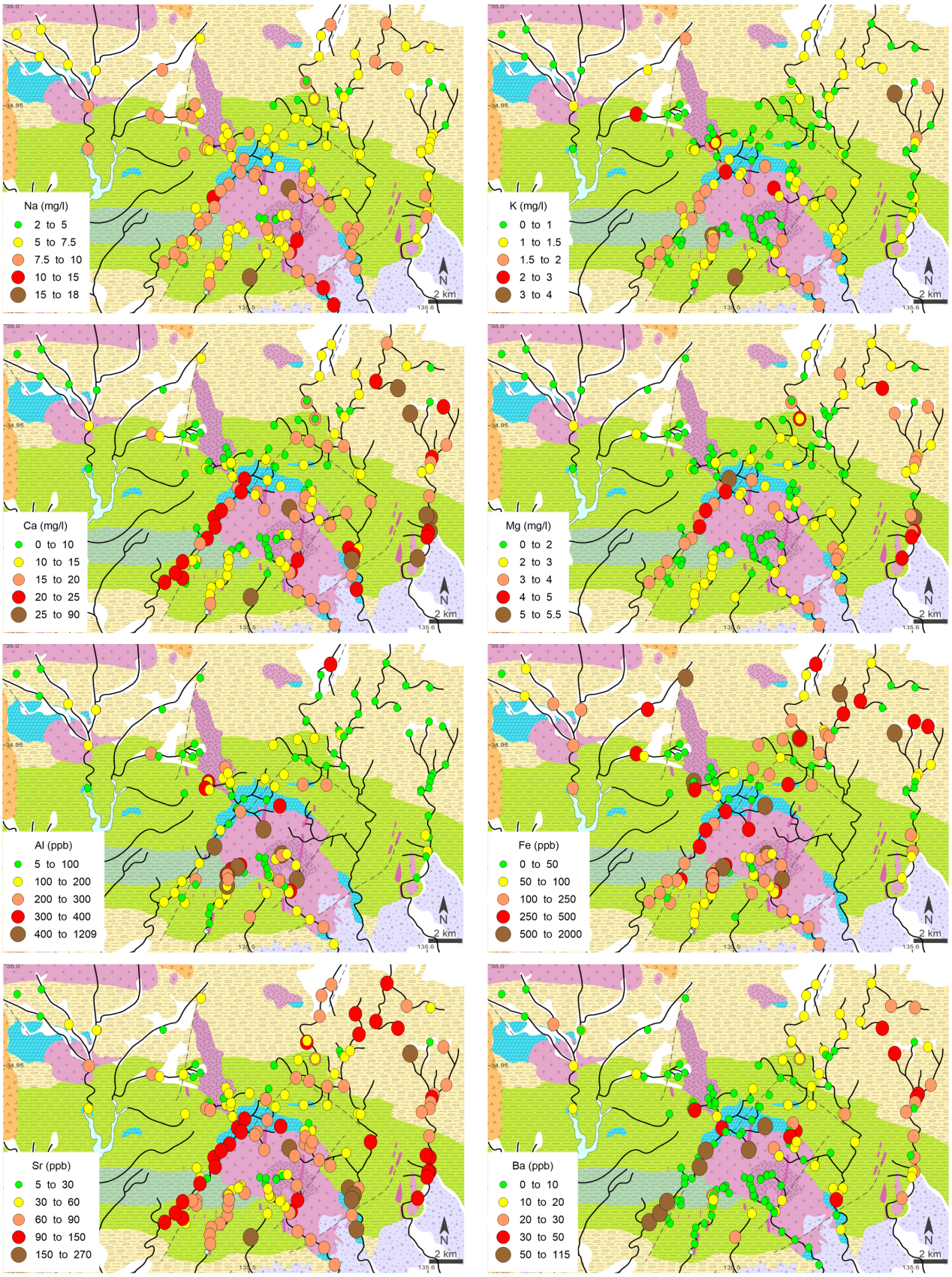

Fig. 4.20 – Distributions of K, Na, Ca, Mg, Al, Fe, Sr, Ba, Mn, Ti, Cu, V, Rb, Ni, Cr, Pb, Co, Cd, Ce, La, Y and Nd in river waters in the Hokusetsu area.

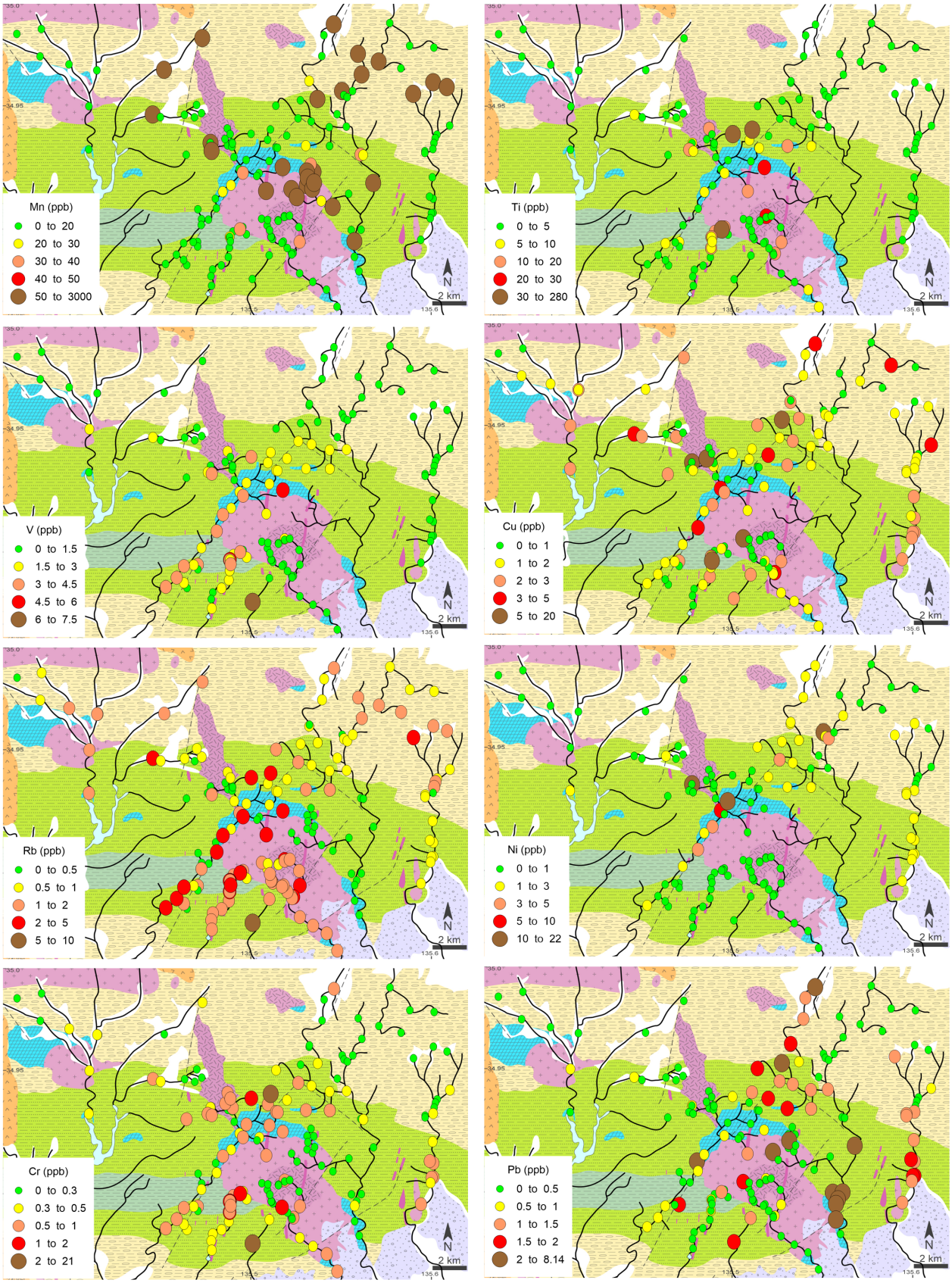

Fig. 4.20 – (continued).

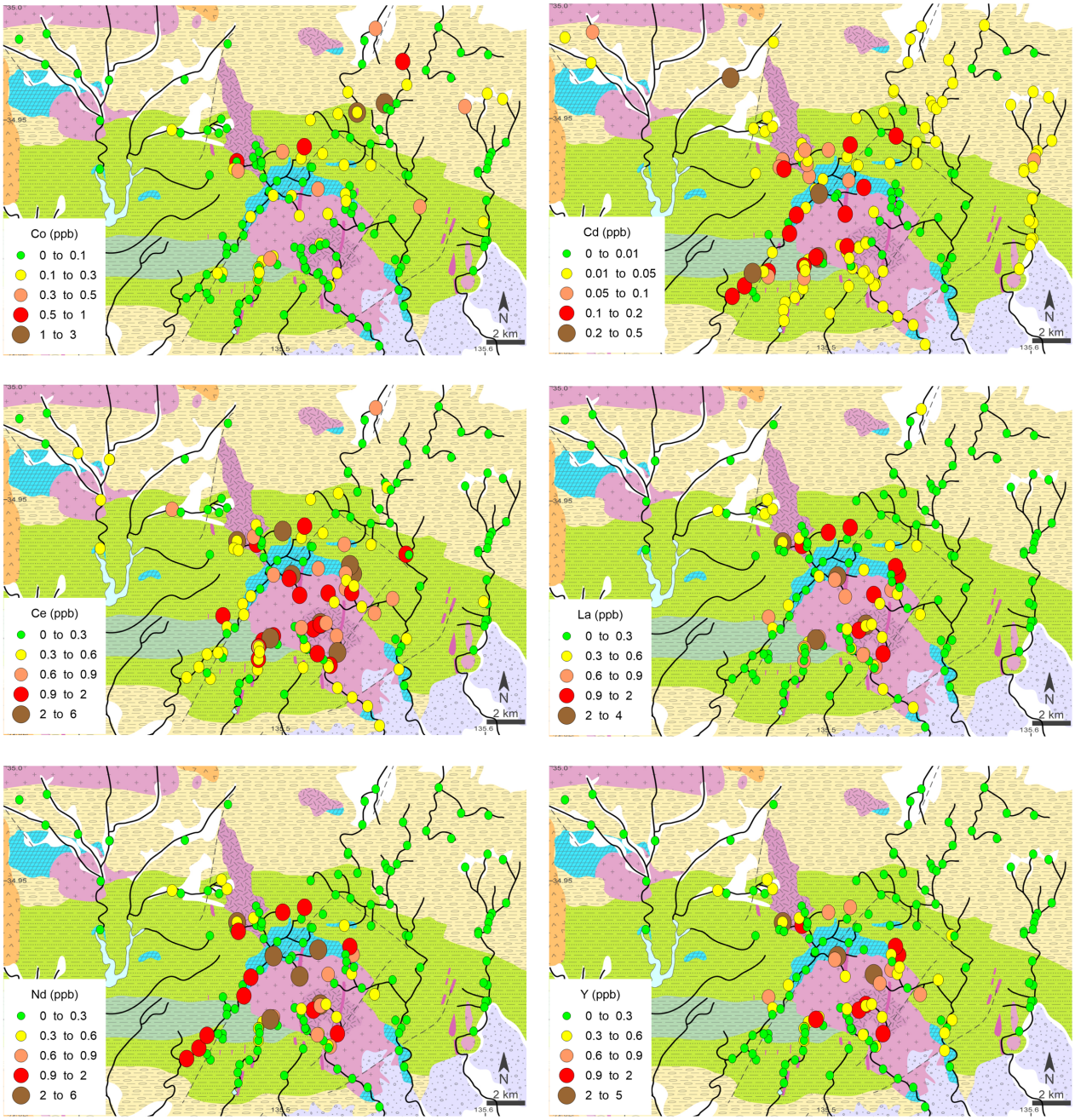

Fig. 4.20 – (continued)

On the other hand, concentrations of Fe, Ti, Mn and Ba were very low in most of the analyzed river waters even these were high in the contact sediments. Concentrations of Mn, Ti, and Fe and Ba were remarkably high in the uppermost reaches, and immediately lowered downstream. This phenomenon was also observed for Co concentrations. The Al was low in the Tamba Terrane, and comparably high in the Ultra-Tamba Terrane and within granitic areas. Distributions of the

studied REYs barely spread outside of areas of the igneous rocks bodies (with a few exceptions for Nd likely from contamination during sampling), indicating the impact of lithology on these components and their rapid depletion in river waters

Cu and Pb concentrations, which did not relate with each other, highly scattered in the studied rivers and did not seem to be affected by the surface geology or the river hydraulics (such as distance from spring area, flow rate, etc.). V and Cd were concentrated in the Yono River waters around the quartz-diorite and granodiorite, and Cd was also concentrated in the sedimentary areas. The Cd distribution was different from that of other heavy metals, as the high concentration waters were spreading along the Yono River without being attenuated. Ni was low throughout the study area, with a few exceptions on the Yono river reach flowing through the quartz-diorite and one location on the Ai River. Apart from the source-rock, adsorption onto the suspended particles and/or dilution or mixing of multiple-sourced waters would constrain the elemental distributions; these aspects will be examined in relation to elemental partitioning further below.

Table 12

Data summary of the total (unfiltered) element concentrations of river waters in the study area

Element	Unit	n	Min	Max	Median	Mean
K	ppm	174	0,34	3,90	0,98	1,10
Na	ppm	175	2,06	17,89	6,95	7,06
Ca	ppm	175	0,30	87,73	12,09	13,37
Mg	ppm	175	0,24	5,41	1,98	2,07
Al	ppb	142	5,60	1208,59	92,06	143,98
As	ppb	173	0,00	**38,33**	0,79	2,27
Ba	ppb	173	n.d.	112,89	9,00	14,41
Cd	ppb	164	n.d.	0,43	0,02	0,04
Ce	ppb	173	0,02	5,27	0,31	0,52
Co	ppb	173	0,01	2,80	0,06	0,11
Cr	ppb	173	n.d.	20,03	0,31	0,52
Cu	ppb	145	n.d.	17,10	1,42	1,73
Fe	ppb	145	2,70	1952,54	82,21	174,46
La	ppb	173	0,01	3,63	0,20	0,35
Mn	ppb	173	0,10	2864,38	6,46	62,31
Nd	ppb	174	n.d.	5,73	0,17	0,36
Ni	ppb	145	0,03	**21,32**	0,41	1,27
Pb	ppb	173	n.d.	8,14	0,24	0,70
Rb	ppb	173	n.d.	7,59	0,88	1,03
Sr	ppb	173	5,44	263,67	61,02	69,36
Ti	ppb	145	0,17	279,38	2,32	11,21
V	ppb	145	0,08	7,32	0,96	1,33
Y	ppb	173	0,01	4,85	0,19	0,32

Bold numbers indicate concentration above the Japan Drinking Water Quality Standard

Based on the Japan Drinking Water Quality Standards that set the MCL (see Section 1.1), concentrations of the hazardous trace metals Cr, Ni, and Pb in the studied rivers did not exceed the standard values ($MCL_{Ni\&Pb}$ =10 ppb, MCL_{Cr} = 50 ppb), except for 3 samples where Ni was >10 to 25 ppb. No MCL is set for Co, but its concentration remained very low at <3 ppb. Cd concentrations were extremely low (few tens of ppt) and rarely exceeded 0.1 ppb (MCL_{Cd} = 10 ppb).

To summarize the distribution of concentrations of river waters, the elements were qualitatively plotted in Fig. 4.21, according to two criteria: 1) host-rocks of the basement flow, i.e., river flowing through sedimentary or igneous formations, and 2) solubility in surface water conditions, i.e., high concentrations kept along the river course or constrained only at the upper reaches. The first geological criterion potentially pointed at the source rocks of the elements, while the second criterion reflected the conservation or attenuation of element concentrations along with the flow.

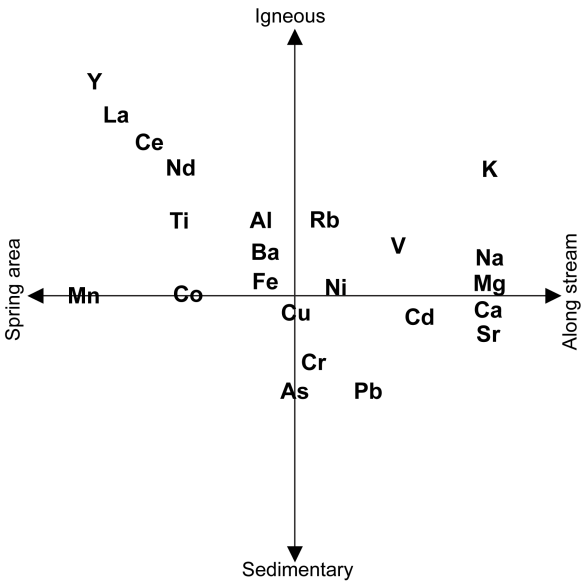

Fig. 4.21 – Qualitative Repartition of elements in river waters according to their distribution in igneous or sedimentary formations, and their high concentrations being restrained to spring area or along the river courses

.

The most immobile elements were the REYs, of which the highest concentrations were specifically restrained to the igneous formations and appeared in only in the upper reaches of rivers, but with noticeable exceptions for Nd in the lower reaches of the Yono River. The attenuation criterion was the largest for Mn with high concentrations at spring areas that strikingly decreased downstream. Opposite to these elements, Na, Ca, Mg and Sr were ubiquitously dissolved in waters

flowing through areas of either sedimentary or igneous rock, and high concentrations were not constrained to the upper reaches of rivers, as noted above.

Although the high concentrations of the trace transition metal concentrations were mostly observed in the rivers flowing through the granitoids and within the Ultra-Tamba sedimentary rocks, those concentrations along the stream were diverse; e.g., Co concentrated only in the upper reaches of studied rivers whereas Cu concentrations did not change along Yono River, or slightly increased toward downstream along Rivers Hitokuraoroji, Ibaraki and Akuta. Cd was high in concentrations only both in spring areas and in lower reaches of rivers.

As previously explained in Section 4.1.2 (Fig. 4.2), the high concentrations of As appeared mostly in the rivers flowing through sedimentary formations around the Nose pluton. These high concentrations were usually found in spring areas and were rapidly mitigated by dilution with As-free baseflow, as the river discharge increased.

Partitioning of arsenic, trace elements and organic matter in river water

Arsenic – The concentrations of Fe, Al, Mn, and As were compared in filtered and unfiltered river waters to assess the partitioning of these elements in between the particulate and dissolved phases by mean of dissolved transport index (DTI) that indicates the percentage of an element in the dissolved phase.

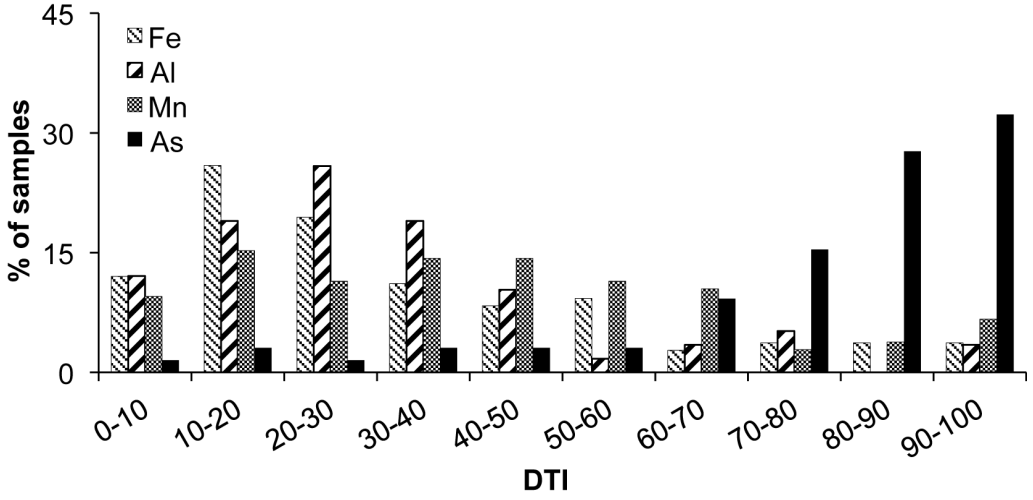

Fig. 4.22 - Distribution of Dissolved Transport Index (DTI) for Fe, Al, Mn and As. Most of DTI_{As} range between 70 and 100, while DTI_{Fe}, DTI_{Al} and DTI_{Mn} range mostly below 40. Fe n=107; Al n=56; Mn n=104; As n=66. DTI = Dissolved (< 0.45 μm) conc. / Total conc. x 100.

Fig. 4.22 represents the distribution of the DTI for Fe, Al, Mn, and As. It shows the DTI_{As} was >70 for 75% of the samples, meaning that at least 70% of As was in the dissolved fraction in three quarters (i.e., 75%) of the studied river waters, rather than adsorbed onto >0.45μm particles. The percentages of river water samples with a DTI ≥ 70 were only 11, 9, and 13% for Fe, Al, and Mn, respectively. Most of the DTIs for these elements were <40, and their respective median DTI reckoned at 24, 25 and 40. Therefore, As existed primarily as a dissolved species in water, whereas most of the Fe, Mn, and Al were present within the >0.45μm particulate fraction, likely as clay particles, amorphous oxides, colloids, and/or adsorbed onto those phases.

The sorption of As onto Fe oxyhydroxides/oxides particles can be argued from the plot of DTI_{Fe} and DTI_{As} in Fig. 4.23. No clear correlation was observable, except for the low values of DTI (<25 and <50 for Fe and As, respectively) from water samples with very low concentrations of As (<1ppb) collected from the upper reaches of the Ibaraki and Yono Rivers in As-depleted granite. These results suggest that the adsorption of As onto the Fe-oxyhydroxides/oxides was maximal when the concentration was lower than the background level. At concentrations higher than 3ppb, the adsorption was least, and As thus remained in the dissolved fraction of the water column along the streams.

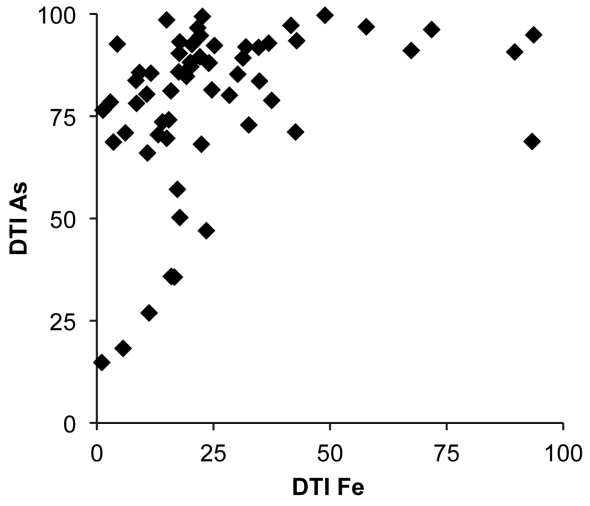

Fig. 4.23 - Biplot of DTI_{Fe} and DTI_{As}. Most of DTI_{As} plot between 70 and 100, meaning that As is mainly present as a dissolved phase in water. For DTI_{As} < 50, DTI_{Fe} and DTI_{As} behave together, showing that for low As concentrations (<1 ppb, samples from Ibaraki River), most of the element is absorbed on Fe particles.

Trace elements other than As– Table 13 shows the average DTI of analyzed elements classified into quartile bins. The average DTIs were calculated from the concentrations of waters of Yono, Minoh and Ibaraki rivers sampled twice, in March (Yono) and May (Minoh, Ibaraki), and in July (all three rivers) (complete analytical results in Annex 2). Duration calculation, values of DTI>100 were excluded since those represented a dissolved concentration exceeding the total concentration, likely due to analytical error.

Table 13
Average DTI of elements in river waters

DTI≤25		25<DTI≤50		50<DTI≤75		75<DTI≤100	
Elem.	Average	Elem.	Average	Elem.	Average	Elem.	Average
Ti	25	Ce	28	Cr	51	V	76
Fe	25	Al	31	Cu	56	**As**	76
		Pb	31	Ni	63	Cd	76
		Nd	38	Ba	74	Rb	77
		La	39			Sr	92
		Mn	41				
		Co	41				
		Y	46				

The DTIs were consistent with the previous observations based on the element mapping and evolution of concentrations in the rivers, e.g., when it was observed that element concentrations were decreasing along the flow, the average DTI of that element was correspondingly low. This was prominent for Mn, Ti, Fe, Co and REYs. In those cases, the low DTI meant that most of the elements were comprised within the particulate fraction that was retained on the 0.45-µm filter during sampling filtration. Consequently, the particulate matter would settle on the river bottom, removing these elements from the water column and causing the decrease of their concentrations.

Overall, the elements sorted similarly to the DTI classification of Martin and Meybeck (1979) (Fig.4.24), e.g., As, Ni, Cu had higher DTI than Fe, Al, Mn and Ti, and REYs were in the low ranges. However, DTI values of the present study were generally higher than those in the list of Martin and Meybeck (1979).

Table IIB. Dissolved transport index (DTI), calculated as the percentage dissolved transport divided by total transport

DTI (%)	Characteristic
90–50: Br, I, Sa, Cl, Ca, Na, Sr	High solubility
50–10: Li, N, Sb, As, Mg, B, Mo, F, Cu, Zn, Ba, K	↓
10–1: P, Ni, Si, Rb, U, Co, Mn, Th, Pb, V, Cs	
<1: Ga, Tm, Lu, Gd, Ti, Er, Nd, Ho, La, Sm, Tb, Yb, Fe, Eu, Ce, Pr, Al	Low solubility

Fig. 4.24 – DTI classification of Martin in Meybeck (1979). From Foster and Charlesworth (1996)

As previously noted, Fe, Mn and Al are the main constituents of suspended matter in the water column, and consequently they had low DTI. Ti had the lowest average DTI, which would be classified in the element working as an adsorbent, similar to Fe, Mn and Al. Indeed, titanium dioxide (mainly as rutile in natural conditions) is very stable in the hydrosphere and can be a highly reactive catalyst used for As remediation of water (Dutta et al., 2004).

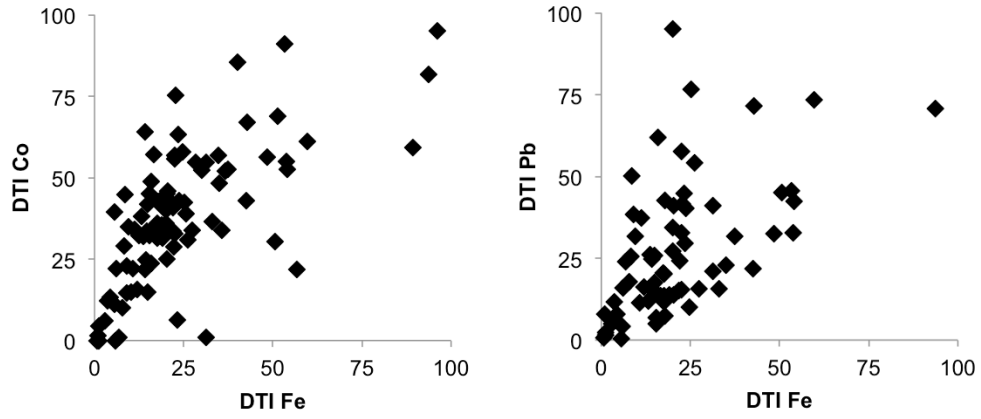

Fig. 4.25 - Biplot of DTI of Fe/Co and Fe/Pb. The correlated plot of DIT Co and Pb with DTI of Fe tended to highlight the non-conservative behavior of these elements, likely in a metal-Fe-bearing phase condition.

The DTIs of studied trace metals were consistent with the binding strength sequence on iron oxides Pb > Cu > Cd > Ni, established by Tessier et al. (1985). The low DTIs of Pb and Co were indicative of the occurrence of these elements mainly in the particulate phase, especially with Fe-oxyhydroxides/oxides as suggested by the positive correlations of DTIs shown in Fig.4.25. Ni, Cu and Cd had higher DTIs, indicating little binding onto >0.45μm-particles, and were considered to

behave as dissolved components. DTI of Sr was also high throughout the sample sets, which corroborated the dissociative character of Sr, which remains as a dissolved phase in the river waters.

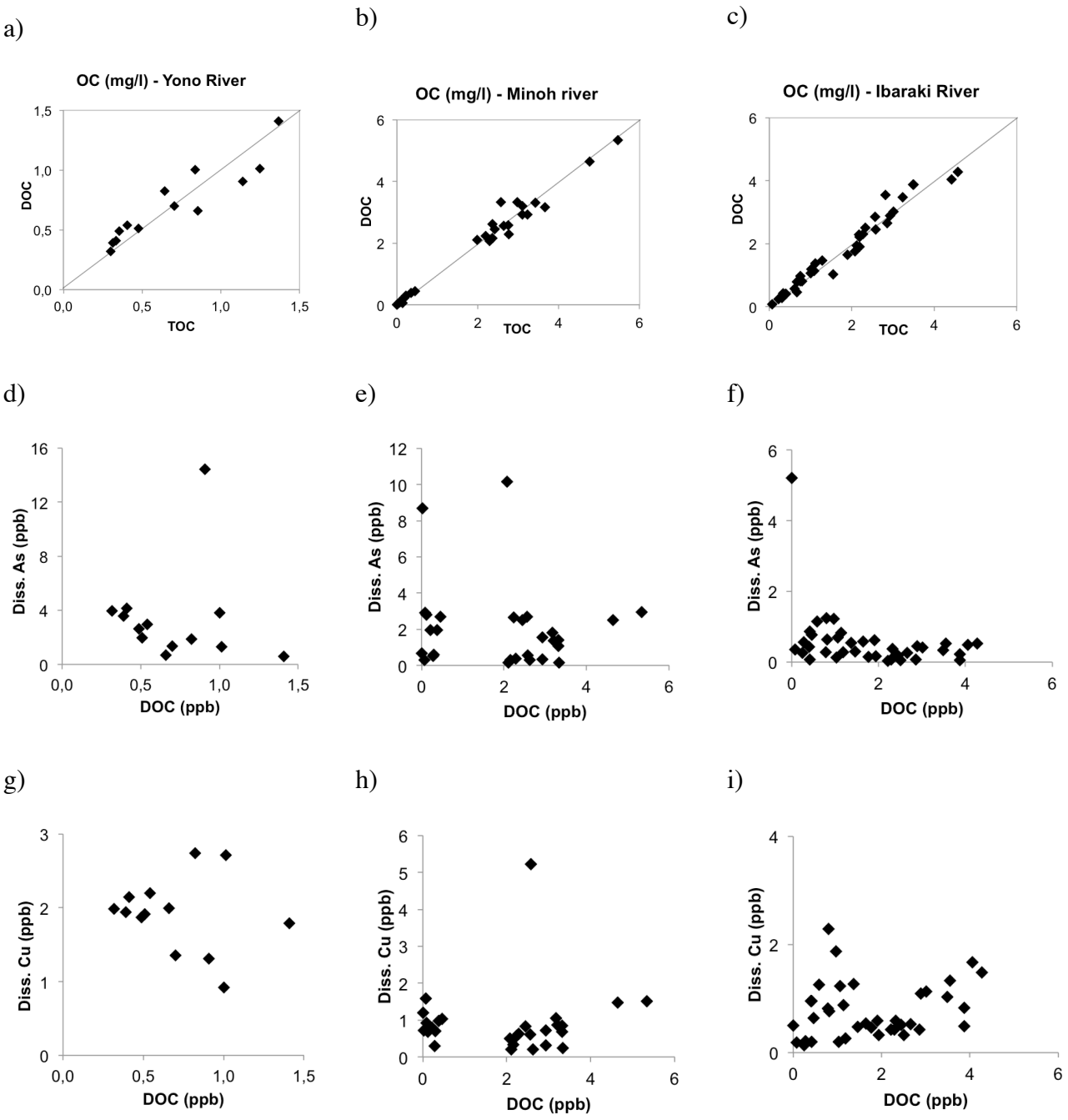

Fig. 4.26 – Biplots of total and dissolved organic carbon (TOC/DOC) (a, b, c; the line represents the 1:1 ratio), DOC and dissolved As (d, e, f) and DOC vs dissolved Cu (g, h, i) in Yono, Minoh and Ibaraki Rivers, respectively.

Organic Matter – The role of organic mater, analyzed as organic carbon (OC) in the present study, was assessed on its role as a ligands for As and trace elements. OC was measured in the total and the

dissolved fraction of river waters, and the concentrations in both fractions were minimal, i.e., OC was mainly present in the <0.45µm phase (Fig. 4.26 a, b, c). Apart from binding onto mineral oxides, trace metals would also bind with organic molecules, either fluvic or humic acid in natural waters. However, below the <0.45µm cut off, there was an lack of relationship between DOC and dissolved concentrations of trace metal, as seen on Fig. 4.26 d, e, f for As, and g, h, i for Cu.

4.3.2 Discussion

Influence of the surface geology on trace element distributions

The geochemical mapping and the statistical analysis of riverbed sediment chemistry showed the influence of the surface geology on the major geochemistry of sediments at each sampling site. K enrichment of the sediments from the central part of the Nose pluton was likely due to the abundance of K-feldspars in the granite rock, whereas these minerals are almost absent in the adjacent quartz-diorite (Tainosho, 1971). Among the others large-ion lithophile elements (LILEs), Rb and Ba followed the behavior of K, and remained in the residual melt to partition in the K-feldspar of the later crystallized adamellite (Icenhower and London, 1996), whereas Sr preferentially partitioned in plagioclase (Nash and Crecraft, 1985) in quartz-diorite during the early differential crystallization of the Nose pluton.

The strong association of Mg and Fe in the sediments from the quartz-diorite area must be due to the mafic minerals such as biotite, hornblende and pyroxenes that are absent in the adamellite of the Nose and Myoken plutons. The highest Ti concentrations, strongly associated with Fe, Mg and Ca, appeared in the Yono river sediments from quartz diorite and flushed downstream. This enrichment would be explained by the occurrences of ilmenite in the quartz-diorite (Tainosho, 1971), and/or plagioclase, in which Ti was concentrated by preferential partitioning during the early differentiation (Salmonsen et al., 2011).

Masuda et al. (1972) showed that the central part of the Nose pluton was enriched in La and Ce, while heavy REEs had no distinctive change throughout the granitic sequence. CM and PCA in Set_{AsInc} suggested Y, associated with K and Rb, originated from the most felsic rocks, while Ce, higher in quartz-diorite areas, would come from the Ce-rich hornblende (Masuda et al., 1972). The statistics analysis also emphasized a behavior of REYs similar to Al, Mn and Ti. Thus, the deposition of suspended matter composed of Al, Mn, Ti, and adsorbing REYs, as explained below, would

readily enrich these elements in the sediments, especially in the case of Ce, which had the lowest DTI of REYs.

Riverbed sediments from the Tamba Belt were commonly enriched in trace metals, compared to the sediments derived from igneous rock bodies. This was especially noticeable for Co and Cr that were enriched in the sediments from the Ultra-Tamba Belt. Ohta et al. (2005) suggested that ultramafic and mafic nature of rocks in the accretionary formations of Central Japan would cause enrichment of Co, Cr and Ni in riverbed sediments, even if the outcrop was small. The Ni and Cr enrichment of bed sediments in Inagawa district from greenstone of Tamba Belt was also suggested by Kagawa et al. (2007). Thus, even if greenstones, i.e., seafloor basalt, are seldom in the Ultra-Tama formation, they still contributed to the enrichment of Co, Cr and other metals Ni and V.

Zn and Cu concentrations were higher in the western part of the study area, where many subvolcanic ore-deposits were located, but the multivariate analysis narrowly supported a clear relationship between these elements and Pb. Only Pb was correlated with Cu and Zn, especially the Cu distribution was similar to that of Pb along the Yono river. Ohta et al. (2005) emphasized that urbanization was a possible cause for enrichment of Pb in the sediments. High concentrations of Pb in the lower reach of the Yono River on the upper and lower reaches of Ai River might indeed be attributed to the light urban area found upstream, a dumping site, and/or highway works and. Considering the small scale of urbanization in the area and the numerous occurrences of base metal mines in the study area, the Cu and Zn is plausibly originated from ore mineralization, while the Pb may have dual or more origins.

Behavior and fate of arsenic in the studied rivers

The fate of As along the river courses is an important process to document the cycle of this element in the hydrosphere. Many studies emphasized the role of amorphous Al, Mn, and Fe oxides/hydroxides/ oxyhydroxides as salient absorbents of As. This is especially the case for arsenate, the most abundant As species under oxic and neutral pH conditions (Bowell, 1994; Grosbois et al., 2011; Zhang et al., 2012) as those in the rivers of the study area.

Previous works already pointed out that the As in surface waters was present as dissolved species rather than associated with suspended particles (Foster and Charlesworth, 1996; Pokrovsky et al., 2005; Tanizaki et al., 1992). Indeed, adsorption of As onto suspended particles in water was not significant in the present study, as shown by the high DTI value (average = 76) of As. Our data also

showed a totally different behavior between As and Fe, Al and Mn throughout the entire studied river system, i.e., As dominantly (at least >70%) existed as dissolved species, whereas the other three elements were predominant in the particulate phase. Thus the particulate matters were not an important factor controlling the As distribution in the studied rivers. In the studied river system, the dissolved As would be transported down along the river course and would not accumulate in the sediment pools. The same observations were reported by Dittmar (2004) who explained the conservative behavior of As (in the dominant arsenate form) in the Elqui River by its inefficiency to bind on iron hydroxide because of high pH.

Previous studies examined the sorption capacities of As onto Fe oxides and clays (e.g., Pierce and Moore, 1982; Manning and Goldberg, 1997; Zeng, 2004). One of important results is a severe desorption of As(III) and the inefficient adsorption of As(V) at pH >7 (Manning et al., 1998). In our study, the adsorption of As onto suspended particles or riverbed sediments, i.e., observation of low DTI_{As}, was prominent only when the As concentrations were very low (<1 ppb) in the upper reaches of streams flowing through granitic areas (Ibaraki and Yono rivers). The exchange of As between the aqueous and adsorbing/solid phases in the water column would actually be constrained by the competition with other chemical species present in the water, such as sulfates (Wilkie and Hering, 1996). Therefore, only the dilution of contaminated water by an As-free inflow seemed to be effective for the auto-remediation of As in the studied river system.

Behavior and fate of trace elements in studied rivers

The behavior of trace metals in this study was generally consistent with those in the previous works that investigated the partitioning of trace metals in fresh and estuarine waters, and the binding affinity onto Al-, Mn- or Fe-oxides. The similar sequence of the DTI obtained in this study and the order of binding strength onto natural iron hydroxides from Tessier et al. (1985) suggested these adsorbent phases were the main carriers of trace metals in the studied river system. The elements most readily adsorbed onto suspended matter were Pb, Co and Cr, while Cu, Ni and Cd were retained as dissolved species longer than those in the water column.

The strong affinity of Fe, Mn, Al and Ti to bind with oxygen would explain the high concentrations at spring area and their rapid decrease downstream. Indeed, as the redox condition changed when the groundwater issued from spring and contacted with air, these elements were oxidized and readily formed oxides/hydroxides. These reactions were more dramatic for Mn that

immediately precipitated, while it was less obvious for Fe and Al, likely because the Mn oxides complex more readily. E.g., Dong et al. (2000) showed that Pb was adsorbed preferentially onto Mn oxides rather than onto Fe or Al oxides in river water.

Fe and Al acted as main ligands to adsorb and/or form complex with other trace elements, as illustrated by their DTI. Pb and Co in the studied riverwaters were typical trace metals with the lowest DTIs, and their behaviors were indeed related to Fe-bearing minerals. E.g., the highest concentrations of Co were found at spring, with concentrations dropping by a factor of 3 immediately downstream. Kohler (2010) also reported the decrease of Pb and Co in filtered waters up to a factor of 4 (corresponding to DTI ~25) compared with those of the unfiltered waters, and the correlated behavior of both elements with Fe in Swedish river waters. Coston et al. (1995) also showed that Pb was readily bound to Fe-site than Al-site of oxides minerals on aquifer sand coatings. Additionally, detrital clay particles derived from the erosion of the surface geology would also be important adsorbents for the trace elements, as they were within rock before erosion. Thus, concentrations of trace metals in the studied rivers were greatly influenced by their affinity to bind onto the particulate phase, resulting in a non-conservative behavior along the river course. Those decreasing concentrations by co-precipitation with the aforementioned carriers contributed to the auto-remediation of some rivers.

Ni, Cd, V and Cu were dominantly present as dissolved species, which prevented from their removal by precipitation from the column water. Ni concentrations >10ppb appeared in the quartz-diorite area, where the bed sediments were also Ni-rich. Concentrations of Ni seemed to gradually decrease along the river flow. As it was hypothesized for arsenic, the decreasing Ni concentrations outside the quartz-diorite area were induced by dilution with a Ni-free groundwater. This phenomenon was not observed for Cd, V and Cu, which concentrations did not change (Cd, V) or slightly increased (Cu). These elements demonstrate a high solubility in the water column and can be transported downstream, spreading contamination. Such high mobility would have contributed to the contamination process of the massive Cd contamination of the Jinzu River that started from the Kamioka Mine in Gifu Prefecture, and spread further down to Toyama city (distant from several tens km).

Trace elements with higher DTI may be adsorbed on other phases of the river water, namely natural organic matter (NOM). The present study established a partitioning of elements at the 0.45µm size (or 0.45µm cut off), although trace metals would bind to the organic matters and colloids <0.45µm. For example, Sigg et al. (2000) reported Cu being mainly present as a complex

strongly binding to dissolved organic mater (DOM) in the ultra-filtered (10kD or 25nm) waters of the Thur River (Swiss). The total and dissolved (<0.45µm) fractions of organic matter (analyzed as organic carbon) were investigated in the present study. Organic matter was essentially dissolved, however, any correlated behavior was not found between the trace metals and the DOM. The main carrier phase of As, Ni, Cu and other dissolved trace elements was plausibly present <0.45µm fractions, and the cut off at this size was not enough to specify the host phase of dissolved trace metals. Further investigations at downsize filtration are thus required.

5. CONCLUSION

The occurrence and fate of As in river waters of the heavily mineralized Hokusetsu area, where the Paleozoic-Mesozoic sedimentary rocks (Tamba and Ultra-Tamba formations) were intruded by granitic complexes (e.g., Ibaraki granitoids), area were investigated via geochemical mapping of river water and bed sediments, in order to assess the extension of contamination and specify the contamination mechanism.

The geochemical mapping demonstrated the concordant distribution of conservative major and trace elements, including As, in waters and sediments of rivers with the surface geology, indicating that the baseflow, of which chemistry was formed via the water-rock interaction, is the primary factor that controls the element distribution. In the sedimentary rocks far from the igneous intrusions, As concentrations of river waters were <3ppb and riverbed sediments had As levels similar to the average concentrations of sedimentary formations of Central Japan. In these areas, the background concentration was mainly due to the weathering of the volcanogenic sedimentary rocks, e.g., As-rich meta-basalt that is occasionally found in the Tamba Belt formations.

High levels of As in sediments and river water appeared around the Ibaraki granitic complex. Thus, the igneous activities that induced the numerous ore-deposits of the area were presumably involved in the As contamination of river by dissolution of the sulfide-ores hosted in country rocks. Petrological analysis of the present study confirmed that those sulfide minerals from these activities were the source of As. Arsenic was detected in the sulfides at every site where the As contamination was observed from the geochemical mapping, and the isotopic and mineralogical analysis showed that sulfides were formed at two different ore mineralizations epochs, i.e., a Pre-Cretaceous subvolcanism and a Late-Cretaceous/Early Paleogene magmatism.

The highest As contamination (38ppb) of river waters was generated by the oxidation-dissolution of pyrite hosted by the Paleozoic/Mesozoic sedimentary rocks nearby fossil faults, which promoted the infiltration of oxic surface water into the host rocks and enhanced the dissolution of As-bearing sulfides. At this sampling site, colloform assemblages of magnetite/chalcopyrite, which were related to the Pre-Cretaceous (Paleozoic/Mesozoic) subseafloor volcanogenic cupriferous stratiform ore-deposits, were identified as an As source. Arsenic was concentrated in the magnetite (0.35 wt%), which occurred as the relics of pyrite altered by the Late-Cretaceous intrusions. Sulpharsenides were also found in the shale of the same area. These hydrothermally altered As-

bearing minerals would dissolve more easily due to the lower crystallinity, especially in fault areas where the oxic water infiltration triggered local As contamination.

Arsenic was also detected in sulfides minerals related to the Late Cretaceous/Early Paleogene magmatism that intruded into the sedimentary rocks and induced hydrothermal ore deposits in the western part of study area. The highest As level in riverbed sediments was found in a quartzite. The quartzite was mainly disseminated with As-bearing pyrrhotite that precipitated from gaseous emanations during contact-metamorphism of the quartz-diorite intrusion of the Ibaraki granitic complex, although the river waters flowing in this area had mild As concentrations (<10ppb). Several hydrothermal ore deposits that include As-bearing minerals were found in the study area, however, it was notable that such ore deposits rarely caused a serious As contamination of river waters in their vicinity.

Along with As, the sulfides from all types of ore deposits contained important amount of Ni, Co and Pb that would be released in the environment after the sulfide oxidation-dissolution. Results of the partitioning analysis of the present study showed that As fractionated mostly in the dissolved phase of the water column. The same behavior was also observed for the trace metals Ni, Cd, V and Cu. Fe, Mn and Al are the major constituents of suspended particles that include oxides and clay particles, which are usually considered as the main carriers of As. Indeed, results showed these elements were present in the particulate phase of the water column, meaning they were not important career phases of As and aforementioned trace metals. On the other hand, a non-conservative behavior was observed for Pb and Co, which were associated with Fe, implying that these harmful trace metals bound on particles, leading to a rapid decrease of concentrations in the water column due to the precipitation.

As-contaminated waters widely appear in the world, and extensive studies have been conducted especially for groundwaters because of the importance for these water resources. Throughout the studies, sources of As causing a natural contamination have been believed to be mainly sulfides derived from hydrothermal activities and ore deposits. The most serious contaminations are known to occur in Holocene aquifers, and for this case, primary sources have been thought to be mostly sulfides found in the source areas of the river basins (e.g., Smedley and Kinniburgh, 2002). Even though, there are not so many reports in which the As-source minerals are specified and the dissolution process can be traced back throughout the water natural cycle free from anthropogenic impacts, e.g., As released from marcasite in the mercury ore deposit in association with water incorporated along fault in New Zealand (Craw et al., 2000), and from fossil

hydrothermal vein in granitic body in India (Acharyya et al., 2005). The present work is thus an important contribution to the knowledge of the fate of As from the source minerals to surface waters. It showed that a wide distribution of As, even at low concentration, and the infiltration of oxic waters through fractures promoting chemical weathering are important mechanisms that contributed to extend the As contamination. The study also documented the As cycle in the deep crust at a convergent margin. Magmatic and hydrothermal activities play a primary role in incorporating As into the Earth's crust. Here, As was supplied from an island arc magmatism at its early stage of differentiation, into the accreted sedimentary formations, in which As originated from seafloor volcanism was also included.

REFERENCES

Acharyya, S.K., Shah, B.A., Ashyiya, I.D., Pandey, Y., 2005. Arsenic contamination in groundwater from parts of Ambagarh-Chowki block, Chhattisgarh, India: source and release mechanism. Environ. Geol. 49, 148–158.

Andersen, L.C.D., Bruland, K.W., 1991. Biogeochemistry of arsenic in natural waters: The importance of methylated species. Environ. Sci. Technol. 25, 420–427.

Ashida, K., Yamamoto, J., Kobuke, Y., 2001. Spatial and Temporal Distributions of Arsenic and Other Heavy Metals and Their Causes in the Ina River System. J. Japan Soc. Water Environ. 24, 466–472.

Augustithis, S., 1995. Atlas of the textural patterns of ore minerals and metallogenic processes. Walter de Gruyter.

Baeyens, W., Brauwere, A. de, Brion, N., Gieter, M. De, Leermakers, M., 2007. Arsenic speciation in the River Zenne, Belgium. Sci. Total Environ. 384, 409–419.

Bajwah, Z., Seccombe, P., Offler, R., 1987. Trace element distribution, Co: Ni ratios and genesis of the Big Cadia iron-copper deposit, New South Wales, Australia. Miner. Depos.

Baker, L.A., Qureshi, T.M., Wyman, M.M., 1998. Sources and mobility of arsenic in the Salt River Watershed, Arizona. Water Resour. Res. 34, 1543–1552.

Beauchemin, S., Kwong, Y., 2006. Impact of redox conditions on arsenic mobilization from tailings in a wetland with neutral drainage. Environ. Sci. Technol.

Beermann, O., Botcharnikov, R.E., Nowak, M., 2015. Partitioning of sulfur and chlorine between aqueous fluid and basaltic melt at 1050°C, 100 and 200MPa. Chem. Geol. 418, 132–157.

Benjamin, M.M., Leckie, J.O., 1981. Competitive adsorption of cd, cu, zn, and pb on amorphous iron oxyhydroxide. J. Colloid Interface Sci. 83, 410–419.

Borůvka, L., Vacek, O., Jehlička, J., 2005. Principal component analysis as a tool to indicate the origin of potentially toxic elements in soils. Geoderma 128, 289–300.

Bralia, A., Sabatini, G., Troja, F., 1979. A revaluation of the Co/Ni ratio in pyrite as geochemical tool in ore genesis problems. Miner. Depos. 14, 353–374. doi:10.1007/BF00206365

British Geological Survey (BGS), Department of Public Health Engineering (DPHE), 2001. Arsenic contamination of groundwater in Bangladesh, British Geological Survey Technical Report WC/00/19. British Geological Survey, London.

Bruce A. Manning, *,†, Scott E. Fendorf, ‡ and, Goldberg†, S., 1998. Surface Structures and Stability of Arsenic(III) on Goethite: Spectroscopic Evidence for Inner-Sphere Complexes.

Campbell, F., Ethier, V., 1984. Nickel and cobalt in pyrrhotite and pyrite from the Faro and Sullivan

orebodies. Can. Mineral.

Canfield, D.E., 2004. The evolution of the Earth surface sulfur reservoir. Am. J. Sci. 304, 839–861.

Cenci, R.M., Martin, J.-M., 2004. Concentration and fate of trace metals in Mekong River Delta. Sci. Total Environ. 332, 167–182.

Charvet, J., 2013. Late Paleozoic–Mesozoic tectonic evolution of SW Japan: A review – Reappraisal of the accretionary orogeny and revalidation of the collisional model. J. Asian Earth Sci. 72, 88–101.

Cook, N.J., Ciobanu, C.L., Pring, A., Skinner, W., Shimizu, M., Danyushevsky, L., Saini-Eidukat, B., Melcher, F., 2009. Trace and minor elements in sphalerite: A LA-ICPMS study. Geochim. Cosmochim. Acta 73, 4761–4791.

Costagliola, P., Benvenuti, M., Benvenuti, M.G., Innocenti, A., Mascaro, L., Paolieri, M., Rossato, L., Tanelli, G., 2004. Arsenic Distribution In The QuaternarySediments Of The Median Valley Of The PecoraStream (Grosseto, Italy). WIT Trans. Ecol. Environ. 70.

Coston, J.A., Fuller, C.C., Davis, J.A., 1995. Pb2+ and Zn2+ adsorption by a natural aluminum- and iron-bearing surface coating on an aquifer sand. Geochim. Cosmochim. Acta 59, 3535–3547.

Craw, D., Chappell, D., Reay, A., 2000. Environmental mercury and arsenic sources in fossil hydrothermal systems, Northland, New Zealand. Environ. Geol. 39, 875–887.

Davidson, C., 1962. On the cobalt-nickel ratio in ore deposits. Min. Mag. 106, 78–85.

Deer, W.A. (William A., Howie, R.A. (Robert A., Zussman, J., Mineralogical Society (Great Britain), 2012. An introduction to the rock-forming minerals. Mineralogical Society of Great Britain and Ireland.

Dittmar, T., 2004. Hydrochemical processes controlling arsenic and heavy metal contamination in the Elqui river system (Chile). Sci. Total Environ. 325, 193–207.

Dixit, S., Hering, J.G., 2003. Comparison of Arsenic(V) and Arsenic(III) Sorption onto Iron Oxide Minerals: Implications for Arsenic Mobility. Environ. Sci. Technol. 37, 4182–4189.

Dong, D., Nelson, Y.M., Lion, L.W., Shuler, M.L., Ghiorse, W.C., 2000. Adsorption of Pb and Cd onto metal oxides and organic material in natural surface coatings as determined by selective extractions: new evidence for the importance of Mn and Fe oxides. Water Res. 34, 427–436.

Dutta, P.K., Ray, A.K., Sharma, V.K., Millero, F.J., 2004. Adsorption of arsenate and arsenite on titanium dioxide suspensions. J. Colloid Interface Sci. 278, 270–275.

Dzombak, D.A., Morel, F., 1990. Surface complexation modeling : hydrous ferric oxide. Wiley.

El-Gemmizi, M.A., 1996. Super gene alternation of magnetite and pyrite and the role of their alternation products in the fixation of uranium from the circulating media. Vol. 3.

Essozv, J., Stevens, R., Vincent, E., 1965. Aspects of the geochemistry of arsenic and antimony, exemplified by the Skaergaard intrusion. Mineral. Mag. 35, 88–107.

Ewart, A., Griffin, W.L., 1994. Application of proton-microprobe data to trace-element partitioning in volcanic rocks. Chem. Geol. 117, 251–284.

Fanlo, I., Subías, I., Gervilla, F., 2004. The composition of Co–Ni–Fe sulfarsenides, diarsenides and triarsenides from the San Juan de Plan deposit, Central Pyrenees, Spain. Canadian.

Farley, K.J., Dzombak, D.A., Morel, F.M.., 1985. A surface precipitation model for the sorption of cations on metal oxides. J. Colloid Interface Sci. 106, 226–242.

Fendorf, S., Michael, H., Geen, A. van, 2010. Spatial and temporal variations of groundwater arsenic in South and Southeast Asia. Science (80). 328, 1123–1127.

Field, C.W., 1966. Sulfur isotopic method for discriminating between sulfates of hypogene and supergene origin. Econ. Geol. 61, 1428–1435.

Foster, I.D.L., Charlesworth, S.M., 1996. Heavy metals in the hydrological cycle: Trends and explanation. Hydrol. Process. 10, 227–261.

Fukuoka, M., Hirowatari, F., 1980. On minerals in the system Ni Co As S from the bedded manganese ore deposits in the eastern part of Yamaguchi Prefecture: on the chemical compositions of gersdorffite cobaltite solid solution. Sci. Rep. Fac. Sci. Kyushu Univ. Geol. 13, 239–249.

GSJ/AIST, 2011. Bouguer Gravity Anomalies. Density: 2.67 g/cm3. Map 5235-00, 1st mesh. Gravity Database Japan - DVD Ed.

Halamić, J., Peh, Z., Bukovec, D., Miko, S., Galović, L., 2001. A factor model of the relationship between stream sediment geochemistry and adjacent drainage basin lithology, Medvednica Mt., Croatia. Geol. Croat. 54, 37–51.

Hedenquist, J.W., Lowenstern, J.B., 1994. The role of magmas in the formation of hydrothermal ore deposits. Nature 370, 519–527.

Helmy, H.M., Ballhaus, C., Wohlgemuth-Ueberwasser, C., Fonseca, R.O.C., Laurenz, V., 2010. Partitioning of Se, As, Sb, Te and Bi between monosulfide solid solution and sulfide melt – Application to magmatic sulfide deposits. Geochim. Cosmochim. Acta 74, 6174–6179.

Hem, S.R., Makovicky, E., Gervilla, F., 2001. Compositional trends in Fe, Co and Ni sulfarsenides and their crystal-chemical implication: Results from the arroyo de la cueva deposits, ronda peridotite, Southern Spain. Can. Mineral. 39, 831–853.

Hunter, R.H., Sparks, R.S.J., 1987. The differentiation of the Skaergaard Intrusion. Contrib. to Mineral. Petrol. 95, 451–461.

Icenhower, J., London, D., 1996. Experimental partitioning of Rb, Cs, Sr, and Ba between alkali feldspar and peraluminous melt. Am. Mineral. 81, 719–734.

Imai, H., Lee, M.S., Iida, K., Fujiki, Y., Takenouchi, S., 1975. Geologic structure and mineralization of the xenothermal vein-type deposits in Japan. Econ. Geol. 70, 647–676.

Imai, N., Terashima, S., Ohta, A., Mikoshiba, M., 2004. Database of elemental distribution (geochemical map) in Japan. Chikyukagaku (Geochemistry) 38, 203–222.

Imai, N., Terashima, S., Takashi, O., Yutaka, K., Masumi, M., Atsuyuki, O., Yoshiko, T., Hikari, K., Shigeko, T., Matsuhisa, Y., 2003. Geochemical map of Japan. Geochim. Cosmochim. Acta Suppl. 67, 170.

Ishiga, H., 1990. Ultra-Tamba Terrane, in: Ichikawa, K., Mizutani, S., Hara, I., Hada, S., Yao, A. (Eds.), Pre-Cretaceous Terranes of Japan. Publication of IGCP Project No. 224: Pre-Jurassic Evolution of Eastern Asia. Osaka, pp. 97–107.

Ishihara, S., 1978. Metallogenesis in the Japanese island arc system. J. Geol. Soc. London. 135, 389–406.

Ishihara, S., Sasaki, A., 2002. Paired Sulfur Isotopic Belts: Late Cretaceous-Paleogene Ore Deposits of Southwest Japan. Bull. Geol. Surv. Japan 53, 461–477.

Ishihara, S., Sasaki, A., 1991. Ore Deposits Related to Granitic Magmatism in Japan: A Magmatic Viewpoint. Episodes.

Ishizaka, K., 1971. A Rb-Sr isotopic study of the Ibaragi granitic complex, Osaka, Japan. J. Geol. Soc. Japan 77, 731–740.

Isozaki, Y., 1997. Jurassic accretion tectonics of Japan. Isl. Arc 6, 25–51.

Ito, H., Masuda, H., Kusakabe, M., 2003. Some factors controlling arsenic concentrations of groundwater in the northern part of Osaka Prefecture. J. Groundw. Hydrol. 45, 3–18.

Ixer, R., Stanley, C., Vaughan, D., 1979. Cobalt-, nickel-, and iron-bearing sulpharsenides from the north of England. Mineral. Mag.

Janzen, M.P., Nicholson, R. V, Scharer, J.M., 2000. Pyrrhotite reaction kinetics: reaction rates for oxidation by oxygen, ferric iron, and for nonoxidative dissolution. Geochim. Cosmochim. Acta 64, 1511–1522.

Japan Oil Gas and Metals National Corporation, 2013. JOGMEC's activities in Japan : Mine Pollution Control http://www.jogmec.go.jp/english/mp_control/mp_control_metal_10_000005.html

Kagawa, Y., Imamura, K., Okabe, M., Okauchi, K., Osaki, S., Shibata, H., Tanaka, M., Tog, Y., Yamamura, H., Tsuboi, M., 2007. Geochemical map of the Hanshin area, Southwest Japan, in: 114th (2007 Sapporo) Annual Meeting of the Geological Society of Japan. Geological Society of Japan, p. 614.

Kamiga, M., Tagiri, M., 2003. The present pollution of river-bed sediments and soil in the Watarase-river basin and the Miyata-river basin: The pollution level after abandoned working of the Ashio copper mine and the Hitachi mine. J. Geol. Soc. Japan 109, 533–547.

Kanehira, K., Tatsumi, T., 1970. Bedded cupriferous iron sulfide deposits in Japan: A review., in: Tatsumi, T. (Ed.), Volcanism and Ore Genesis. University of Tokyo Press, Tokyo, pp. 51–76.

Kasama, T., Yoshida, H., 1976. Volcanostratigraphy of the late Mesozoic acid pyroclastic rocks of the Arima Group, southwest Japan. J. Geosci. Osaka City Univ. 20, 19–42.

Kelly, W.C., Turneaure, F.S., 1970. Mineralogy, paragenesis and geothermometry of the tin and tungsten deposits of the eastern Andes, Bolivia. Econ. Geol. 65, 609–680.

Keppler, H., Wallace, P.J., Gerlach, T.M., Kress, V., Gerlach, T.M., McGee, K.A., Luhr, J.F., Carmichael, I.S., Varekamp, J.C., Sigurdson, H., Carey, S., Palais, J.M., Devine, J., Bluth, G.J.S., Schnetzler, C.C., Krueger, A.J., Walter, L.S., McCormick, M.P., Thomason, L.W., Trepte, C.R., Bekki, S., Devine, J.D., Sigurdsson, H., Davis, A.N., Self, S., Oppenheimer, C., Williams, S.N., Scaillet, B., Clemente, B., Evans, B.W., Pichavant, M., Chou, I.M., Carroll, M.R., Rutherford, M.J., 1999. Experimental evidence for the source of excess sulfur in explosive volcanic eruptions. Science 284, 1652–4.

Klemm, D.D., 1965. Synthesen und Analysen in den Dreiecksdiagrammen FeS - CoAsS - NiAsS und FeS2 - CoS2 - NiS2. Neues Jahrb. Miner. 103, 205–255.

Kobayashi, J., Morii, F., Muramoto, S., Nakashima, S., 1970. Effects of Air and Water Pollution on Agricultural Products by Cd, Pb, Zn Attributed to Mine Refinery in Annaka City, Gunma Prefecture. Nippon Eiseigaku Zasshi (Japanese J. Hyg. 25, 364–375.

Koga, M., Nishida, M., Yoshida, I., 2004. Determination of calcium in natural water samples by atomic absorption spectrometry by adding reduced amounts of lanthanum chloride. Bunseki Kagaku 53, 173–176.

Kohler, S., 2010. Comparing filtered and unfiltered metal concentrations in some swedish surface waters. Uppsala.

Kosyakov, V.I., Sinyakova, E.F., 2015. Peculiarities of behavior of trace elements during fractional crystallization of sulfide magmas. Dokl. Earth Sci. 460, 179–182.

Laznicka, P., 1985. Empirical Metallogeny: Depositional Environments, Lithologic Associations, and Metallic Ores, Vol. 1: Phanerozoic Environments, Associations, and Deposits- Part A. Elsevier Science, Amsertdam.

Lindgren, W., 1933. Mineral deposits, 4th Editio. ed. McGraw-HillBook Co, New York.

Loftus-Hills, G., Solomon, M., 1967. Cobalt, nickel and selenium in sulphides as indicators of ore genesis. Miner. Depos. 2, 228–242.

Lu, L., Wang, R., Chen, F., Xue, J., Zhang, P., Lu, J., 2005. Element mobility during pyrite weathering: implications for acid and heavy metal pollution at mining-impacted sites. Environ. Geol. 49, 82–89.

Martin, J.M., Meybeck, M., 1979. Elemental mass-balance of material carried by major world rivers. Mar. Chem. 7, 173–206.

Masuda, H., Ibuki, Y., Tonokai, K., 1999. Mechanism of Natural Arsenic Pollution of Shallow Groundwater in the Northern Part of Osaka Prefecture, Japan. J. Groundw. Hydrol. 41, 133–

146.

Masuda, Y., Yagi, S., Nishimura, S., Asayama, T., 1972. Rare-earth distributions in the Ibaragi granitic complex, Osaka prefecture, Japan. J. Geol. Soc. Japan 78, 521–530.

Matsuura, H., Kurimoto, C., Sanagawa, A., Bunno, M., 1995. Geology of the Hirone district. With Geological Sheet Map at 1:50,000.

Ministry of Land InfrastructureTransport and Tourism, 2013. Water Information System [WWW Document]. URL http://www1.river.go.jp/ (accessed 4.1.16).

Ministry of the Environment, 2008. On the health effects of diphenylarsinic acid - Organic arsenic compound contamination in Kamisu City, Ibaraki Prefecture.

Mitsuno, C., 1988. Stratiform Sulfide Ore Deposits of the Upper Palaeozoic in Eastern Chugoku and Western Kinki Regions, Southwestern Japan. Min. Geol. 38, 247–262.

Miyachi, Y., Kusunoki, T., Musashino, M., Tainosho, Y., Imoto, N., 2005. Geology of the Kyoto Seinanbu District., Quadrangle Series, Scale 1: 50,000. Geological Survey of Japan, AIST.

Miyamura, M., Ishida, S., Komura, Y., 1972. Subsurface geology, Kyoto-Seinanbu, in: Economic Planning Agency (Ed.), Fundamental Land Classification Survey - Geomorphology, Subsurface Geology & Soil, Kyoto-Seinanbu 1:50,000. p. 65.

Miyoshi, T., Nakamura, T., Kusakabe, M., 1988. Sulfur isotopic study of vein deposits in the Kinki district, Inner Zone of Southwest Japan. Min. Geol. 38, 323–333.

Mizota, C., Sasaki, A., 1996. Sulfur isotope composition of soils and fertilizers: differences between Northern and Southern Hemispheres. Geoderma 71, 77–93.

Nakadaira, H., Yamamoto, M., Katoh, K., 1995. Arsenic levels in soil of a town polluted 35 years ago (Nakajo, Japan). Bull. Environ. Contam. Toxicol. 55, 650–7.

Nakae, S., 1993. Jurassic accretionary complex of the Tamba Terrane southwest Japan and its formative process. J. Geosci. Osaka City Univ. 36, 15–70.

Nakahara, H., Yanokura, M., Murakami, Y., 1978. Environmental effects of geothermal waste water on the nearby river system. J. Radioanal. Chem. 45, 25–36.

Nakamura, T., 1990. Pre-Cretaceous strata-bound ore deposits, in: Ichikawa, K., Mizutani, S., Hara, I., Hada, S., Yao, A. (Eds.), Pre-Cretaceous Terranes of Japan. IGCP, Osaka, pp. 381–99.

Nakamura, T., Imoto, N., Shimizu, D., Tomita, K., 1987. Mining resources, in: Nakazawa, K., Ichikawa, K., Itihana, M. (Eds.), Regional Geology of Japan. Part 6 - Kinki. Kyoritsu Shuppan Co. Ltd., Tokyo, pp. 215–231.

Nakamura, T., Kim, M.Y., 1982. Macrostructures of vein filling in ore veins, with special reference to those of plutonic tungsten-tin-copper veins at the Otani mine, Kyoto Prefecture, Japan. Min. Geol. 32, 85–94.

Nash, W.P., Crecraft, H.R., 1985. Partition coefficients for trace elements in silicic magmas.

Geochim. Cosmochim. Acta 49, 2309–2322.

Nicholson, R. V., Scharer, J.M., 1993. Laboratory Studies of Pyrrhotite Oxidation Kinetics. pp. 14–30.

Nimick, D.A., Moore, J.N., Dalby, C.E., Savka, M.W., 1998. The fate of geothermal arsenic in the Madison and Missouri Rivers, Montana and Wyoming. Water Resour. Res. 34, 3051–3067.

Nishiyama, T., Ito, T., 2012. On trace elements in sulfides of the Otani Mine, in: Nagahara, S. (Ed.), Otani Mine Site Prospection. Nishiyama, Takashi, Kyoto, Japan, pp. 119–124.

Nordstrom, D.K., Wright, W.G., Mast, M.A., Bove, D.J., Rye, R.O., 2007. Aqueous-sulfate stable isotopes—a study of mining-affected and undisturbed acidic drainage, in: Church, S.E., Guerard, P. von, Finger, S.E. (Eds.), Integrated Investigations of Environmental Effects of Historical Mining in the Animas River Watershed, San Juan County, Colorado. U.S. Geological Survey.

Ogoshi, K., Mori, I., Gotoh, K., Ogawa, K., 1996. Did Arsenic Contamination in the Inagawa River Occur in Geogenic Relation to the Great Hanshin (Kobe) Earthquake of 1995? Appl. Organomet. Chem. 10, 757–760.

Ohta, A., Imai, N., Terashima, S., Tachibana, Y., 2005. Application of multi-element statistical analysis for regional geochemical mapping in Central Japan. Appl. geochemistry 20, 1017–1037.

Okada, A., Togo, M., 2000. Active Faults in the Kinki Area, Central Japan: Sheet Maps and Inventories. Tokai University Press.

Osaka Mining Supervisory Bureau, 1933. List of Mine concessions within the jurisdction of the Osaka Mining Supervisory Bureau - As of Showa 8 July 1st. Kogyosha, Osaka.

Osaka Mining Supervisory Office, 1911. List of Mine concessions within the jurisdction of the Osaka Mining Supervisory Office - As of Meiji 44 July 1st. Osaka Mining Supervisory Office, Osaka.

Osaka Prefecture Government, 2016. On the results of monitoring the quality of the Senri River. http://www.pref.osaka.lg.jp/jigyoshoshido/kawachiiki/s-top.html (accessed 4.1.16).

Oyarzun, R., Guevara, S., Oyarzún, J., Lillo, J., Maturana, H., Higueras, P., 2006. The As-Contaminated Elqui River Basin: a Long Lasting Perspective (1975–1995) Covering the Initiation and Development of Au–Cu–As Mining in the High Andes of Northern Chile. Environ. Geochem. Health 28, 431–443.

Pokrovsky, O., Schott, J., Dupré, B., 2006. Trace element fractionation and transport in boreal rivers and soil porewaters of permafrost-dominated basaltic terrain in Central Siberia. Geochim. Cosmochim. Acta.

Pokrovsky, O.S., Dupré, B., Schott, J., 2005. Fe–Al–organic Colloids Control of Trace Elements in Peat Soil Solutions: Results of Ultrafiltration and Dialysis. Aquat. Geochemistry 11, 241–278.

Robinson, B., Outred, H., Brooks, R., Kirkman, J., 2015. The distribution and fate of arsenic in the Waikato River system, North Island, New Zealand. Chem. Speciat. Bioavailab.

Sakaguchi, S., 1961. Stratigraphy and Palaeontology of the South Tamba District. Part I Stratigraphy. Osaka University of the Liberal Arts and Education.

Salminen, R., Tarvainen, T., Demetriades, A., 1998. FOREGS geochemical mapping field manual.

Salmonsen, L., Tegner, C., Humphreys, M., 2011. Titanium in plagioclase as a monitor of magma differentiation in the Skaergaard Intrusion. Am. Geophys. Union, Fall Meet. 2011, Abstr. #V43A-2566.

Sano, S., Tazaki, K., 1989. Greenstones in the Tamba belt. Mem. Geol. Soc. Japan 53–67.

Sasaki, A., Ishihara, S., 1979. Sulfur isotopic composition of the magnetite-series and ilmenite-series granitoids in Japan. Contrib. to Mineral. Petrol. 68, 107–115.

Sato, K., Kase, K., 1996. Pre-accretionary mineralization of Japan. Isl. Arc 5, 216–228.

Schieber, J., 2004. Marcasite in Sediments and Sedimentary Rocks - Conundrum and Opportunity, in: American Geophysical Union, Fall Meeting 2004, Abstract #OS14A-05.

Seal, R.R., 2006. Sulfur Isotope Geochemistry of Sulfide Minerals. Rev. Mineral. Geochemistry 61, 633–677.

Seddique, A., Masuda, H., Mitamura, M., 2008. Arsenic release from biotite into a Holocene groundwater aquifer in Bangladesh. Appl. Geochemistry 23, 2236–2248.

Shimada, N., 1996. Geochemical Conditions Enhancing the Solubilization of Arsenic into Groundwater in Japan. Appl. Organomet. Chem. 10, 667–674.

Shimazaki, H., 1985. Regional variation of isotopic composition of hydrothermal ore sulfur in Japan. J. Fac. Sci. Univ. Tokyo, Sect. 2 Geol. Mineral. Geogr. Geophys. 21, 81–100.

Sigg, L., Xue, H., Kistler, D., Sshönenberger, R., 2000. Size Fractionation (Dissolved, Colloidal and Particulate) of Trace Metals in the Thur River, Switzerland. Aquat. Geochemistry 6, 413–434.

Simon, A.C., Pettke, T., Candela, P.A., Piccoli, P.M., Heinrich, C.A., 2007. The partitioning behavior of As and Au in S-free and S-bearing magmatic assemblages. Geochim. Cosmochim. Acta 71, 1764–1782.

Smedley, P.L., Kinniburgh, D.G., 2002. A review of the source, behaviour and distribution of arsenic in natural waters. Appl. Geochemistry 17, 517–568.

Sohrin, Y., Matsui, M., Kawashima, M., Hojo, M., 1997. Arsenic biogeochemistry affected by eutrophication in Lake Biwa, Japan. Environmental.

Sugamori, Y., 2006. Upper Permian Takatsuki Formation, Middle Triassic Shimamoto Formation and Triassic sedimentary complex in the Nishiyama area, Osaka and Kyoto prefectures, SW Japan. J. Geol. Soc. Japan 112, 390–406.

Suzuki, T., Hirata, T., Ohara, S., 2015. iQuant2 - Isotope Quantitative Imaging.

Tainosho, Y., 1971. Petrology of the Ibaragi granitic complex in the northern part of Osaka Prefecture, Japan. Jour. Geol. Soc. Japan 77, 57–70.

Tainosho, Y., Nakajima, W., Ikegaki, K., 1977. The Mikusayama Quartz Gabbro and Granophyre Complex at the Hyogo Osaka Prefecture Border. J. Japanese Assoc. Mineral. Petrol. Econ. Geol. 72, 263–276.

Takimoto, K., 1973. Mineral resources of Japan - Kinki Region, 2nd Ed. ed. Asakura Publishing (In Japanese), Tokyo.

Tanizaki, Y., Shimokawa, T., Yamazaki, M., 1992. Physico-chemical speciation of trace elements in urban streams by size fractionation. Water Res. 26, 55–63.

Tatsumi, T., Sekine, Y., Kanehira, K., 1970. Mineral deposits of volcanic affinity in Japan: Metallogeny, in: Volcanism and Ore Genesis. University Tokyo Press, Tokyo, pp. 3–47.

Tessier, A., Rapin, F., Carignan, R., 1985. Trace metals in oxic lake sediments: possible adsorption onto iron oxyhydroxides. Geochim. Cosmochim. Acta 49, 183–194.

Timperley, M.H., Huser, B.A., 1996. Inflows of geothermal fluid chemicals to the Waikato River catchment, New Zealand. New Zeal. J. Mar. Freshw. Res. 30, 525–535.

Tonokai, K., Mitamura, M., 1998. Arsenic in springs and groundwaters and geological effects. Arsenic in springs and groundwaters of North Osaka Prefecture and its origin., in: Hideo, M., Geological Survey of Japan (Eds.), Environmental Problems Surrounding Arsenic. Natural and Artificial Geological Hazards. Geological Environment and Global Environment Series. Tokai University Press, Tokyo, pp. 63–94.

Toran, L., Harris, R., 1989. Interpretation of sulfur and oxygen isotopes in biological and abiological sulfide oxidation. Geochim. Cosmochim. Acta.

Tsuchiya, K., 1977. Various effects of arsenic in Japan depending on type of exposure. Environ. Health Perspect. 19, 35–42.

Wada, K., Fukushima, M., 1997. Arsenic Concentration in Ina-gawa River after the 1995 South Hyogo Earthquake. J. Japan Soc. Water Environ. 20, 860–864.

Wager, L.R., Vincent, E.A., Smales, A.A., 1957. Sulphides in the Skaergaard intrusion, East Greenland. Econ. Geol. 52, 855–903.

Watanabe, T., 1957. Genesis of Bedded Manganese Deposits and Cupriferous Pyrite Deposits in Japan. Min. Geol. 7, 87–97.

Watanabe, Y., Takagi, T., Kaneko, N., Suzuki, Y., 2016. Mineral and hydrocarbon resources, in: Moreno, T., Wallis, S.R., Kojima, T., Gibbons, W. (Eds.), Geology of Japan. Geological Society, London, pp. 431–455.

Webster, J.G., 2010. Chemical processes affecting trace metal transport in the Waihou River and

estuary, New Zealand.

White, J., Gammons, C., Zieg, G., 2014. Paragenesis of cobalt and nickel in the Black Butte shale-hosted copper deposit, Belt Basin, Montana, USA. Miner. Depos.

Wilkie, J., Hering, J., 1998. Rapid oxidation of geothermal arsenic (III) in streamwaters of the eastern Sierra Nevada. Environ. Sci. Technol.

Woitke, P., Wellmitz, J., Helm, D., Kube, P., Lepom, P., 2003. Analysis and assessment of heavy metal pollution in suspended solids and sediments of the river Danube. Chemosphere.

Wones, D.R., Eugter, H.P., 1965. Stability of biotite: experiment, theory an application. Am. Mineral. 50, 1228–1272.

Yamamoto, M., 1974. Distribution of sulfur isotopes in the Ryusei vein of the Akenobe mine, Hyogo Prefecture, Japan. Geochem. J.

Yamaoka, K., 1959. Geology and Mineralization of the Toroku Mine, Miyazaki Prefecture. Min. Geol. 9, 69–81.

Yamaoka, K., 1958. Spectrographic Studies on the Trace Elements in Pyrite. Kumamoto J. Sci. Ser. B, Sect. 1 Geol. 3, 31–37.

Yanagisawa, F., Sakai, H., 1983. Thermal decomposition of barium sulfate-vanadium pentoxide-silica glass mixtures for preparation of sulfur dioxide in sulfur isotope ratio measurements. Anal. Chem. 55, 985–987.

Yang, C., Telmer, K., Veizer, J., 1996. Chemical dynamics of the St. Lawrence riverine system: δDH_2O, $\delta^{18}OH_2O$, $\delta^{13}CDIC$, $\delta^{34}S$sulfate, and dissolved $^{87}Sr/^{86}Sr$. Geochim. Cosmochim. Acta 60, 851–866.

ANNEXES

Annex 1 – Map of sampling locations for river waters.

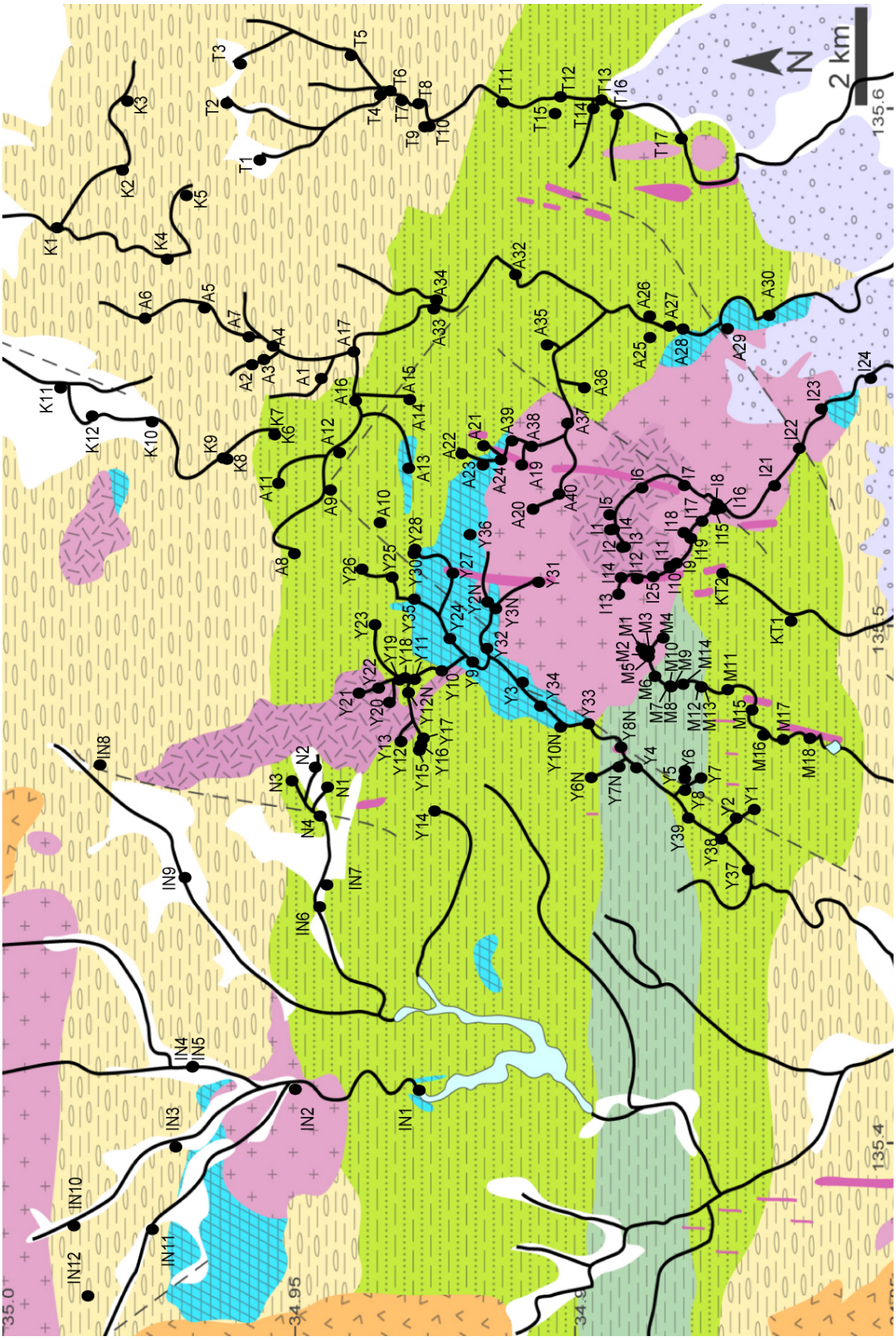

Annex 2 – Geochemistry of river waters of the study area

N.B. - Geochemical data for the Ai (samples AXX and #X on map of Annex 1), Kastura (KXX) and Tano (TXX) Rivers are described in Nojima et al. (2011) (#X sapmples) and Shibata et al. (2015) (others). The following are the geochemical data for waters sampled from the Yono (YXX and YXXJ, J indicates that water was sampled a second time in July), Minoh (MXX) and Ibaraki (IXX) Rivers.

YONOGAWA

Sample#	Y-01	Y-02	Y-03	Y-04	Y-05	Y-06	Y-07	Y-08	Y-09	Y-10
Date (y/m/d)	16/03/13	16/03/13	16/03/13	16/03/13	16/03/13	16/03/13	23/03/13	23/03/13	23/03/13	23/03/13
GPS	34,87	34,88	34,89	34,89	34,89	34,89	34,88	34,89	34,92	34,93
	135,46	135,46	135,47	135,47	135,47	135,47	135,47	135,47	135,49	135,49
Temp°C	8,40	16,10	11,60	10,70	6,70	12,10	7,70	9,20	--	11,90
pH	6,92	8,46	7,92	7,78	7,06	7,62	7,12	7,65	7,78	7,61
EC (uS/cm)	60,80	133,10	141,00	130,60	38,50	78,50	49,10	71,50	138,40	73,70
EC 25°C	40,61	109,41	103,21	93,25	24,41	58,25	32,11	48,91	--	54,39
TDS (mg/l)	18,28	49,23	46,45	41,96	10,98	26,21	14,45	22,01	--	24,48
DO (mg/l)	7,70	8,23	9,29	7,23	6,45	8,09	8,16	7,79	6,92	5,78
ORP (mV)	264,00	365,00	357,00	383,00	394,00	448,00	296,00	305,00	260,00	257,00
TOC (mg/l)										
DOC (mg/l)										
HCO3- (mg/l)	18,30	**69,24**	68,02	64,05	15,25	46,97	16,01	37,92	55,92	39,45
F (mg/l)	0,07	0,22	0,23	0,22	0,10	0,16	0,11	0,14	0,20	0,23
Cl (mg/l)	4,04	4,91	9,61	7,29	4,54	4,12	4,79	4,25	7,02	6,86
Br (mg/l)	n.d.	n.d.	n.d.	n.d.	n.d.	n.d.	n.d.	n.d.	n.d.	n.d.
NO3 (mg/l)	2,28	0,94	0,68	0,79	0,91	0,57	1,50	0,94	0,87	0,38
PO4 (mg/l)	n.d.	n.d.	n.d.	n.d.	n.d.	n.d.	0,15	0,07	n.d.	n.d.
SO4 (mg/l)	6,82	17,85	13,77	12,85	4,60	9,31	10,40	8,70	17,03	5,81
Na+ (gm/l)	4,26	9,42	9,75	8,14	5,90	7,51	6,99	6,93	8,47	6,75
K+ (mg/l)	0,41	0,49	1,28	1,20	0,61	0,59	0,79	0,64	1,75	0,91
Ca2+ (mg/l)	9,22	22,78	19,47	16,02	2,90	11,62	4,18	10,66	16,78	10,17
Mg2+ (mg/l)	1,22	1,90	4,48	3,56	0,99	1,57	1,37	1,92	3,38	1,66
∑ cation (meq/l)	0,76	1,72	1,80	1,48	0,50	1,05	0,65	1,01	1,53	0,96
∑ anions (meq/l)	0,72	1,72	1,73	1,59	0,54	1,13	0,73	1,00	1,54	1,00
CBE (%)	2	0	2	-4	-4	-4	-6	0	0	-2

Total (in ppb)	Y-01	Y-02	Y-03	Y-04	Y-05	Y-06	Y-07	Y-08	Y-09	Y-10
Mn	2,55	0,59	22,58	7,82	2,65	10,23	2,30	6,08	15,71	3,32
Fe	117,80	11,10	102,71	109,35	94,19	295,48	66,81	212,08	36,77	64,47
As	0,22	38,33	1,22	2,37	1,21	34,08	2,00	17,01	2,01	0,87
Ti	3,18	0,39	2,39	3,24		6,53	1,86	3,70	1,07	0,92
V	0,39	2,31	1,87	1,74		3,40	0,44	1,74	1,71	1,02
Cr	0,35	0,34	0,36	0,39		0,72	0,19	0,44	0,31	0,25
Co	0,06	0,01	0,09	0,07		0,22	0,06	0,13	0,05	0,03
Ni	0,23	0,08	4,56	1,96		0,77	0,74	0,26	9,15	0,11
Cu	0,76	0,82	2,11	1,46		2,65	0,84	1,71	3,48	0,81
Al	140,26	28,63	73,27	123,37		260,71	77,27		39,82	57,20
Rb	0,34	1,33	0,91	1,01		1,50	0,45	0,87	1,11	0,94
Sr	37,55	138,75	95,41	98,09		74,13	80,45	79,11	92,41	54,60
Y	0,14	0,02	0,09	0,11		0,17	0,10	0,11	0,05	0,05
Cd	0,00	0,00	0,01	0,02		0,13	0,07	0,04	0,04	0,06
Ba	5,39	0,77	6,61	6,27		2,43	1,39	2,99	40,55	16,55
La	0,17	0,02	0,14	0,13		0,26	0,11	0,17	0,04	0,05
Ce	0,52	0,02	0,18	0,22		0,59	0,19	0,34	0,05	0,07
Nd	0,17	0,02	0,09	0,11		0,22	0,13	0,16	0,04	0,05
Pb	d.l.	d.l.	d.l.	d.l.		1,77	d.l.	0,38	d.l.	d.l.

Filtered (in ppb)	Y-01	Y-02	Y-03	Y-04	Y-05	Y-06	Y-07	Y-08	Y-09	Y-10
Mn	2,42	0,15	19,87	2,71	0,45	0,71	0,79	0,41	16,63	4,34
Fe	134,44	5,71	41,09	20,48	18,04	23,18	59,66	19,18	34,40	98,79
As	0,18	39,70	1,82	2,61	1,33	36,94	2,73	18,24	2,18	0,94
Ti	4,19	0,19	0,52	0,37	0,47	1,15	12,89	0,11	0,63	1,83
V	0,47	2,45	1,84	1,80	0,36	3,11	0,55	1,52	1,90	1,18
Cr	0,47	0,31	0,26	0,29	0,16	0,39	0,20	0,21	0,28	0,32
Co	0,07	0,01	0,08	0,03	0,02	0,02	0,04	0,02	0,05	0,04
Ni	0,30	0,06	4,81	1,89	0,14	0,31	0,18	0,11	10,59	0,29
Cu	0,30	0,13	0,86	0,65	0,27	0,59	0,10	0,02	2,06	0,73
Al	289,39	20,43	33,99	29,41	30,55	35,40	92,62	19,02	30,70	110,65
Rb	0,48	0,86	0,83	0,75	0,30	0,60	0,36	0,49	1,07	1,00
Sr	54,77	133,31	92,73	89,93	54,16	68,42	82,79	76,06	88,70	51,17
Y	0,15	0,02	0,04	0,03	0,06	0,03	0,07	0,03	0,04	0,07
Cd	0,00	0,00	0,05	0,03	0,02	0,05	0,01	0,03	0,05	0,06
Ba	55,91	32,67	14,47	50,08	22,82	44,12	8,46	7,84	39,60	6,26
La	0,15	0,01	0,03	0,03	0,06	1,64	0,07	0,03	0,03	0,07
Ce	0,54	0,02	0,04	0,03	0,08	2,39	0,10	0,03	0,04	0,10
Nd	0,15	0,01	0,03	0,02	0,05	0,53	0,06	0,02	0,02	0,06
Pb	0,13	0,14	0,12	0,07	0,10	0,31	0,22	0,15	0,30	0,13

DTI	Y-01	Y-02	Y-03	Y-04	Y-05	Y-06	Y-07	Y-08	Y-09	Y-10
Mn	95	26	88	35	17	7	34	7	106	131
Fe	114	51	40	19	19	8	89	9	94	153
As	82	104	150	110	109	108	136	107	108	108
Ti	132	49	22	11		18	693	3	59	199
V	120	106	98	103		92	125	88	111	115
Cr	135	91	72	75		54	109	49	90	130
Co	114	69	85	36		10	59	15	106	132
Ni	128	69	106	97		40	25	43	116	254
Cu	40	15	40	45		22	11	1	59	91
Al	206	71	46	24		14	120		77	193
Rb	141	65	91	74		40	79	56	96	106
Sr	146	96	97	92		92	103	96	96	94
Y	106	70	45	32		20	73	23	74	136
Cd	110	124	446	138		36	12	77	111	100
Ba	1038	4266	219	799		1818	609	263	98	38
La	88	52	21	20		621	58	15	75	135
Ce	103	99	22	15		405	51	10	71	149
Nd	89	32	28	22		236	51	15	57	115
Pb						18		38		

YONOGAWA

Sample#	**Y-11**	**Y-12**	**Y-13**	**Y-14**	**Y-15**	**Y-16**	**Y-17**	**Y-18**	**Y-19**	**Y-20**
Date (y/m/d)	23/03/13	23/03/13	23/03/13	23/03/13	23/03/13	23/03/13	23/03/13			
GPS	34,93	34,93	34,93	34,93	34,93	34,93	34,93	34,93	34,93	34,93
	135,49	135,48	135,48	135,46	135,48	135,48	135,48	135,49	135,49	135,49
Temp°C	12,10	10,80	8,70	10,80	9,00	7,10	6,70	10,80	11,60	9,20
pH	7,74	7,37	7,50	7,15	7,86	7,57	7,63	7,57	7,85	7,49
EC (uS/cm)	80,80	79,60	47,70	70,50	88,90	64,50	39,70	49,50	81,20	33,50
EC 25°C	*59,95*	*56,99*	*32,15*	*50,48*	*60,45*	*41,41*	*25,17*	*35,44*	*59,44*	*22,91*
TDS (mg/l)	*26,98*	*25,65*	*14,47*	*22,72*	*27,20*	*18,63*	*11,33*	*15,95*	*26,75*	*10,31*
DO (mg/l)	5,11	7,26	7,23	6,09	6,00	5,73	6,71	7,65	6,15	6,06
ORP (mV)	258,00	242,00	302,00	293,00	287,00	271,00	298,00	270,00	288,00	278,00
TOC (mg/l)										
DOC (mg/l)										
HCO3- (mg/l)	38,13	17,54	17,84	25,77	62,53	31,42	18,30	34,16	52,46	14,82
F (mg/l)	0,24	0,06	0,06	0,13	0,19	0,22	0,13	0,19	0,29	0,29
Cl (mg/l)	7,12	20,04	9,34	7,38	6,65	11,02	7,57	6,17	7,63	3,10
Br (mg/l)	n.d.	n.d.	n.d.	n.d.	n.d.	0,02	n.d.	n.d.	n.d.	n.d.
NO3 (mg/l)	0,41	0,48	0,09	1,73	0,91	1,01	0,16	0,41	0,41	0,07
PO4 (mg/l)	n.d.	n.d.	n.d.	n.d.	n.d.	n.d.	n.d.	n.d.	n.d.	n.d.
SO4 (mg/l)	5,46	5,12	5,98	5,80	0,96	2,66	1,61	4,61	5,74	3,96
Na+ (gm/l)	6,77	8,83	8,06	9,33	8,99	7,14	6,74	7,45	7,89	5,66
K+ (mg/l)	0,93	0,75	0,53	0,77	1,29	0,96	0,56	2,17	1,14	0,37
Ca2+ (mg/l)	9,92	9,28	4,04	5,73	13,19	8,68	2,89	7,08	13,48	2,55
Mg2+ (mg/l)	1,50	1,23	0,33	1,62	2,75	1,70	0,84	1,26	2,24	0,43
∑ cation (meq/l)	0,94	0,97	0,59	0,84	1,31	0,91	0,52	0,84	1,23	0,42
∑ anions (meq/l)	0,98	1,00	0,69	0,88	1,31	0,97	0,57	0,87	1,24	0,43
CBE (%)	-2	-1	-8	-2	0	-3	-4	-2	0	-2
Unfiltered (in ppb)	**Y-11**	**Y-12**	**Y-13**	**Y-14**	**Y-15**	**Y-16**	**Y-17**	**Y-18**	**Y-19**	**Y-20**
Mn	4,48	120,82	0,61	0,10	0,56	*missing*	0,30	0,49	0,99	2,36
Fe	67,37	1952,54	11,21	2,70	23,90		5,79	8,81	13,24	21,08
As	1,01	0,34	0,13	0,36	0,22		0,40	0,39	2,00	0,16
Ti	1,33	5,66	1,45	1,12	14,56		2,08	3,26	3,21	2,58
V	0,89	0,49	0,19	0,51	2,20		0,42	0,80	1,44	0,25
Cr	0,23	0,39	0,36	0,55	0,92		0,30	0,42	0,52	0,62
Co	0,03	0,62	0,03	0,02	0,10		0,04	0,04	0,06	0,05
Ni	0,14	21,32	0,16	0,19	0,46		0,15	0,86	0,24	0,52
Cu	1,80	17,10	0,61	3,00	0,60		0,48	0,56	0,81	7,59
Al	54,85	300,76	112,44	19,77	365,02		80,84	104,59	128,06	140,91
Rb										
Sr	32,44	31,96	8,48	54,50	87,14		24,86	24,11	44,29	7,02
Y	0,09	4,85	0,57	0,01	0,21		0,20	0,16	0,11	0,54
Cd	0,09	0,06	0,05	0,05	0,05		0,03	0,01	0,03	0,02
Ba	6,04	13,72	5,92	1,10	3,43		4,38	5,43	7,50	3,63
La	0,10	3,63	0,49	0,01	0,26		0,22	0,16	0,12	0,43
Ce	0,13	3,08	0,45	0,08	0,42		0,21	0,23	0,19	0,62
Nd	0,08	3,69	0,46	0,01	0,22		0,19	0,13	0,10	0,43
Pb	0,10	0,91	0,33	0,22	0,32		0,15	0,14	0,18	0,46

Filtered (in ppb)	Y-11	Y-12	Y-13	Y-14	Y-15	Y-16	Y-17	Y-18	Y-19	Y-20
Mn	4,05	6,33	3,35	0,13	0,49	0,78	1,48	1,69	3,85	8,23
Fe	64,79	20,17	151,95	3,05	13,54	24,91	42,07	59,54	36,57	119,31
As	1,10	0,05	0,15	0,03	0,26	1,26	0,45	0,37	0,31	2,01
Ti	0,97	0,17	1,70	0,03	0,39	0,53	0,51	0,90	0,58	1,90
V	0,92	0,00	0,24	0,05	1,84	1,02	0,40	0,42	0,80	1,56
Cr	0,25	0,23	0,41	0,02	0,31	0,31	0,32	0,34	0,26	0,38
Co	0,03	0,01	0,31	0,01	0,02	0,06	0,07	0,07	0,05	0,15
Ni	0,19	0,09	0,98	0,06	0,40	0,75	0,66	0,69	1,66	0,94
Cu	0,78	0,11	1,98	0,30	0,13	0,59	0,26	0,87	3,42	1,21
Al	57,55	27,02	127,76	2,42	27,21	38,39	62,94	64,02	37,24	86,16
Rb	1,05	0,92	1,02	0,02	0,27	0,81	0,52	0,53	2,11	1,03
Sr	46,56	49,67	16,25	8,00	119,90	69,19	36,09	36,26	37,87	62,57
Y	0,06	0,11	0,31	0,00	0,02	0,02	0,11	0,11	0,07	0,05
Cd	0,04	0,05	0,06	0,04	0,10	0,25	0,06	0,06	0,07	0,03
Ba	13,79	124,41	47,74	1,31	8,53	99,04	119,02	125,50	12,83	37,14
La	0,06	0,06	0,27	0,00	0,02	0,02	0,11	0,11	0,05	0,05
Ce	0,09	0,05	0,23	0,00	0,02	0,02	0,08	0,08	0,06	0,06
Nd	0,05	0,05	0,22	0,00	0,01	0,01	0,11	0,11	0,05	0,03
Pb	0,29	0,07	0,70	0,00	0,00	0,06	0,05	0,13	0,13	0,12

DTI	Y-11	Y-12	Y-13	Y-14	Y-15	Y-16	Y-17	Y-18	Y-19	Y-20
Mn	90	5	546	127	87		497	341	390	348
Fe	96	1	1356	113	57		727	676	276	566
As	109	15	117	9	115		112	96	16	1255
Ti	73	3	117	3	3		25	28	18	74
V	104	1	126	10	84		96	53	56	635
Cr	112	59	113	3	34		109	80	49	61
Co	95	1	996	33	22		172	157	94	321
Ni	138	0	602	31	88		432	81	683	182
Cu	43	1	325	10	22		55	156	425	16
Al	105	9	114	12	7		78	61	29	61
Rb										
Sr	144	155	192	15	138		145	150	85	892
Y	63	2	55	10	7		58	73	61	8
Cd	49	90	123	84	189		220	669	228	203
Ba	228	907	806	118	248		2720	2310	171	1022
La	54	2	54	7	6		51	74	43	12
Ce	71	2	51	6	4		39	36	30	9
Nd	56	1	48	4	5		56	80	48	8
Pb	302	8	210	2	-1		33	94	73	26

YONOGAWA

Sample#	Y-21	Y-22	Y-23	Y-24	Y-25	Y-26	Y-27	Y-28	Y-30	Y-31
Date (y/m/d)										08/07/2013
GPS	34,94	34,94	34,94	34,92	34,93	34,94	34,92	34,93	34,93	34,8741
	135,49	135,49	135,50	135,50	135,51	135,51	135,51	135,51	135,52	135,4648
Temp°C	11,10	12,60	10,50	14,70	14,30	9,60	12,60	10,00	9,30	22,10
pH	8,00	7,81	7,95	8,23	8,26	7,33	7,86	7,87	8,05	7,85
EC (uS/cm)	57,10	58,60	49,80	169,50	82,80	31,30	92,50	46,40	48,20	142,50
EC 25°C	*41,23*	*44,07*	*35,36*	*134,58*	*65,08*	*21,66*	*69,56*	*30,50*	*31,86*	*151,27*
TDS (mg/l)	*18,55*	*19,83*	*15,91*	*60,56*	*29,29*	*9,75*	*31,30*	*13,73*	*14,34*	*68,07*
DO (mg/l)	5,36	7,12	7,16	6,08	5,70	5,64	5,68	6,18	154,00	4,49
ORP (mV)	87,00	143,00	104,00	108,00	127,00	208,00	187,00	194,00	6,14	968,00
TOC (mg/l)										1,37
DOC (mg/l)										1,41
HCO3- (mg/l)	32,94	33,92	26,96	73,20	51,24	16,84	56,97	31,72	28,06	63,44
F (mg/l)	0,15	0,17	0,13	0,14	0,11	0,06	0,09	0,10	0,09	0,27
Cl (mg/l)	4,00	4,02	5,98	6,01	4,43	3,74	5,39	3,29	4,10	6,13
Br (mg/l)	n.d.	n.d.	n.d.	n.d.	n.d.	n.d.	n.d.	n.d.	n.d.	0,04
NO3 (mg/l)	0,25	0,26	0,43	1,53	0,14	0,47	0,39	0,10	0,35	0,26
PO4 (mg/l)	n.d.	n.d.	n.d.	n.d.	n.d.	n.d.	0,03	n.d.	n.d.	n.d.
SO4 (mg/l)	4,13	4,38	2,46	31,72	4,28	2,71	6,43	2,05	2,90	9,23
Na+ (gm/l)	6,12	6,12	7,62	9,47	7,41	5,15	6,99	5,96	5,87	7,25
K+ (mg/l)	0,47	0,56	0,51	1,28	0,66	0,70	0,90	0,77	0,53	1,63
Ca2+ (mg/l)	7,00	7,30	4,46	23,83	11,17	2,97	12,91	4,84	5,49	17,29
Mg2+ (mg/l)	1,35	1,30	1,12	5,22	2,06	0,88	3,20	1,47	1,36	2,76
∑ cation (meq/l)	0,74	0,75	0,66	2,06	1,07	0,46	1,23	0,64	0,65	1,45
∑ anions (meq/l)	0,76	0,79	0,70	2,15	1,07	0,47	1,25	0,67	0,67	1,44
CBE (%)	-2	-2	-3	-2	0	-1	-1	-2	-1	0
Unfiltered (in ppb)	**Y-21**	**Y-22**	**Y-23**	**Y-24**	**Y-25**	**Y-26**	**Y-27**	**Y-28**	**Y-30**	**Y-31**
Mn	1,01	0,59	2,15	3,07	1,22	8,47	3,71	0,26	0,30	60,07
Fe	22,75	10,18	94,03	8,23	22,34	121,15	14,50	8,64	10,21	458,90
As	0,47	0,44	6,28	4,20	8,97	5,00	4,94	10,67	6,31	0,86
Ti	10,43	3,94	56,50	1,58	5,18	39,74	4,15	3,48	5,04	12,99
V	1,58	1,18	3,34	2,94	1,87	2,50	2,66	1,84	2,01	2,56
Cr	0,67	0,50	1,96	0,58	0,87	2,14	0,67	0,56	0,60	0,62
Co	0,09	0,04	0,37	0,07	0,10	0,70	0,07	0,05	0,05	0,23
Ni	0,32	0,33	0,92	19,21	0,36	0,91	0,18	0,23	0,19	0,61
Cu	0,59	0,62	1,55	0,73	1,17	1,45	0,68	0,60	0,66	1,32
Al	298,37	123,21		34,51	175,55		79,41	92,56	103,31	485,94
Rb	0,69	0,72	2,30	0,56	0,76	2,74	0,58	0,88	0,66	3,29
Sr	30,51	31,97	32,56	138,34	62,41	26,22	80,41	42,73	44,83	89,29
Y	0,22	0,09	4,90	0,06	0,15	0,84	0,07	0,11	0,09	0,58
Cd	0,01	0,08	0,06	0,02	0,02	0,11	0,08	0,03	0,01	0,13
Ba	6,18	5,83	13,38	7,83	4,31	10,19	7,78	5,36	3,48	64,86
La	0,27	0,14	1,27	0,05	0,20	0,99	0,07	0,14	0,11	0,81
Ce	0,44	0,21	2,01	0,06	0,38	1,67	0,13	0,24	0,17	1,63
Nd	0,22	0,13	1,11	0,04	0,18	0,91	0,07	0,14	0,10	5,73
Pb	0,20	0,16	0,67	0,04	0,34	1,34	0,25	0,15	0,15	1,19

Filtered (in ppb)	Y-21	Y-22	Y-23	Y-24	Y-25	Y-26	Y-27	Y-28	Y-30	Y-31
Mn	4,14	4,40	1,84	32,69	6,71	53,13	39,13	1,55	1,61	45,78
Fe	42,49	96,49	163,84	100,76	130,85	960,19	47,22	103,60	60,21	62,98
As	0,49	0,46	6,78	5,12	11,33	4,64	6,13	13,13	7,77	0,59
Ti	0,49	1,05	4,96	0,94	2,97	39,55	0,74	2,85	2,55	21,42
V	1,42	1,24	1,58	3,64	2,08	2,10	3,04	2,38	2,33	1,80
Cr	0,28	0,30	0,47	0,45	0,49	1,42	0,40	0,49	0,42	0,37
Co	0,05	0,20	0,12	0,17	0,07	0,49	0,06	0,04	0,03	0,07
Ni	0,68	0,74	0,84	23,24	0,88	2,45	0,32	0,63	0,52	1,15
Cu	0,37	0,50	0,71	0,56	1,63	4,57	0,32	0,48	0,24	1,79
Al	68,71	65,98	482,74	32,08	188,40	1385,90	36,75	122,88	108,98	64,54
Rb	0,47	0,54	0,51	0,55	0,58	2,11	0,48	0,64	0,51	2,69
Sr	38,08	37,14	44,72	128,67	66,27	29,34	83,22	46,11	45,67	93,54
Y	0,06	0,07	0,16	0,04	0,08	0,48	0,04	0,05	0,06	0,12
Cd	0,03	0,02	0,05	0,06	0,07	0,20	0,07	0,06	0,04	0,21
Ba	10,30	39,56	168,19	53,79	141,51	123,00	27,45	93,27	66,05	271,28
La	0,06	0,07	0,22	0,05	0,08	0,56	0,03	0,05	0,05	0,15
Ce	0,07	0,07	0,25	0,04	0,14	1,02	0,04	0,07	0,07	0,19
Nd	0,05	0,05	0,18	0,03	0,07	0,49	0,03	0,05	0,05	8,67
Pb	0,08	0,15	0,18	0,13	0,11	0,84	0,33	0,10	0,19	0,31

DTI	Y-21	Y-22	Y-23	Y-24	Y-25	Y-26	Y-27	Y-28	Y-30	Y-31
Mn	410	741	86	1066	551	628	1056	596	533	76
Fe	187	948	174	1224	586	793	326	1199	590	14
As	104	104	108	122	126	93	124	123	123	69
Ti	5	27	9	60	57	100	18	82	51	165
V	90	105	47	124	111	84	114	129	116	70
Cr	42	59	24	78	56	66	59	88	70	59
Co	57	446	33	237	70	70	82	73	61	32
Ni	214	221	91	121	242	270	175	275	276	188
Cu	62	81	46	77	139	314	47	81	36	136
Al	23	54		93	107		46	133	105	13
Rb	69	76	22	98	77	77	82	74	77	82
Sr	125	116	137	93	106	112	103	108	102	105
Y	28	71	3	70	49	57	58	45	60	20
Cd	180	24	91	266	325	179	82	230	325	165
Ba	167	678	1257	687	3281	1207	353	1740	1899	418
La	24	48	17	97	40	56	43	40	46	18
Ce	16	32	12	63	36	61	33	28	39	11
Nd	24	39	16	69	40	54	38	34	45	151
Pb	40	94	26	362	31	63	131	67	123	26

YONOGAWA

Sample#	Y-03J	Y-32	Y-04J	Y-09J	Y-33	Y-11J	Y-34	Y-35	Y-36
Date (y/m/d)	08/07/2013	08/07/2013	09/07/2013	07/07/2013	09/07/2013	07/07/2013	09/07/2013	08/07/2013	08/07/2013
GPS	34,8936	34,8935	34,8934	34,9204	34,9014	34,9312	34,9095	34,9292	34,9332
	135,4729	135,4728	135,4729	135,4940	135,4814	135,4900	135,4848	135,4786	135,4899
Temp°C	25,60	25,80	24,80	26,80	25,00	25,00	26,10	20,90	23,40
pH	7,63	7,89	8,24	7,68	8,31	7,43	8,02	7,74	7,82
EC (uS/cm)	195,80	200,80	181,20	196,90	187,80	148,40	200,00	70,10	126,60
EC 25°C	*193,48*	*197,64*	*181,93*	*190,06*	*187,80*	*148,40*	*195,69*	*76,36*	*130,79*
TDS (mg/l)	*87,07*	*88,94*	*81,87*	*85,53*	*84,51*	*66,78*	*88,06*	*34,36*	*58,85*
DO (mg/l)	5,49	4,57	4,62	5,24	4,80	5,28	4,95	5,73	5,35
ORP (mV)	930,00	884,00	879,00	904,00	876,00	897,00	948,00	867,00	863,00
TOC (mg/l)	0,64	0,85	0,40		0,35	1,25	0,48	1,14	0,71
DOC (mg/l)	0,82	0,66	0,54		0,49	1,01	0,51	0,91	0,70
HCO3- (mg/l)	81,74	90,28	75,88	79,30	80,52	56,12	85,40	32,21	79,30
F (mg/l)	0,23	0,21	0,23	0,25	0,26	0,27	0,25	0,12	0,11
Cl (mg/l)	7,32	7,32	7,20	7,18	7,37	9,13	7,45	3,88	5,39
Br (mg/l)	n.d.	0,06	0,05	n.d.	0,02	n.d.	n.d.	n.d.	0,02
NO3 (mg/l)	0,53	0,42	0,66	0,49	0,58	0,56	0,51	0,24	0,55
PO4 (mg/l)	0,10	n.d.	0,19	0,19	0,12	n.d.	0,13	0,19	0,17
SO4 (mg/l)	11,10	10,75	11,09	12,57	11,00	6,03	11,11	2,41	7,07
Na+ (gm/l)	8,44	8,51	7,99	8,28	8,79	7,59	8,43	5,12	5,98
K+ (mg/l)	2,08	2,06	1,80	2,12	1,79	2,19	1,88	1,14	1,75
Ca2+ (mg/l)	21,94	23,57	21,00	21,26	22,08	16,19	22,42	7,03	14,38
Mg2+ (mg/l)	4,41	4,63	3,99	4,34	4,35	2,43	4,51	1,69	2,97
∑ cation (meq/l)	1,88	1,98	1,77	1,83	1,89	1,39	1,90	0,74	1,27
∑ anions (meq/l)	1,83	1,95	1,74	1,82	1,82	1,36	1,89	0,72	1,65
CBE (%)	1	1	1	0	2	1	0	2	-13
Total (in ppb)	**Y-03J**	**Y-32**	**Y-04J**	**Y-09J**	**Y-33**	**Y-11J**	**Y-34**	**Y-35**	**Y-36**
Mn	32,00	38,35	9,32	36,60	15,46	13,39	28,48	87,92	66,49
Fe	270,42	340,52	191,29	207,22	320,65	156,98	268,63	385,04	614,06
As	2,17	0,90	3,77	4,40	3,39	1,91	2,67	19,68	1,90
Ti	5,61	6,54	6,12	3,91	10,13	2,35	6,42	6,24	20,39
V	3,24	3,30	3,06	3,77	3,55	1,62	3,27	4,16	4,80
Cr	0,48	0,58	0,52	0,44	0,75	0,33	0,57	0,52	0,87
Co	0,13	0,15	0,10	0,09	0,12	0,06	0,12	0,31	0,30
Ni	1,70	0,50	0,87	3,28	1,15	0,42	1,33	0,77	0,63
Cu	2,61	2,10	1,67	3,47	1,64	2,09	1,55	1,16	1,63
Al	188,44	235,37	174,90	89,25	419,02	89,32	194,77	168,44	332,69
Rb	2,28	2,53	2,03	2,19	2,58	3,94	2,10	1,76	2,55
Sr	128,37	136,91	123,60	127,04	143,27	94,41	142,38	63,06	98,28
Y	0,20	0,26	0,15	0,11	0,22	0,13	0,19	0,20	0,26
Cd	0,18	0,24	0,13	0,15	0,17	0,19	0,12	0,10	0,19
Ba	75,50	74,01	62,69	79,31	78,13	112,87	82,23	48,48	112,89
La	0,24	0,35	0,20	0,12	0,26	0,14	0,23	0,22	0,31
Ce	0,49	0,72	0,40	0,22	0,54	0,22	0,46	0,42	0,62
Nd	1,73	2,59	1,42	0,88	1,95	1,03	1,66	1,74	2,25
Pb	1,20	0,88	0,71	0,45	0,87	0,47	0,68	0,42	0,59

Filtered (in ppb)	Y-03J	Y-32	Y-04J	Y-09J	Y-33	Y-11J	Y-34	Y-35	Y-36
Mn	21,91	21,78	1,90	26,68	4,46	9,47	19,79	75,59	35,55
Fe	89,20	93,43	38,95	100,42	46,03	84,49	145,26	205,53	94,55
As	1,88	0,67	2,96	3,22	2,62	1,29	1,97	14,45	1,35
Ti	55,49	6,92	13,74	9,87	8,34	6,69	41,68	15,25	20,60
V	2,75	2,75	2,57	3,33	2,73	1,37	2,82	3,57	3,43
Cr	0,32	0,30	0,31	1,01	0,42	0,18	0,39	0,23	0,35
Co	0,05	0,05	0,02	0,05	0,03	0,03	0,06	0,29	0,10
Ni	4,48	0,72	2,45	9,14	2,74	1,11	3,77	2,15	1,04
Cu	2,74	1,99	2,20	2,25	1,87	2,72	1,91	1,31	1,36
Al	35,27	46,86	34,91	53,66	38,13	30,67	109,31	65,00	29,05
Rb	1,92	2,14	1,86	1,78	1,57	3,47	1,85	1,37	1,77
Sr	130,17	138,77	127,44	126,13	130,62	87,95	134,08	61,75	93,62
Y	0,07	0,09	0,05	0,06	0,05	0,07	0,11	0,14	0,04
Cd	0,16	0,17	0,11	0,12	0,17	0,18	0,11	0,10	0,08
Ba	171,39	125,41	93,42	158,74	854,87	220,27	217,61	234,16	213,51
La	0,07	0,10	0,05	0,05	0,05	0,07	0,12	0,13	0,04
Ce	0,11	0,14	0,07	0,11	0,06	0,09	0,21	0,22	0,06
Nd	5,18	6,55	3,52	3,99	3,14	5,14	8,32	12,78	3,12
Pb	0,19	0,14	0,10	0,15	0,13	0,15	0,29	0,19	0,04

DTI	Y-03J	Y-32	Y-04J	Y-09J	Y-33	Y-11J	Y-34	Y-35	Y-36
Mn	68	57	20	73	29	71	69	86	53
Fe	33	27	20	48	14	54	54	53	15
As	86	75	78	73	77	68	74	73	71
Ti	989	106	225	253	82	284	649	244	101
V	85	83	84	88	77	85	86	86	71
Cr	66	52	60	230	56	55	68	44	40
Co	36	34	25	56	25	55	52	91	32
Ni	264	144	282	279	239	263	282	279	165
Cu	105	95	132	65	114	130	123	114	83
Al	19	20	20	60	9	34	56	39	9
Rb	84	85	92	81	61	88	88	78	69
Sr	101	101	103	99	91	93	94	98	95
Y	37	35	35	51	24	56	58	69	17
Cd	89	71	83	79	105	93	92	94	43
Ba	227	169	149	200	1094	195	265	483	189
La	31	27	27	45	18	52	53	61	14
Ce	22	19	18	51	11	40	47	53	9
Nd	299	253	249	453	161	497	500	736	138
Pb	16	16	14	32	15	33	42	46	7

YONOGAWA

Sample#	**Y-26J**	**Y-37**	**Y-38**	**Y-39**
Date (y/m/d)	08/07/2013	09/07/2013	09/07/2013	09/07/2013
GPS	34,9395 135,5114	34,8746 135,4532	34,8791 135,4591	34,8846 135,4632
Temp°C	19,60	25,50	24,40	24,60
pH	7,71	7,97	8,11	8,12
EC (uS/cm)	46,40	184,40	184,20	179,80
EC 25°C	*52,02*	*182,57*	*186,44*	*181,25*
TDS (mg/l)	*23,41*	*82,16*	*83,90*	*81,56*
DO (mg/l)	6,51	4,85	5,24	5,07
ORP (mV)	928,00	947,00	905,00	880,00
TOC (mg/l)	0,84	0,33	0,30	0,31
DOC (mg/l)	1,00	0,41	0,32	0,39
HCO3- (mg/l)	43,92	75,64	75,64	75,64
F (mg/l)	0,05	0,22	0,23	0,23
Cl (mg/l)	2,84	7,04	6,85	6,96
Br (mg/l)	n.d.	n.d.	0,03	0,01
NO3 (mg/l)	0,28	0,68	0,68	0,68
PO4 (mg/l)	n.d.	n.d.	0,10	n.d.
SO4 (mg/l)	2,87	11,67	11,20	11,18
Na+ (gm/l)	4,30	7,98	7,88	8,57
K+ (mg/l)	0,88	1,89	1,81	1,78
Ca2+ (mg/l)	4,38	21,30	20,96	20,98
Mg2+ (mg/l)	1,12	3,85	3,87	3,89
∑ cation (meq/l)	0,52	1,78	1,75	1,79
∑ anions (meq/l)	0,88	1,74	1,73	1,73
CBE (%)	-26	1	1	2
Unfiltered (in ppb)	**Y-26J**	**Y-37**	**Y-38**	**Y-39**
Mn	21,69	8,51	7,69	8,93
Fe	269,17	165,19	169,62	181,99
As	5,26	5,70	5,21	4,89
Ti	8,21	4,48	4,44	5,39
V	0,78	3,00	3,11	3,22
Cr	0,52	0,60	0,62	0,57
Co	0,14	0,08	0,09	0,10
Ni	0,33	1,01	0,80	0,88
Cu	0,54	1,84	1,59	1,79
Al	251,30	139,48	159,59	174,95
Rb	2,55	2,21	2,16	2,28
Sr	41,90	137,69	137,81	138,18
Y	0,21	0,12	0,13	0,15
Cd	0,08	0,17	0,19	0,20
Ba	47,13	65,78	67,93	67,07
La	0,20	0,16	0,17	0,19
Ce	0,37	0,32	0,35	0,38
Nd	1,63	1,13	1,25	1,38
Pb	0,42	0,55	0,73	0,99

Filtered (in ppb)	Y-26J	Y-37	Y-38	Y-39
Mn	14,64	2,65	2,16	2,52
Fe	160,78	29,01	32,17	41,05
As	3,80	4,16	3,96	3,56
Ti	37,78	14,21	12,69	14,39
V	0,58	2,50	2,52	2,66
Cr	0,40	0,39	0,39	0,54
Co	0,08	0,03	0,03	0,03
Ni	0,85	2,34	2,23	2,54
Cu	0,92	2,15	1,99	1,94
Al	147,17	30,43	34,19	72,66
Rb	1,49	1,80	1,77	1,62
Sr	40,52	126,38	125,60	125,50
Y	0,16	0,04	0,05	0,06
Cd	0,11	0,14	0,22	0,35
Ba	570,59	196,25	161,18	994,02
La	0,14	0,04	0,05	0,05
Ce	0,26	0,06	0,07	0,07
Nd	12,17	2,87	3,46	3,67
Pb	0,31	0,11	0,10	0,15

DTI	Y-26J	Y-37	Y-38	Y-39
Mn				
Fe				
As				
Ti				
V				
Cr				
Co				
Ni				
Cu				
Al				
Rb				
Sr				
Y				
Cd				
Ba				
La				
Ce				
Nd				
Pb				

MINOGAWA

Sample#	M-01	M-02	M-03	M-04	M-05	M-06	M-07	M-08	M-09	M-10
Date (j/m/y)	01/05/13	01/05/13	01/05/13	01/05/13	01/05/13	01/05/13	01/05/13	01/05/13	01/05/13	01/05/13
GPS	34,892442 135,49597	34,891907 135,49488	34,891298 135,49553	34,88886 135,4981	34,89025 135,4906	34,891363 135,49443	34,887679 135,48870	34,887601 135,48861	34,887506 135,48861	34,88769 135,4888
Temp°C	9,8	9	8,6	8,7	12,1	10	13,2	11,1	11,9	12,2
pH	7,45	7,69	7,6	7,54	7,76	7,54	7,54	7,43	7,24	7,67
EC (uS/cm)	51,3	43,6	45,5	63,5	58,5	53,1	88,5	88,4	86,3	78,6
EC 25°C	*73,7*	*64,1*	*67,7*	*94,2*	*78,8*	*75,9*	*115,8*	*122,4*	*116,9*	*105,6*
DO (mg/l)	6,72	7,07	5,95	5,41	6,48	6,27	5,2	5,57	4,99	6,28
ORP (mV)	282	281	281	268	267	244	214	228	238	224
TOC (mg/l)	2,58	1,99	3,23	2,36	2,76	2,36	5,47	2,75	4,77	2,97
DOC (mg/l)	3,33	2,10	2,92	2,16	2,28	2,62	5,34	2,58	4,64	3,32
HCO3- (mg/l)	19,17	15,25	20,92	35,95	24,40	21,79	35,95	17,21	32,90	32,25
F (mg/l)	0,14	0,11	0,11	0,13	0,15	0,15	0,40	0,08	0,33	0,23
Cl (mg/l)	4,28	4,10	4,83	5,42	4,50	4,19	8,29	10,44	8,90	6,72
Br (mg/l)	n.d.	n.d.	n.d.	n.d.	n.d.	0,02	n.d.	n.d.	n.d.	n.d.
NO3 (mg/l)	1,38	1,40	0,91	1,28	1,01	1,12	0,86	3,39	1,36	1,00
PO4 (mg/l)	n.d.	n.d.	n.d.	0,09	0,10	n.d.	0,2864	0,2226	0,1511	n.d.
SO4 (mg/l)	4,69	4,46	3,87	3,64	4,59	3,43	8,33	10,87	8,77	7,46
Na+ (mg/l)	5,66	5,09	5,03	5,55	5,12	5,23	6,52	6,62	6,37	5,60
K+ (mg/l)	0,66	0,59	0,64	0,84	0,77	0,60	1,58	3,24	1,94	1,12
Ca2+ (mg/l)	6,40	5,77	7,47	11,01	8,39	7,29	12,80	11,29	12,52	11,34
Mg2+ (mg/l)	1,16	1,05	1,51	2,20	1,52	1,27	2,22	2,24	2,28	2,15
∑ cation	0,68	0,61	0,73	0,99	0,79	0,71	1,15	1,12	1,14	1,02
∑ anions	0,64	0,56	0,63	0,92	0,71	0,63	1,09	1,06	1,09	0,96
CBE (%)	3	4	7	4	5	6	3	3	2	3

Total (in ppb)	M-01	M-02	M-03	M-04	M-05	M-06	M-07	M-08	M-09	M-10
Mn	8,61	2,86	1,91	1,06	6,46	32,91	22,58	3,29	16,48	7,02
Fe	275,16	79,39	56,58	22,22	222,58	854,54	408,53	59,27	257,68	130,45
As	0,21	0,18	0,28	0,33	0,38	0,37	3,43	0,57	2,58	1,22
Ti	12,13	3,11	2,32	1,11	10,64	35,45	16,53	2,60	9,84	6,51
V	1,27	0,75	1,00	1,85	2,10	3,09	5,30	0,66	4,19	2,95
Cr	0,32	0,18	0,23	0,38	0,68	1,25	1,47	0,56	1,17	0,69
Co	0,12	0,04	0,09	0,03	0,12	0,37	0,19	0,05	0,14	0,08
Ni	0,14	0,10	0,20	0,10	0,28	0,53	0,76	0,37	0,58	0,27
Cu	0,76	0,44	0,80	0,46	0,72	1,19	2,32	1,79	2,31	1,38
Al	347,86	108,24	90,17	35,82	348,26	1208,59	587,89	71,75	377,46	211,37
Rb	1,84	1,17	0,80	0,57	1,25	2,65	2,52	3,54	2,60	1,45
Sr	41,25	33,98	37,64	63,69	42,66	38,61	55,19	72,52	59,58	52,88
Y	0,54	0,32	0,26	0,14	0,44	2,00	0,51	0,21	0,38	0,24
Cd	0,01	0,01	0,23	0,01	0,01	0,11	0,03	0,16	0,12	0,01
Ba	6,55	5,49	4,38	4,94	6,67	9,02	12,82	28,00	15,65	7,67
La	0,72	0,41	0,31	0,10	0,58	2,74	0,63	0,14	0,44	0,29
Ce	1,21	0,49	0,28	0,11	1,03	4,95	1,16	0,15	0,79	0,47
Nd	0,61	0,35	0,28	0,10	0,50	2,32	0,59	0,15	0,39	0,25
Pb	0,27	0,12	0,09	0,05	0,32	1,09	0,63	0,17	0,48	0,21

Filtered (in ppb)	M-01	M-02	M-03	M-04	M-05	M-06	M-07	M-08	M-09	M-10
Mn	0,41	0,33	0,34	0,31	6,30	1,37	15,15	1,64	12,57	3,72
Fe	9,75	6,67	8,01	9,52	208,47	24,75	71,65	13,40	55,80	26,25
As	0,14	0,15	0,32	0,31	0,36	0,29	2,94	0,56	2,49	1,06
Ti	0,76	0,81	0,26	0,66	8,55	0,93	1,29	0,41	1,06	1,58
V	0,74	0,64	0,83	1,73	1,95	0,96	4,12	0,53	3,39	2,45
Cr	0,17	0,17	0,24	0,41	0,67	0,33	0,63	0,41	0,49	0,47
Co	0,01	0,01	0,02	0,02	0,09	0,02	0,06	0,03	0,06	0,03
Ni	0,15	0,10	0,12	0,32	0,39	0,14	0,33	0,31	0,42	0,33
Cu	0,24	0,21	0,31	0,33	0,62	0,20	1,51	5,23	1,48	0,68
Al	21,20	15,07	19,68	11,37	342,56	54,60	97,96	22,75	63,43	64,64
Rb	0,82	0,99	0,59	0,57	1,24	0,68	1,66	3,50	2,22	1,32
Sr	40,20	34,63	38,26	65,51	45,02	37,67	56,25	75,53	60,38	54,48
Y	0,14	0,14	0,17	0,11	0,45	0,12	0,13	0,17	0,13	0,10
Cd	0,01	0,01	0,05	0,05	0,13	0,13	0,07	0,10	0,09	0,06
Ba	32,18	9,83	52,61	9,64	5,76	58,41	98,72	30,55	24,42	18,69
La	0,15	0,15	0,18	0,09	0,56	0,13	0,12	0,07	0,11	0,09
Ce	0,05	0,04	0,05	0,02	1,01	0,15	0,20	0,05	0,16	0,11
Nd	1,29	1,29	1,59	0,57	4,60	1,01	1,14	0,83	1,00	0,80
Pb	0,03	0,03	0,02	0,04	0,23	0,06	0,09	0,05	0,07	0,06

DTI	M-01	M-02	M-03	M-04	M-05	M-06	M-07	M-08	M-09	M-10
Mn	5	11	18	29	98	4	67	50	76	53
Fe	4	8	14	43	94	3	18	23	22	20
As	69	84	113	93	95	78	86	99	97	87
Ti	6	26	11	59	80	3	8	16	11	24
V	59	85	83	94	93	31	78	80	81	83
Cr	52	92	106	107	99	26	43	73	42	68
Co	12	29	22	67	82	6	31	57	42	36
Ni	108	101	58	320	139	27	43	84	73	123
Cu	31	47	39	72	87	17	65	292	64	49
Al	6	14	22	32	98	5	17	32	17	31
Rb	44	84	73	100	99	26	66	99	86	91
Sr	97	102	102	103	106	98	102	104	101	103
Y	26	44	67	80	103	6	26	83	34	40
Cd	93	113	23	680	1129	117	237	58	79	389
Ba	491	179	1201	195	86	647	770	109	156	244
La	21	37	59	88	98	5	20	54	24	30
Ce	4	8	18	24	99	3	18	34	20	24
Nd	211	368	562	586	920	43	194	564	256	320
Pb	12	26	25	71	71	5	13	33	15	27

MINOGAWA

Sample#	M-11	M-12	M-13	M-14	M-15	M-16	M-17	M-18
Date (j/m/y)	01/05/13	02/05/13	02/05/13	02/05/13	02/05/13	02/05/13	02/05/13	02/05/13
GPS	34,87801	34,88249	34,88242	34,88552	34,87393	34,871983	34,86868	34,864191
	135,48804	135,48859	135,48854	135,4891	135,4841	135,479239	135,478379	135,478597
Temp°C	12,8	12,9	13,6	12,9	13,3	11,5	11,5	**13,5**
pH	7,79	7,74	7,82	7,74	7,89	7,92	7,94	8,07
EC (uS/cm)	88	114,3	85,1	96,6	88,6	82,7	80,7	99,9
EC 25°C	*116,4*	*150,8*	*110,2*	*127,4*	*115,7*	*113,3*	*110,5*	***129,7***
DO (mg/l)	6,18	5,46	5,78	5,76	6,16	5,64	6,57	5,26
ORP (mV)	218	213	176	133	184	190	191	201
TOC (mg/l)	3,10	3,43	3,11	3,66	2,64	2,20	2,42	2,30
DOC (mg/l)	2,94	3,31	3,20	3,17	2,56	2,23	2,45	2,07
HCO3- (mg/l)	28,54	29,85	29,55	33,77	35,08	35,08	44,80	34,82
F (mg/l)	0,19	0,23	0,22	0,29	0,17	0,15	0,16	0,18
Cl (mg/l)	7,98	8,25	8,21	9,46	8,98	8,57	8,69	7,71
Br (mg/l)	0,0132	n.d.	n.d.	0,0393	0,0286	n.d.	n.d.	n.d.
NO3 (mg/l)	1,02	1,27	1,18	1,35	0,91	0,96	0,94	0,88
PO4 (mg/l)	0,07	0,2106	0,1965	0,1852	0,1158	n.d.	n.d.	n.d.
SO4 (mg/l)	7,28	7,87	7,76	8,77	7,44	7,41	7,32	**10,43**
Na+ (mg/l)	5,97	6,02	6,12	6,72	7,61	7,21	7,24	8,70
K+ (mg/l)	1,31	1,59	1,51	1,77	1,30	1,17	1,16	1,00
Ca2+ (mg/l)	10,59	11,31	11,30	13,06	12,09	12,16	11,95	15,18
Mg2+ (mg/l)	2,02	2,16	2,14	2,37	2,02	2,03	2,02	2,05
∑ cation	0,99	1,04	1,04	1,18	1,13	1,12	1,11	1,33
∑ anions	0,93	1,00	0,98	1,12	1,06	1,05	1,21	1,08
CBE (%)	3	2	3	3	3	3	-4	10

Unfiltered (in ppb)	M-11	M-12	M-13	M-14	M-15	M-16	M-17	M-18
Mn	3,00	16,55	4,20	12,46	3,35	2,08	2,08	2,09
Fe	98,56	421,73	118,84	194,01	71,12	60,33	54,59	54,72
As	1,68	1,52	1,47	1,95	3,01	3,10	3,14	11,50
Ti	4,36	18,01	5,47	8,27	2,71	2,72	2,29	2,45
V	1,86	3,00	2,21	3,07	1,62	1,41	1,34	1,57
Cr	0,49	1,05	0,60	0,75	0,49	0,44	0,43	0,43
Co	0,06	0,21	0,07	0,11	0,04	0,03	0,03	0,03
Ni	0,28	0,58	0,35	0,39	0,25	0,18	0,18	0,20
Cu	2,18	1,86	1,41	5,37	1,55	1,00	0,90	0,95
Al	160,01	557,65	194,51	248,85	148,47	73,40	78,84	80,78
Rb	1,57	2,32	1,70	2,17	1,67	1,51	1,48	1,52
Sr	61,02	60,22	60,51	61,02	62,32	61,83	61,89	78,68
Y	0,16	0,53	0,18	0,25	0,11	0,07	0,07	0,07
Cd	0,04	0,02	0,05	0,03	0,03	0,04	0,03	0,03
Ba	8,04	12,72	8,82	12,30	8,11	7,52	6,78	4,55
La	0,18	0,67	0,21	0,29	0,12	0,08	0,09	0,08
Ce	0,31	1,19	0,36	0,51	0,21	0,15	0,16	0,13
Nd	0,17	0,60	0,19	0,27	0,11	0,07	0,07	0,07
Pb	0,08	0,64	0,16	0,22	0,34	0,03	0,01	0,11

Filtered (in ppb)	M-11	M-12	M-13	M-14	M-15	M-16	M-17	M-18
Mn	0,94	2,06	1,65	6,67	1,78	0,74	0,82	0,75
Fe	24,86	18,49	24,20	34,46	22,25	18,22	15,51	10,96
As	1,55	1,41	1,36	1,81	2,68	2,64	2,52	10,14
Ti	1,04	0,57	0,89	0,65	0,48	0,64	0,56	0,36
V	1,54	1,83	1,79	2,40	1,35	1,17	1,10	1,30
Cr	0,36	0,37	0,38	0,44	0,45	0,52	0,36	0,30
Co	0,02	0,03	0,03	0,04	0,02	0,02	0,02	0,02
Ni	0,22	0,22	0,21	0,23	0,53	0,26	0,38	0,13
Cu	0,71	0,84	0,86	1,05	0,61	0,58	0,83	0,49
Al	59,70	34,73	67,21	84,36	42,11	33,52	28,85	27,69
Rb	1,46	1,65	1,60	0,91	1,82	1,51	1,54	1,46
Sr	60,79	59,42	62,28	75,84	58,17	61,99	65,50	62,77
Y	0,07	0,07	0,08	0,09	0,08	0,05	0,06	0,04
Cd	0,03	0,03	0,04	0,03	0,03	0,02	0,04	0,04
Ba	14,15	15,40	15,37	23,52	15,31	11,34	12,44	10,89
La	0,06	0,05	0,08	0,09	0,07	0,04	0,12	0,03
Ce	0,09	0,07	0,11	0,20	0,09	0,06	0,06	0,05
Nd	0,55	0,54	0,64	0,89	0,60	0,35	0,38	0,28
Pb	0,06	0,05	0,07	0,09	0,07	0,03	0,03	0,04

DTI	M-11	M-12	M-13	M-14	M-15	M-16	M-17	M-18
Mn	31	12	39	54	53	36	39	36
Fe	25	4	20	18	31	30	28	20
As	92	93	93	93	89	85	80	88
Ti	24	3	16	8	18	23	24	15
V	83	61	81	78	84	83	82	83
Cr	73	35	63	59	92	119	84	69
Co	42	13	45	35	55	52	55	44
Ni	79	38	60	58	210	141	211	67
Cu	33	45	61	19	40	58	93	52
Al	37	6	35	34	28	46	37	34
Rb	93	71	94	42	109	100	103	96
Sr	100	99	103	124	93	100	106	80
Y	45	14	46	34	76	65	79	52
Cd	96	111	80	127	80	56	143	157
Ba	176	121	174	191	189	151	183	239
La	32	8	39	29	54	47	134	42
Ce	29	6	30	38	44	40	38	37
Nd	318	90	337	328	565	481	514	396
Pb	77	8	41	43	21	118	256	34

MINOGAWA	July 2013									
Sample #	**M-01J**	**M-04J**	**M-05J**	**M-08J**	**M-09J**	**M-11J**	**M-13J**	**M-15J**	**M-17J**	**M-18J**
Date (j/m/y)	41461,00	41461,00	41461,00	41461,00	41461,00	41461,00	41461,00	41461,00	41461,00	41461,00
GPS	34,8924	34,8889	34,8902	34,8876	34,8875	34,8780	34,8820	34,8739	34,8687	34,8642
	135,4958	135,4981	135,4906	135,4886	135,4886	135,4880	135,4888	135,4841	135,4784	135,4786
Temp°C	16,10	15,10	20,00	18,90	21,00	21,10	21,70	21,60	21,70	21,40
pH	7,06	6,87	7,42	6,87	7,21	7,37	7,29	7,78	7,79	7,78
EC (uS/cm)	56,90	88,70	81,80	115,00	116,30	103,90	109,60	112,80	112,10	122,80
EC 25°C	*68,89*	*110,05*	*90,49*	*130,39*	*125,87*	*112,20*	*116,84*	*120,51*	*119,51*	*131,76*
DO (mg/l)	8,03	7,73	7,28	4,15	4,53	4,33	4,59	4,36	4,46	4,28
ORP (mV)	922,00	806,00	748,00	885,00	876,00	890,00	905,00	889,00	869,00	884,00
TOC (mg/l)	0,14	0,20	0,22	n,d,	0,44	0,18	0,35	0,08	0,07	0,02
DOC (mg/l)	0,06	0,27	0,30	n.d.	0,45	0,22	0,38	0,12	0,08	0,02
HCO3- (mg/l)	10,98	23,42	18,06	10,61	22,08	19,28	19,40	21,35	20,62	24,89
F (mg/l)	0,17	0,15	0,17	0,07	0,28	0,17	0,21	0,15	0,15	0,17
Cl (mg/l)	4,23	5,30	4,87	9,97	7,00	7,41	7,09	8,07	7,55	6,81
Br (mg/l)	n.d.	0,04	n,d,	n,d,	n,d,	n,d,	n,d,	n,d,	n,d,	n,d,
NO3 (mg/l)	1,41	1,43	0,82	4,01	1,35	1,04	1,22	0,96	1,00	1,03
PO4 (mg/l)	0,09	0,18	0,20	0,31	0,22	0,09	0,15	0,14	0,15	0,11
SO4 (mg/l)	4,64	4,03	5,30	11,60	7,72	7,12	7,35	7,19	7,11	9,50
Na+ (mg/l)	6,28		5,44	6,09	6,17	6,70	6,81	7,36	7,19	8,61
K+ (mg/l)	0,87		1,17	3,55	2,09	1,72	1,87	1,57	1,41	1,27
Ca2+ (mg/l)	16,47		9,10	6,79	6,08	8,21	6,64	7,67	8,55	5,80
Mg2+ (mg/l)	1,12		1,68	2,42	2,35	2,17	2,22	2,14	2,07	2,03
∑ cation	1,21		0,86	0,89	0,82	0,92	0,86	0,92	0,95	0,86
∑ anions	0,51	0,73	0,62	1,00	0,84	0,76	0,77	0,81	0,78	0,88
CBE (%)	41		16	-5	-1	10	5	6	9	-1

Unfiltered (in pbb)	**M-01J**	**M-04J**	**M-05J**	**M-08J**	**M-09J**	**M-11J**	**M-13J**	**M-15J**	**M-17J**	**M-18J**
Mn	9,00	1,30	8,70	9,42	29,12	4,45	10,36	6,16	4,48	3,54
Fe	245,63	57,01	253,28	191,47	272,28	120,32	234,47	132,32	107,01	82,87
As	0,31	0,58	0,66	0,98	3,75	2,63	2,66	3,81	4,05	12,45
Ti	8,23	1,38	10,03	6,10	8,01	3,58	6,59	3,21	2,71	2,26
V	1,52	2,76	2,94	1,12	3,41	2,13	2,75	1,95	1,82	1,85
Cr	0,37	0,48	0,75	0,86	0,69	0,56	0,71	0,54	0,49	0,49
Co	0,10	0,04	0,11	0,11	0,12	0,07	0,11	0,06	0,06	0,05
Ni	0,15	0,17	0,47	0,44	0,55	0,51	0,34	0,28	0,24	0,10
Cu	0,52	0,49	1,05	1,79	7,59	1,16	1,69	1,16	1,30	1,10
Al	276,01	75,31	309,91	191,54	209,31	123,35	228,27	123,01	101,37	85,32
Rb	1,99	0,98	1,76	4,78	2,99	2,28	2,63	2,35	2,13	1,93
Sr	44,35	76,92	58,12	88,59	71,48	75,00	68,60	74,27	72,89	83,47
Y	0,71	0,18	0,44	0,32	0,25	0,16	0,25	0,13	0,11	0,10
Cd	0,01	0,01	0,03	0,05	0,04	0,03	0,02	0,01	0,06	0,04
Ba	8,37	8,98	9,51	34,35	16,29	12,40	14,02	10,90	10,54	8,79
La	0,91	0,14	0,55	0,32	0,26	0,19	0,29	0,17	0,13	0,12
Ce	1,29	0,17	0,96	0,43	0,42	0,30	0,49	0,29	0,22	0,20
Nd	0,64	0,11	0,40	0,27	0,20	0,14	0,22	0,13	0,10	0,09
Pb	0,22	0,06	0,27	0,48	0,25	0,20	0,31	0,15	0,22	0,16

Filtered (in ppb)	M-01J	M-04J	M-05J	M-08J	M-09J	M-11J	M-13J	M-15J	M-17J	M-18J
Mn	8,21	0,41	1,65	2,19	21,32	1,51	2,87	2,70	1,37	1,54
Fe	317,40	5,37	17,16	22,88	64,80	27,32	35,23	34,57	24,76	25,93
As	0,31	0,52	0,57	0,66	2,68	1,96	1,95	2,79	2,92	8,68
Ti	12,26	0,35	0,62	0,87	0,76	0,77	0,69	0,74	2,84	0,74
V	1,66	2,40	2,30	0,80	2,83	1,83	2,22	1,64	1,52	1,59
Cr	0,41	0,24	0,31	0,39	0,28	0,30	0,40	0,27	0,26	0,32
Co	0,12	0,01	0,00	0,02	0,05	0,05	0,02	0,02	0,00	0,00
Ni	0,31	0,07	0,32	0,30	0,33	0,24	0,27	0,17	0,24	0,23
Cu	1,58	0,30	0,69	1,21	1,03	0,80	0,97	0,68	0,92	0,71
Al	404,75	7,88	33,77	37,68	30,00	41,87	52,62	30,78	38,05	65,18
Rb	1,55	0,86	1,05	3,78	2,65	1,76	1,95	1,59	1,69	1,46
Sr	38,57	70,41	50,24	79,55	64,86	67,06	63,30	65,26	66,07	75,61
Y	0,49	0,12	0,08	0,13	0,10	0,07	0,08	0,04	0,11	0,04
Cd	0,02	0,01	0,04	0,05	0,04	0,03	0,03	0,06	0,04	0,03
Ba	114,94	16,53	50,91	80,24	22,07	78,05	110,00	53,92	61,58	109,01
La	0,57	0,04	0,07	0,08	0,07	0,05	0,05	0,03	0,11	0,02
Ce	0,72	0,02	0,08	0,08	0,10	0,08	0,08	0,05	0,14	0,05
Nd	4,82	0,68	0,68	0,98	0,79	0,55	0,57	0,35	0,38	0,32
Pb	0,26	0,02	0,06	0,08	0,10	0,08	0,08	0,08	0,10	0,07

DTI	M-01J	M-04J	M-05J	M-08J	M-09J	M-11J	M-13J	M-15J	M-17J	M-18J
Mn	91	31	19	23	73	34	28	44	31	43
Fe	129	9	7	12	24	23	15	26	23	31
As	99	89	88	68	71	74	73	73	72	70
Ti	149	25	6	14	9	22	10	23	105	33
V	109	87	78	71	83	86	81	84	83	86
Cr	110	51	41	46	40	53	56	50	52	66
Co	121	35	1	16	43	75	15	31	6	1
Ni	205	38	69	68	59	46	81	60	102	224
Cu	304	62	66	67	14	69	58	59	71	65
Al	147	10	11	20	14	34	23	25	38	76
Rb	78	87	59	79	89	77	74	68	79	76
Sr	87	92	86	90	91	89	92	88	91	91
Y	69	64	19	41	39	41	30	33	97	38
Cd	204	140	145	113	115	101	195	417	72	82
Ba	1373	184	535	234	135	630	785	495	584	1241
La	63	33	13	26	28	26	19	16	84	19
Ce	56	11	8	18	25	25	16	18	61	27
Nd	753	638	169	363	394	386	259	271	376	349
Pb	116	32	24	16	40	42	26	54	45	41

IBARAGIGAWA

Sample#	I01	I02	I03	I04	I05	I06	I07	I08	I09	I10
Date (y/m/d)	03/05/13	03/05/13	03/05/13	03/05/13	03/05/13	03/05/13	03/05/13	03/05/13	04/05/13	04/05/13
GPS	34,89774	34,89571	34,89536	34,897217	34,897864	34,89243	34,88532	34,879807	34,886643	34,887735
	135,51902	135,51564	135,515708	135,519118	135,521935	135,52713	135,5276	135,523998	135,512542	135,511922
Temp°C	9,9	9,5	7,9	9,3	10,1	12,1	13,8	13,4	9,1	9,1
pH	7,68	7,02	6,91	7,39	7,63	7,79	7,86	7,73	7,55	7,6
EC (uS/cm)	60,5	34,3	34,6	43,6	75,7	90,4	132,7	132,1	47,4	54,1
EC 25°C	86,7	49,7	52,6	63,6	107,8	121,8	171,0	172,0	69,5	79,3
TDS (ppm)	39,0	22,4	23,7	28,6	48,5	54,8	77,0	77,4	31,3	35,7
DO (mg/l)	7,07	7	6,42	7,39	5,13	4,98	4,71	**	7,87	5,57
ORP (mV)	261	307	296	148	213	231	210	230	274	283
TOC (mg/l)	1,55	3,51	2,33	2,56	2,18	2,86	4,57	4,43	1,90	2,07
DOC (mg/l)	1,03	3,88	2,51	2,86	2,29	2,65	4,28	4,05	1,65	1,76
HCO3- (mg/l)	42,27	10,89	8,50	19,83	35,78	45,76	63,45	62,54	27,02	29,63
F (mg/l)	0,50	0,16	0,15	0,25	0,34	0,39	0,45	0,39	0,31	0,15
Cl (mg/l)	3,23	2,83	3,11	3,49	4,91	5,50	9,97	10,03	4,17	4,62
Br (mg/l)	d.l.	d.l.	d.l.	d.l.	d.l.	d.l.	d.l.	d.l.	d.l.	d.l.
NO3 (mg/l)	0,20	1,16	1,63	0,38	0,39	0,39	1,58	1,54	0,54	0,47
PO4 (mg/l)	d.l.	d.l.	d.l.	d.l.	d.l.	d.l.	0,5843	0,2814	d.l.	d.l.
SO4 (mg/l)	2,79	6,95	5,72	4,86	13,33	11,91	12,48	12,58	3,52	3,23
Na+ (mg/l)	7,23	4,50	4,42	5,12	6,39	7,57	11,55	10,64	5,50	5,19
K+ (mg/l)	0,44	0,60	0,57	0,59	0,79	0,91	1,93	1,95	0,56	0,61
Ca2+ (mg/l)	3,16	2,68	2,50	3,03	5,05	6,88	22,35	20,71	3,08	3,18
Mg2+ (mg/l)	8,81	18,60	14,31	14,74	67,30	81,95	278,99	260,43	10,83	10,29
∑ cation	0,95	0,53	0,51	0,68	1,10	1,25	1,78	1,77	0,76	0,80
∑ anions	0,88	0,49	0,47	0,57	1,05	1,20	1,74	1,71	0,69	0,72
CBE (%)	4	4	4	9	2	2	1	2	5	5

Total (in ppb)	I01	I02	I03	I04	I05	I06	I07	I08	I09	I10
Mn	10,99	1,57	5,00	6,97	3,42	15,00	38,46	17,28	2,10	3,11
Fe	635,54	62,99	104,67	199,59	76,78	170,99	549,65	359,69	34,13	66,39
As	0,17	0,11	0,17	0,14	0,23	0,36	0,65	0,54	0,64	0,29
Ti	29,14	3,19	3,62	4,95	2,70	3,21	18,41	11,01	1,63	2,80
V	2,19	0,59	0,41	0,56	0,68	0,62	1,26	1,09	0,95	1,16
Cr	0,60	0,09	0,14	0,23	0,17	0,18	0,53	0,54	0,22	0,24
Co	0,20	0,02	0,04	0,06	0,04	0,05	0,18	0,12	0,02	0,04
Ni	0,26	0,10	0,10	0,23	0,13	0,09	0,36	0,29	0,09	0,08
Cu	0,49	0,03	0,02	0,52	0,77	0,49	2,95	4,62	0,43	0,07
Al	1035,55	74,95	127,06	228,44	133,65	133,64	675,28	391,56	50,42	106,53
Rb	2,11	0,74	0,62	1,11	1,15	1,18	2,62	2,30	1,08	1,37
Sr	40,18	28,79	28,61	29,24	49,38	66,36	94,65	93,18	35,15	43,34
Y	1,50	0,30	1,24	0,48	0,33	0,34	1,05	0,60	0,13	0,26
Cd	0,03	0,01	0,02	0,03	0,01	0,01	0,03	0,02	0,02	0,01
Ba	5,47	6,19	5,83	5,19	5,50	7,25	12,94	10,83	3,05	3,99
La	2,76	0,46	1,47	0,56	0,48	0,46	1,62	0,88	0,16	0,30
Ce	4,11	0,42	1,20	0,97	0,65	0,64	2,89	1,52	0,19	0,43
Nd	2,12	0,40	1,47	0,62	0,39	0,39	1,37	0,73	0,14	0,26
Pb	0,85	0,12	0,21	0,20	0,20	0,18	0,81	0,65	0,10	0,10

Filetredl (in ppb)	I01	I02	I03	I04	I05	I06	I07	I08	I09	I10
Mn	0,30	0,39	0,57	3,09	0,77	9,43	16,12	6,84	0,43	0,38
Fe	8,11	14,79	11,72	34,41	12,75	72,82	58,77	79,43	11,83	11,79
As	0,13	0,05	0,05	0,08	0,08	0,25	0,52	0,49	0,59	0,14
Ti	0,29	0,66	0,50	0,68	0,58	0,99	0,59	1,87	1,01	0,45
V	0,84	0,51	0,27	0,30	0,56	0,48	0,60	0,73	0,91	1,06
Cr	missing									
Co	0,01	0,02	0,01	0,02	0,02	0,02	0,04	0,04	0,01	0,01
Ni	missing									
Cu	0,20	0,49	0,33	0,42	0,42	0,53	1,49	1,67	0,54	0,46
Al	26,29	33,48	23,77	20,63	30,67	32,98	68,67	94,53	23,56	30,30
Rb	0,26	0,57	0,38	0,58	0,95	0,95	1,62	1,88	1,03	0,98
Sr	37,16	29,03	29,18	30,10	50,01	67,24	97,25	95,72	36,78	44,51
Y	0,05	0,23	0,55	0,19	0,14	0,15	0,14	0,20	0,10	0,07
Cd	0,02	0,02	0,02	0,05	0,03	0,02	0,03	0,02	0,03	0,07
Ba	26,29	21,09	16,55	28,50	32,34	54,50	54,19	19,46	9,35	52,95
La	0,08	0,29	0,48	0,18	0,20	0,16	0,15	0,23	0,11	0,08
Ce	0,06	0,10	0,09	0,19	0,16	0,15	0,22	0,35	0,05	0,04
Nd	0,06	0,24	0,49	0,16	0,13	0,13	0,11	0,17	0,07	0,07
Pb	0,02	0,04	0,08	0,04	0,03	0,04	0,09	0,16	0,34	0,01

DTI	I01	I02	I03	I04	I05	I06	I07	I08	I09	I10
Mn	3	25	11	44	23	63	42	40	20	12
Fe	1	23	11	17	17	43	11	22	35	18
As	76	47	27	57	36	71	80	90	92	50
Ti	1	21	14	14	22	31	3	17	62	16
V	38	86	64	53	82	77	47	67	96	91
Cr										
Co	4	63	34	35	57	43	22	33	57	32
Ni										
Cu	41	1404	1920	80	55	108	50	36	125	658
Al	3	45	19	9	23	25	10	24	47	28
Rb	12	77	61	52	83	81	62	82	96	71
Sr	92	101	102	103	101	101	103	103	105	103
Y	4	75	45	40	43	43	14	34	81	27
Cd	57	146	146	186	405	179	87	121	116	1205
Ba	481	341	284	549	588	751	419	180	307	1326
La	3	64	33	33	40	36	10	27	72	27
Ce	2	23	8	20	24	23	8	23	27	9
Nd	3	61	33	25	34	33	8	24	52	26
Pb	2	29	37	20	14	22	11	24	358	7

IBARAGIGAWA

Sample#	I11	I12	I13	I14	I15	I16	I17	I18	I19	I20
Date (y/m/d)	04/05/13	04/05/13	04/05/13	04/05/13	04/05/13	04/05/13	04/05/13	04/05/13	04/05/13	04/05/13
GPS	34,8877	34,893238	34,89636	34,89594	34,88007	34,87916	34,88234	34,885393	34,88479	34,8774
	135,51165	135,509547	135,50653	135,50975	135,52293	135,52323	135,52068	135,518484	135,5176	153,5212
Temp°C	9,2	9,7	8,9	10,3	15,9	14,6	12,8	13,1	12,1	13,6
pH	7,71	7,74	7,78	7,67	8,04	7,95	7,91	7,95	7,94	7,91
EC (uS/cm)	49,1	42,8	40,7	30,2	91,4	107,2	72,9	67,7	73	106,7
EC 25°C	71,8	61,7	60,0	42,8	111,7	135,4	96,4	88,8	98,4	138,2
TDS (ppm)	32,3	27,8	27,0	19,2	50,3	60,9	43,4	40,0	44,3	62,2
DO (mg/l)	5,47	5,88	6,29	5,34	5,69	5,64	7,03	6,63	6,31	5,38
ORP (mV)	277	282	275	276	249	239	230	374	374	369
TOC (mg/l)	2,18	1,28	2,19	2,11	3,01	3,24	2,27	3,48	2,58	2,92
DOC (mg/l)	1,91	1,46	2,22	1,94	3,01	3,48	2,32	3,87	2,45	2,90
HCO3- (mg/l)	26,36	21,57	21,66	13,38	41,40	50,12	33,34	27,50	35,30	50,33
F (mg/l)	0,34	0,27	0,13	0,11	0,39	0,38	0,37	0,51	0,57	0,38
Cl (mg/l)	4,00	3,69	4,08	2,87	5,96	7,75	5,68	5,43	5,29	8,02
Br (mg/l)	d.l.	d.l.	0,03	d.l.	d.l.	d.l.	d.l.	d.l.	d.l.	d.l.
NO3 (mg/l)	0,55	0,39	0,53	0,29	0,87	1,10	0,70	0,49	0,55	1,17
PO4 (mg/l)	0	d.l.	d.l.	d.l.	d.l.	0,12	d.l.	d.l.	d.l.	d.l.
SO4 (mg/l)	3,65	2,92	2,56	3,17	7,39	10,00	6,71	7,95	6,60	10,05
Na+ (mg/l)	5,45	5,08	4,56	4,39	7,18	8,54	6,53	6,64	6,95	8,72
K+ (mg/l)	0,53	0,38	0,70	0,34	1,00	1,35	0,86	0,92	0,77	1,38
Ca2+ (mg/l)	2,90	1,94	3,19	1,47	7,21	11,57	5,58	6,14	5,37	12,00
Mg2+ (mg/l)	10,59	5,67	8,17	4,66	53,29	115,68	37,44	48,80	35,42	120,65
∑ cation	0,73	0,60	0,61	0,44	1,15	1,41	0,98	0,89	1,00	1,43
∑ anions	0,68	0,56	0,57	0,39	1,08	1,35	0,92	0,83	0,93	1,36
CBE (%)	4	4	4	6	3	2	3	4	3	2

Total (in ppb)	I11	I12	I13	I14	I15	I16	I17	I18	I19	I20
Mn	3,70	2,36	6,91	2,46	5,78	5,76	3,23	6,28	5,67	5,16
Fe	63,31	49,89	69,71	60,46	105,96	99,02	56,23	64,74	119,63	76,84
As	0,76	0,33	0,15	0,13	0,53	0,47	0,55	0,26	0,27	0,67
Ti	2,09	1,47	1,25	1,77	3,65	3,38	2,00	1,83	3,87	2,54
V	1,00	0,82	0,35	0,61	1,09	0,89	0,87	0,67	0,96	0,85
Cr	0,22	0,17	0,14	0,16	0,25	0,25	0,20	0,16	1,04	0,22
Co	0,02	0,02	0,03	0,03	0,05	0,04	0,03	0,03	0,06	0,04
Ni	0,06	0,12	0,17	0,09	0,18	0,17	0,14	0,14	0,27	0,18
Cu	0,83	0,00	7,26	0,29	1,19	1,45	0,91	1,05	0,60	1,30
Al	88,43	76,75	54,34	89,08	149,72	128,53	71,75	132,88	227,69	90,66
Rb	1,11	0,90	1,45	0,83	1,46	1,47	1,22	1,04	1,24	1,42
Sr	33,80	26,98	29,28	17,83	55,58	69,42	47,62	38,37	44,92	72,65
Y	0,19	0,18	0,29	0,32	0,29	0,23	0,18	0,30	0,59	0,20
Cd	0,00	0,01	0,02	0,12	0,02	0,02	0,03	0,02	0,02	0,03
Ba	3,13	2,76	4,60	2,76	4,22	6,48	3,51	3,82	3,38	6,63
La	0,24	0,21	0,23	0,39	0,40	0,30	0,23	0,42	0,84	0,25
Ce	0,31	0,29	0,28	0,62	0,58	0,44	0,30	0,56	1,16	0,36
Nd	0,20	0,18	0,20	0,34	0,33	0,24	0,19	0,36	0,69	0,20
Pb	0,11	0,38	1,68	0,12	0,20	0,27	0,10	0,24	0,26	0,19

Filetredl (in ppb)	I11	I12	I13	I14	I15	I16	I17	I18	I19	I20
Mn	0,49	0,35	0,26	0,83	1,46	1,85	1,30	4,08	0,82	2,10
Fe	10,05	8,81	3,89	12,08	9,00	15,24	8,41	15,95	7,29	17,20
As	0,62	0,30	0,03	0,16	0,42	0,35	0,38	0,22	0,19	0,45
Ti	0,45	0,78	0,11	0,26	0,75	0,30	0,37	0,37	0,51	0,41
V	0,89	0,72	0,26	0,49	0,89	0,75	0,79	0,58	0,75	0,75
Cr										
Co	0,01	0,01	0,01	0,01	0,02	0,02	0,01	0,02	0,01	0,02
Ni										
Cu	0,59	0,48	0,42	0,33	1,13	1,03	0,59	0,83	0,51	1,09
Al	41,69	14,79	11,91	28,00	33,53	31,53	15,23	27,37	26,86	32,12
Rb	0,84	0,87	1,40	0,72	1,42	1,50	1,21	0,99	0,93	1,46
Sr	36,44	28,95	31,84	18,35	58,29	77,10	51,58	41,71	47,25	79,08
Y	0,10	0,09	0,10	0,27	0,10	0,10	0,10	0,14	0,14	0,11
Cd	0,02	0,01	0,02	0,22	0,03	0,03	0,03	0,03	0,02	0,03
Ba	69,13	11,05	13,49	13,54	10,48	12,04	9,97	11,68	50,83	15,85
La	0,09	0,09	0,09	0,18	0,11	0,09	0,09	0,16	0,16	0,10
Ce	0,06	0,05	0,03	0,19	0,07	0,08	0,07	0,12	0,09	0,10
Nd	0,08	0,07	0,08	0,17	0,08	0,07	0,07	0,13	0,13	0,07
Pb	0,07	0,04	0,01	0,11	0,10	0,01	0,02	0,02	0,04	0,11

DTI	I11	I12	I13	I14	I15	I16	I17	I18	I19	I20
Mn	13	15	4	34	25	32	40	65	14	41
Fe	16	18	6	20	8	15	15	25	6	22
As	81	90	18	123	78	74	70	81	71	68
Ti	22	53	8	14	21	9	19	20	13	16
V	89	89	76	81	82	85	91	86	78	89
Cr										
Co	49	43	40	40	45	45	42	58	22	56
Ni										
Cu	71	34395	6	116	95	71	64	79	84	84
Al	47	19	22	31	22	25	21	21	12	35
Rb	76	97	96	87	97	102	100	95	75	103
Sr	108	107	109	103	105	111	108	109	105	109
Y	51	49	36	84	34	45	55	48	24	55
Cd	405	91	78	183	160	162	98	148	124	101
Ba	2208	400	294	490	248	186	284	306	1505	239
La	39	42	39	47	28	31	41	39	19	40
Ce	18	16	12	31	12	19	22	21	8	27
Nd	37	38	39	50	23	29	37	37	18	36
Pb	62	12	0	95	50	5	18	10	16	58

IBARAGIGAWA

Sample#	I21	I22	I23	I24	I02J	I03J	I05J	I06J	I07J	I08J
Date (y/m/d)	04/05/13	04/05/13	04/05/13	04/05/13	07/07/13	07/07/13	07/07/13	07/07/13	07/07/13	07/07/13
GPS	34,87013	34,8559	34,86226	34,85398	135,52	135,52	135,52	135,53	135,53	135,52
	135,52755	135,5262	135,54244	135,54836	34,90	34,90	34,90	34,89	34,89	34,88
Temp°C	13,5	13,8	14,1	13,7	18,50	17,10	20,60	23,90	25,70	22,50
pH	7,8	7,92	7,88	8,05	--	7,36	7,27	7,67	7,60	7,88
EC (uS/cm)	112,6	121,6	123,1	126,8	55,50	49,00	138,10	129,20	193,00	125,20
EC 25°C	146,2	156,7	157,4	163,8	63,79	58,19	151,43	132,11	190,34	131,79
TDS (ppm)	65,8	70,5	70,8	73,7	28,71	26,19	68,14	59,45	85,65	59,31
DO (mg/l)	5,73	5,73	5,62	5,58	5,82	6,41	5,17	4,75	4,51	5,52
ORP (mV)	361	361	356	354	862,00	792,00	931,00	901,00	879,00	916,00
TOC (mg/l)	2,82	**	**	**	1,01	0,23	0,67	1,08	1,01	0,80
DOC (mg/l)	3,55	**	**	**	1,19	0,25	0,46	1,14	1,06	0,81
HCO3- (mg/l)	56,00	62,97	65,37	66,46	5,73	5,49	20,98	26,35	37,09	35,01
F (mg/l)	0,38	0,42	0,47	0,43	0,19	0,13	0,32	0,37	0,40	0,36
Cl (mg/l)	8,4485	8,43	8,43	8,38	3,00	2,84	4,79	4,99	9,79	9,41
Br (mg/l)	d.l.	d.l.	d.l.	d.l.					0,04	
NO3 (mg/l)	0,96	0,93	0,67	0,78	1,55	1,64	0,45	0,45	1,02	1,15
PO4 (mg/l)	0,1803	0,148	d.l.	d.l.					0,42	0,25
SO4 (mg/l)	10,33	11,03	10,24	10,58	6,89	5,62	15,85	10,86	12,39	12,67
Na+ (mg/l)	8,94	9,57	10,28	10,06	5,36	5,43	6,91	7,52	10,03	9,48
K+ (mg/l)	1,45	1,62	1,64	1,78	0,88	0,72	1,18	1,36	2,16	1,98
Ca2+ (mg/l)	12,94	15,48	16,88	17,90	4,46	4,00	14,22	14,98	21,03	20,43
Mg2+ (mg/l)	133,68	170,64	172,83	189,43	0,62	0,64	1,57	1,70	2,56	2,64
∑ cation	1,53	1,66	1,68	1,73	0,53	0,51	1,17	1,25	1,75	1,70
∑ anions	1,47	1,59	1,60	1,62	0,44	0,41	0,86	0,85	1,25	1,21
CBE (%)	2	2	2	3	9	10	15	19	17	17

Total (in ppb)	I21	I22	I23	I24	I02J	I03J	I05J	I06J	I07J	I08J
Mn	5,90	7,23	13,49	14,26	101,11	23,67	14,18	27,57	41,54	12,82
Fe	114,40	90,76	207,64	196,48	1821,33	1034,59	341,88	466,42	300,68	186,82
As	0,74	0,94	1,19	1,11	0,31	0,15	0,28	0,65	0,88	0,70
Ti	4,98	3,74	5,51	5,46	75,63	78,00	12,75	7,91	8,65	4,58
V	1,20	1,23	1,26	1,14	4,43	2,11	1,36	1,48	1,17	3,68
Cr	0,32	0,32	0,56	0,51	0,94	0,43	0,35	0,39	0,30	0,49
Co	0,06	0,05	0,08	0,08	0,70	0,32	0,14	0,11	0,11	0,07
Ni	0,21	0,28	0,76	0,82	0,60	0,30	0,31	0,43	0,51	0,24
Cu	1,14	1,25	1,26	1,26	0,16	0,03	0,11	0,13	0,28	0,16
Al	153,68	120,79	207,59	171,59	1948,98	740,45	571,29	314,46	234,35	160,34
Rb	1,43	1,47	1,63	1,74	7,74	5,60	2,11	1,88	2,18	1,79
Sr	76,64	83,54	79,93	83,71	36,81	32,07	53,17	67,02	96,23	89,18
Y	0,26	0,22	0,26	0,25	4,44	3,06	1,15	0,86	0,56	0,36
Cd	0,02	0,02	0,01	0,02	0,05	0,02	0,02	0,02	0,02	0,01
Ba	7,05	7,17	6,85	7,59	15,41	9,48	6,89	8,85	13,35	11,83
La	0,30	0,25	0,30	0,29	8,72	4,23	1,68	1,18	0,75	0,47
Ce	0,47	0,38	0,50	0,49	19,01	4,56	2,77	1,87	1,07	0,76
Nd	0,26	0,21	0,26	0,25	7,17	3,95	1,42	1,00	0,63	0,41
Pb	0,22	0,16	0,21	0,24	4,31	0,78	0,55	0,53	0,37	0,35

Filetredl (in ppb)	I21	I22	I23	I24	I02J	I03J	I05J	I06J	I07J	I08J
Mn	2,15	4,19	7,43	8,07	1,81	0,77	1,41	13,30	26,74	5,13
Fe	15,04	12,75	77,80	68,48	13,50	13,31	19,72	236,59	110,29	66,76
As	0,52	0,69	0,94	0,93	0,28	0,26	0,77	0,83	0,70	0,63
Ti	0,51	0,40	0,99	0,75	0,84	0,71	0,88	2,16	1,09	0,47
V	1,01	1,10	1,05	0,94	0,80	0,48	0,78	1,19	0,94	1,47
Cr					0,12	0,14	0,10	0,26	0,71	0,42
Co	0,02	0,03	0,04	0,04	d.l.	d.l.	d.l.	0,03	0,06	0,02
Ni					0,17	0,11	0,25	0,20	missing	
Cu	1,33	1,01	1,39	1,13	0,26	0,14	0,64	0,88	1,24	0,76
Al	27,24	22,35	67,05	42,47	37,47	50,30	35,72	80,63		
Rb	1,30	1,33	1,46	1,55	0,52	0,36	1,38	1,22		
Sr	77,72	83,58	78,22	82,94	30,92	28,47	52,06	64,94		
Y	0,12	0,11	0,15	0,14	0,33	0,47	0,18	0,31		
Cd	0,03	0,02	0,02	0,02	0,02	0,02	0,01	0,02		
Ba	12,56	15,51	16,35	15,58	109,70	111,83	24,95	63,50		
La	0,10	0,08	0,15	0,19	0,40	0,38	0,17	0,34		
Ce	0,09	0,10	0,19	0,16	0,14	0,06	0,13	0,42		
Nd	0,07	0,06	0,11	0,10	3,29	3,70	1,52	2,67		
Pb	0,03	-0,01	0,07	0,05	0,04	0,01	0,02	0,24		

DTI	I21	I22	I23	I24	I02J	I03J	I05J	I06J	I07J	I08J
Mn	36	58	55	57	2	3	10	48	64	40
Fe	13	14	37	35	1	1	6	51	37	36
As	70	74	79	84	92	171	280	128	80	91
Ti	10	11	18	14	1	1	7	27	13	10
V	84	89	83	82	18	23	57	81	80	40
Cr					12	33	28	67	240	86
Co	38	64	53	48				30	52	34
Ni					28	39	82	46		
Cu	117	81	110	89	168	457	573	674	448	469
Al	18	18	32	25	2	7	6	26		
Rb	91	90	90	89	7	6	65	65		
Sr	101	100	98	99	84	89	98	97		
Y	46	51	58	54	7	15	16	36		
Cd	153	93	177	91	41	90	65	79		
Ba	178	216	239	205	712	1180	362	718		
La	31	31	48	64	5	9	10	29		
Ce	18	28	37	33	1	1	5	22		
Nd	29	30	44	40	46	94	107	266		
Pb	12	-5	32	23	1	1	4	45		

IBARAGIGAWA

Sample#	I09J	I12J	I13J	I17J	I19J	I20J	I21J	I22J	I23J	I24J	I25J
Date (y/m/d)	07/07/13	07/07/13	07/07/13	07/07/13	07/07/13	08/07/13	08/07/13	08/07/13	08/07/13	08/07/13	07/07/13
GPS	135,51	135,51	135,51	135,52	135,52	153,52	135,53	135,53	135,54	135,55	135,51
	34,89	34,89	34,90	34,88	34,88	34,88	34,87	34,87	34,86	34,85	34,89
Temp°C	20,00	18,70	16,70	24,60	23,30	22,80	23,40	25,40	24,40	25,70	15,50
pH	7,41	7,59	7,06	7,54	7,48	7,77	7,82	7,99	7,91	8,02	6,99
EC (uS/cm)	72,10	56,00	50,40	177,00	97,50	153,90	179,10	195,70	190,30	211,00	74,90
EC 25°C	80,11	64,07	60,43	178,43	100,93	160,98	185,02	194,15	192,61	208,09	92,47
TDS (ppm)	36,05	28,83	27,19	80,29	45,42	72,44	83,26	87,37	86,68	93,64	41,61
DO (mg/l)	5,04	6,84	7,60	4,67	4,74	5,25	4,84	5,04	5,13	5,07	5,40
ORP (mV)	935,00	985,00	1031,00	913,00	941,00	920,00	871,00	878,00	869,00	860,00	951,00
TOC (mg/l)	0,30	0,07	0,33	0,39	0,66	1,12	0,40	0,62	0,75	0,75	m.
DOC (mg/l)	0,27	0,08	0,42	0,41	0,79	1,37	0,41	0,58	0,81	0,97	n.d
HCO3- (mg/l)	15,49	12,20	12,20	27,50	16,23	33,92	37,33	74,42	74,42	80,52	39,77
F (mg/l)	0,28	0,26	0,11	0,37	0,53	0,36	0,37	0,40	0,42	0,42	1,43
Cl (mg/l)	4,06	3,58	3,91	6,56	5,54	8,15	9,08	9,47	9,03	9,48	3,22
Br (mg/l)			0,08	0,06		n.d.	n.d.				
NO3 (mg/l)	0,62	0,44	0,45	0,98	0,76	1,04	1,02	0,95	0,79	0,83	0,20
PO4 (mg/l)					0,12	0,15	0,17	0,17	0,10	0,13	
SO4 (mg/l)	3,90	3,03	2,95	8,53	8,95	10,54	15,30	14,77	14,05	15,56	4,16
Na+ (mg/l)	6,12	5,88	5,12	7,95	7,49	8,50	9,90	10,27	10,51	10,68	7,88
K+ (mg/l)	0,79	0,65	1,00	1,40	1,53	1,78	1,93	2,15	2,11	2,37	0,52
Ca2+ (mg/l)	7,29	5,22	5,30	14,42	9,25	17,92	20,95	22,50	21,75	23,27	9,78
Mg2+ (mg/l)	1,22	0,88	1,07	2,27	1,32	2,57	2,98	3,29	3,42	3,91	0,98
∑ cation	0,75	0,61	0,60	1,29	0,94	1,52	1,77	1,90	1,88	2,01	0,92
∑ anions	0,51	0,41	0,41	0,90	0,69	1,10	1,28	1,89	1,85	2,00	0,92
CBE (%)	19	19	19	18	15	16	16	0	1	0	0

Total (in ppb)	I09J	I12J	I13J	I17J	I19J	I20J	I21J	I22J	I23J	I24J	I25J
Mn	6,13	9,61	8,97	19,78	8,06	8,44	9,03	16,14	23,29	20,62	0,72
Fe	118,64	173,49	113,69	378,55	108,42	142,05	182,07	288,74	437,06	283,46	22,95
As	0,58	0,27	0,11	0,60	0,26	0,58	0,74	1,29	1,42	1,36	5,85
Ti	3,74	4,04	2,21	13,22	3,71	4,49	7,59	14,87	16,81	12,02	1,38
V	1,54	1,30	0,59	1,88	1,19	1,34	1,83	2,24	2,21	2,10	1,21
Cr	0,23	0,25	0,15	0,53	0,17	0,29	0,41	0,52	0,72	0,56	0,24
Co	0,06	0,07	0,05	0,17	0,05	0,07	0,11	0,15	0,19	0,14	0,02
Ni	0,17	0,26	0,26	0,53	0,37	1,07	0,41	2,46	1,10	0,87	0,11
Cu	0,04	0,04	0,04	0,19	0,12	0,32	0,16	0,92	0,24	0,21	0,03
Al	178,11	234,90	94,51	510,78	161,14	155,31	291,92	415,19	574,05	300,45	36,41
Rb	1,68	1,38	1,95	2,31	1,50	1,95	2,07	2,35	2,58	2,43	1,38
Sr	35,59	27,28	30,96	65,82	42,56	78,62	91,43	95,28	94,59	96,21	33,91
Y	0,43	0,60	0,31	1,04	0,60	0,33	0,60	0,72	0,74	0,45	0,07
Cd	0,01	0,01	0,01	0,02	0,02	0,03	0,02	0,01	0,03	0,02	0,02
Ba	3,84	3,09	5,97	8,46	5,04	8,71	8,51	9,35	10,06	10,74	0,73
La	0,58	0,79	0,35	1,50	0,84	0,42	0,83	1,03	1,02	0,61	0,05
Ce	0,87	1,21	0,46	2,46	1,22	0,66	1,26	1,68	1,93	1,09	0,07
Nd	0,50	0,66	0,31	1,28	0,71	0,35	0,69	0,85	0,89	0,52	0,04
Pb	0,17	0,24	0,08	0,62	0,15	0,30	0,28	0,35	0,60	0,36	0,06

Filetredl (in ppb)	I09J	I12J	I13J	I17J	I19J	I20J	I21J	I22J	I23J	I24J	I25J
Mn	0,71	0,95	0,84	1,86	4,08	2,42	2,38	5,61	7,23	11,48	0,65
Fe	18,92	17,73	16,63	20,77	22,32	31,24	22,75	25,81	96,94	72,99	30,23
As	0,56	0,36	0,07	0,43	0,28	0,54	0,87	1,15	1,25	1,22	5,21
Ti	1,01	0,73	0,67	1,09	0,71	0,84	1,15	0,63	2,10	1,68	1,34
V	1,25	0,95	0,44	1,19	1,04	1,20	1,53	1,70	1,50	1,61	1,17
Cr	0,00	0,00	0,00	0,00	0,00	0,00	0,17	0,00	0,00	0,00	0,00
Co	0,01	0,01	0,02	0,02	0,02	0,03	0,03	0,03	0,05	0,05	0,01
Ni											
Cu	0,21	0,18	0,20	0,95	0,82	1,27	0,96	1,26	2,29	1,88	0,50
Al											
Rb											
Sr											
Y											
Cd											
Ba											
La											
Ce											
Nd											
Pb											

DTI	I09J	I12J	I13J	I17J	I19J	I20J	I21J	I22J	I23J	I24J	I25J
Mn	12	10	9	9	51	29	26	35	31	56	91
Fe	16	10	15	5	21	22	12	9	22	26	132
As	96	132	58	72	107	93	118	89	88	89	89
Ti	27	18	30	8	19	19	15	4	12	14	97
V	81	73	75	63	88	89	84	76	68	77	97
Cr	0	0	0	0	0	0	41	0	0	0	0
Co	24	15	34	11	46	41	32	23	29	39	72
Ni											
Cu	500	430	540	493	673	403	603	137	938	894	1691
Al											
Rb											
Sr											
Y											
Cd											
Ba											
La											
Ce											
Nd											
Pb											

Sample	IN1	IN2	IN3	IN4	IN5	IN06	IN07	IN08	IN09	IN10	IN11	IN12	IN13
GPS													
EC (18°C)(µS/cm)	99,9	115,3	69,6	69,6	59,8	140,8	91,4	94,5	78,2	46,7	54,3	36,9	57,1
EC	120,6	139,3	85,1	82,1	71,9	163,0	108,6	112,0	91,4	57,9	66,1	48,2	69,3
pH	7,3	8,4	8,6	8,4	8,2	8,2	8,0	7,9	8,5	8,7	8,0	8,3	8,3
ORP (mV)	245	225	209	205	163	188	176	204	196	184	241	204	**57**
DO(mg/L)	7,4	5,5	5,8	6,8	5,6	6,2	53,2	5,4	5,1	5,8	5,3	5,7	**227,0**
Temp. (°C)	16,4	16,4	15,9	17,4	16,6	18,2	17,1	17,2	17,8	15,3	16,1	13,3	16,2
HCO3 (mg/l)	34,1	49,5	24,3	25,4	24,8	61,2	38,9	48,8	32,2	16,4	23,7	17,3	29,5
F-	0,2	0,2	0,2	0,1	0,1	0,3	0,3	0,1	0,1	0,2	0,2	0,2	0,1
Cl-	7,3	7,9	5,6	6,0	5,1	8,7	6,5	5,8	5,9	5,2	4,4	3,9	4,2
NO3-	0,3	0,2	0,2	0,4	0,2	0,9	0,9	0,2	0,4	0,1	0,2	0,0	0,1
PO43-	n.a.	n.a.	n.a.	n.a.	n.a.	n.a.	n.a.	0,1	0,0	0,0	0,0	0,0	0,0
SO42-	6,1	6,4	4,3	5,6	5,1	10,1	6,2	6,3	5,9	3,4	4,1	3,0	4,8
Na+ (mg/l)	7,6	8,3	6,2	6,5	6,3	9,5	8,2	7,0	7,8	6,1	6,2	5,8	6,7
K+	0,9	1,2	0,7	0,9	0,8	2,3	0,9	1,7	1,2	0,5	0,6	0,4	0,6
Ca2+	8,8	11,3	5,8	7,9	6,7	18,1	11,0	13,8	8,5	4,2	5,8	3,3	6,6
Mg2+	1,0	2,6	0,8	0,8	0,5	2,7	1,3	1,3	1,2	0,4	0,7	0,5	0,8
Total Anion	0,9	1,2	0,7	0,7	0,7	1,5	1,0	1,1	0,9	0,5	0,6	0,5	0,7
Total cation	0,9	1,2	0,6	0,8	0,7	1,6	1,0	1,1	0,9	0,5	0,6	0,5	0,7
CBE (%)	3	1	2	-2	1	-2	0	-1	-3	-2	-1	0	1

TOTAL (ppb)	IN1	IN2	IN3	IN4	IN5	IN06	IN07	IN08	IN09	IN10	IN11	IN12	IN13
Al(27)	95,91	154,89	120,62	134,31	126,55	284,13	79,76	63,74	54,05	34,43	39,42	5,60	29,87
Ti(49)	1,98	3,56	2,17	2,97	3,54	9,94	2,04	0,73	0,57	0,46	0,56	0,17	0,26
V(51)	0,60	1,71	0,44	0,51	0,51	2,94	1,29	1,31	0,62	0,22	0,44	0,16	0,20
Cr(52)	0,36	0,46	0,40	0,43	0,46	0,86	0,44	0,43	0,29	0,24	0,21	0,16	0,28
Mn(55)	10,91	16,69	14,11	19,25	13,10	57,09	4,12	113,35	70,33	0,84	1,78	2,02	24,03
Fe(56)	111,35	215,11	143,25	148,57	120,29	333,25	60,22	722,19	416,97	58,02	75,99	10,19	216,36
Co(59)	0,06	0,09	0,08	0,08	0,08	0,17	0,05	0,02	0,02	0,01	0,02	0,01	0,02
Ni(60)	1,81	0,46	0,26	0,36	0,23	0,71	0,03	0,41	0,29	0,27	0,20	0,15	0,19
Cu(63)	2,47	2,07	1,62	2,10	1,61	3,38	2,40	2,08	1,08	0,54	1,30	0,13	0,34
As(75)	0,57	0,63	0,48	0,46	0,50	1,00	0,67	0,85	0,50	0,40	0,70	0,66	0,66
Rb(85)	1,66	1,40	1,29	1,88	1,43	2,09	0,75	1,23	1,30	0,82	0,73	0,43	0,67
Sr(88)	42,13	61,83	30,37	34,56	31,03	85,84	53,37	54,32	28,61	15,67	21,28	14,03	22,33
Y(89)	0,17	0,20	0,21	0,25	0,20	0,37	0,13	0,08	0,07	0,11	0,06	0,03	0,10
Cd(111)								0,03	0,43	0,06	0,02	0,03	0,02
Ba(137)	16,01	12,73	22,39	11,12	7,87	14,17	5,25	0,06	0,08	0,07	0,07	0,07	0,07
La(139)	0,19	0,22	0,23	0,26	0,20	0,41	0,13	0,09	0,08	0,09	0,05	0,02	0,10
Ce(140)	0,32	0,44	0,39	0,45	0,36	0,75	0,17	0,15	0,11	0,08	0,08	0,02	0,15
Nd(143)	0,16	0,19	0,20	0,22	0,17	0,34	0,11	0,09	0,08	0,09	0,05	0,02	0,10
Pb(203)	0,27	0,53	0,31	0,48	0,40	0,67	0,13	0,30	0,32	0,25	0,22	0,14	0,22

0.45um	IN1	IN2	IN3	IN4	IN5	IN06	IN07	IN08	IN09	IN10	IN11	IN12	IN13
Al (27)	35,9	111,2	35,5	65,6	52,1	111,5	48,6	67,6	65,1	36,4	45,5	12,5	32,2
Ti (49)	0,7	1,9	0,4	0,7	0,5	1,8	0,6	0,9	1,0	0,3	0,5	0,0	0,2
V (51)	0,5	1,2	0,3	0,4	0,4	2,4	1,3	1,4	0,7	0,2	0,5	0,2	0,3
Cr (52)	0,2	0,3	0,2	0,4	0,2	0,5	0,3	0,4	0,3	0,2	0,3	0,2	0,2
Mn (55)	6,6	12,5	6,7	11,4	7,5	22,9	2,7	47,7	30,7	1,9	2,4	0,7	11,7
Fe (56)	36,5	86,0	31,8	34,3	24,1	80,2	21,3	184,5	101,8	15,7	21,5	4,3	55,2
Co (59)	0,0	0,1	0,0	0,0	0,0	0,1	0,0	0,1	0,0	0,0	0,0	0,0	0,0
Ni (60)	1,2	0,4	0,2	0,3	0,2	0,8	0,2	0,4	0,3	0,2	0,2	0,2	0,2
Cu (63)	1,1	1,2	0,5	1,0	1,1	2,9	1,4	1,8	1,0	0,1	1,3	0,0	0,3
As (75)	0,6	0,7	0,5	0,5	0,5	0,9	0,7	0,9	0,5	0,5	0,9	0,6	0,7
Rb (85)	1,1	1,1	0,8	1,4	1,0	1,6	0,6	1,2	1,3	0,8	0,7	0,4	0,7
Sr (88)	39,3	59,1	28,2	35,8	30,7	86,7	55,6	75,9	40,3	22,7	30,5	20,8	32,1
Y (89)	0,1	0,1	0,1	0,1	0,1	0,1	0,1	0,1	0,1	0,1	0,0	0,0	0,1
Cd (111)	0,0	0,0	0,0	0,0	0,0	0,0	0,0	0,0	0,4	0,1	0,0	0,0	0,0
Ba (137)													
La (139)	0,0	0,1	0,0	0,1	0,1	0,1	0,1	0,1	0,1	0,1	0,0	0,0	0,1
Ce (140)	0,1	0,1	0,1	0,1	0,1	0,2	0,0	0,1	0,1	0,0	0,0	0,0	0,1
Nd (143)													
Pb (208)	0,1	0,1	0,1	0,2	0,1	0,2	0,1	0,1	0,1	0,0	0,1	0,0	0,1

DTI	IN1	IN2	IN3	IN4	IN5	IN06	IN07	IN08	IN09	IN10	IN11	IN12	IN13
Al (27)	37	72	29	49	41	39	61	106	120	106	115	223	108
Ti (49)	33	53	20	22	14	19	28	120	170	72	96		79
V (51)	84	72	70	79	81	80	101	108	110	91	111	126	140
Cr (52)	56	62	42	82	46	56	68	84	97	103	129	110	62
Mn (55)	60	75	47	59	57	40	65	42	44	224	135	34	49
Fe (56)	33	40	22	23	20	24	35	26	24	27	28	42	26
Co (59)	52	59	37	48	36	38	58	279	241	83	129	42	143
Ni (60)	66	86	78	86	93	107	711	102	102	79	95	148	104
Cu (63)	44	59	30	46	71	87	59	86	89	16	98		84
As (75)	107	112	95	115	102	88	109	111	105	117	122	98	106
Rb (85)	68	75	63	74	68	77	81	98	97	95	96	96	97
Sr (88)	93	96	93	104	99	101	104	140	141	145	143	148	144
Y (89)	37	40	31	37	35	31	58	90	93	88	89	78	92
Cd (111)								80	91	95	93	98	97
Ba (137)													
La (139)	27	33	21	25	25	24	45	82	84	82	82	61	84
Ce (140)	18	30	14	18	17	21	27	74	78	58	61	-21	70
Nd (143)													
Pb (208)	41	26	20	35	18	34	42	39	46	19	25	0	31

Annex 3 – Map of sampling locations for riverbed sediments.

N.B. - Geochemical data for the samples labeled #X are described in Nojima et al. (2011).

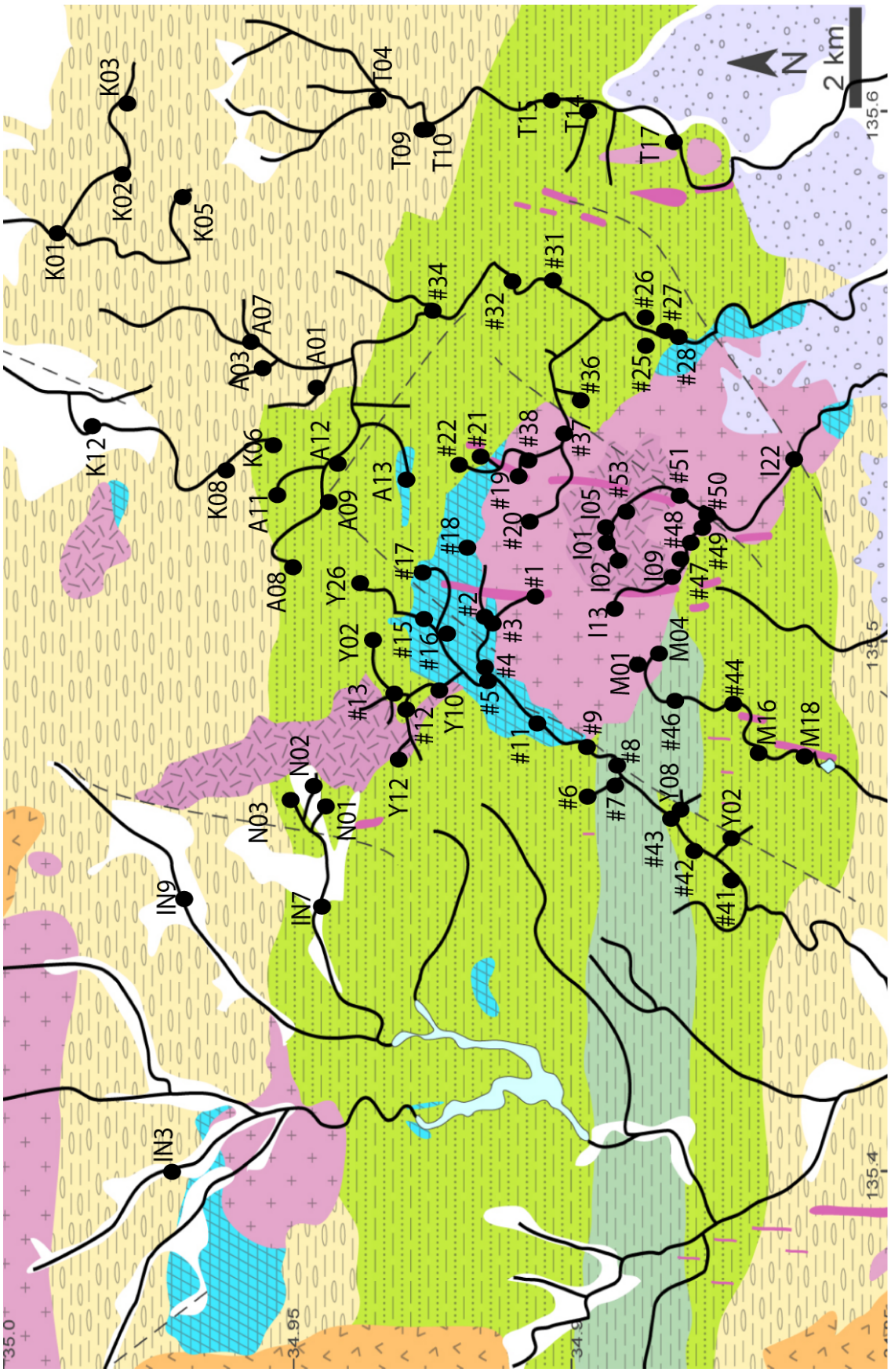

Annex 4 – Geochemistry of riverbed sediments of the study area

Sample	longitude	latitude	SiO2 wt%	TiO2 wt%	Al2O3 wt%	T-Fe2O3 wt%	MnO wt%	MgO wt%	CaO wt%	Na2O wt%
Y02	135,4631	34,8766	69,45	0,71	15,49	5,06	0,12	1,87	1,46	2,57
Y08	135,4685	34,8852	65,85	0,84	18,34	5,63	0,12	1,66	0,83	1,92
Y10	135,4911	34,9261	70,00	0,51	15,13	4,53	0,10	1,06	1,59	2,01
Y12	135,4780	34,9330	68,54	0,34	15,86	5,35	0,86	0,39	0,87	2,35
Y02	135,5006	34,9373	71,70	0,68	14,42	5,50	0,17	1,44	1,13	0,68
Y26	135,5114	34,9395	71,00	0,72	14,64	5,79	0,21	1,44	1,27	1,29
A01	135,5483	34,9469	71,84	0,74	14,55	4,56	0,16	1,10	0,42	1,52
A03	135,5520	34,9560	70,85	0,75	16,06	4,93	0,26	1,06	0,30	0,89
A07	135,5570	34,9580	72,94	0,63	14,24	4,19	0,25	0,99	0,37	1,09
A08	135,5144	34,9509	65,71	0,81	16,84	6,02	0,14	1,29	3,08	1,41
A09	135,5267	34,9448	66,67	0,78	15,22	5,66	0,19	1,63	3,02	1,63
A11	135,5280	34,9535	67,72	1,04	15,98	6,85	0,24	1,87	0,88	1,32
A12	135,5340	34,9433	70,85	0,76	15,05	5,57	0,16	1,46	1,77	1,38
A13	135,5309	34,9317	74,81	0,73	12,11	3,97	0,13	1,09	1,17	1,23
M01	135,4960	34,8924	66,96	0,62	17,06	4,70	0,09	1,11	0,84	1,17
M04	135,4981	34,8889	64,64	1,99	16,76	7,58	0,22	1,68	1,95	1,16
M16	135,4792	34,8720	70,09	0,76	14,82	5,30	0,11	1,48	1,42	1,32
M18	135,4786	34,8642	69,63	0,98	15,29	5,50	0,14	1,43	1,54	1,37
I01	135,5190	34,8977	70,35	0,47	14,82	2,84	0,06	0,57	0,97	1,64
I02	135,5156	34,8957	70,38	0,48	14,86	2,75	0,04	0,64	0,80	1,63
I05	135,5219	34,8979	72,54	0,55	13,44	2,68	0,06	0,55	0,72	1,57
I09	135,5125	34,8866	68,59	0,64	15,24	4,38	0,08	1,08	1,17	1,43
I13	135,5065	34,8964	71,04	0,57	14,26	3,77	0,12	0,77	0,67	0,91
I22	135,5348	34,8660	66,71	0,73	16,17	4,86	0,10	1,31	1,77	2,02
K01	135,5775	34,9908	76,51	0,51	12,86	2,77	0,09	0,64	0,25	1,65
K02	135,5887	34,9798	76,36	0,53	12,70	2,76	0,06	0,64	0,27	1,27
K03	135,6021	34,9790	74,91	0,54	13,46	3,06	0,06	0,72	0,23	1,32
K05	135,5838	34,9690	67,48	0,70	17,70	5,24	0,22	1,10	0,76	1,33
K06	135,5375	34,9542	69,43	1,37	14,10	5,40	0,14	1,24	1,46	1,62
K08	135,5327	34,9622	74,66	1,32	10,62	4,54	0,15	1,00	1,55	1,46
K12	135,5411	34,9849	73,52	0,76	13,09	4,00	0,20	0,91	0,66	1,51
T04	135,6038	34,9369	67,96	0,79	17,51	5,26	0,21	1,34	0,54	1,26
T09	135,5971	34,9290	71,35	0,77	14,77	5,03	0,14	1,39	0,48	1,59
T10	135,5972	34,9282	72,32	0,77	13,94	4,95	0,14	1,41	0,77	1,86
T14	135,6006	34,8991	73,13	0,76	14,39	4,36	0,08	1,17	0,56	1,37
T15	135,5997	34,9070	65,11	0,79	16,33	6,60	0,31	2,07	2,01	2,16
T17	135,5948	34,8863	69,39	0,87	15,49	5,45	0,17	1,41	0,55	1,51
N01	135,4692	34,9453	67,66	0,61	16,98	4,94	0,13	1,03	1,68	3,31
N02	135,4730	34,9474	69,22	0,48	17,73	3,67	0,09	0,26	1,05	3,96
N03	135,4704	34,9513	72,06	0,42	15,78	3,08	0,08	0,28	0,85	3,10
IN3	135,3995	34,9708	73,97	0,57	13,01	3,50	0,13	0,57	0,87	2,34
IN7	135,4502	34,9454	68,61	0,57	15,79	4,90	0,16	1,13	1,60	2,03
IN9	135,4522	34,9682	74,52	0,53	12,41	4,12	0,35	0,65	0,82	1,45

Sample	K2O wt%	P2O5 wt%	*Total*	V ppm	Cr ppm	Co ppm	Ni ppm	Cu ppm	Zn ppm	Rb ppm	Sr ppm
Y02	2,45	0,09	*99,27*	162,89	109,08	40,29	44,71	30,86	113,70	98,03	256,84
Y08	3,71	0,10	*99,01*	192,97	97,32	44,20	44,92	43,25	189,32	160,46	141,20
Y10	4,25	0,10	*99,29*	114,46	63,04	30,82	29,74	36,83	172,37	167,25	130,34
Y12	4,83	0,03	*99,41*	54,57	9,37	34,31	36,19	16,67	225,46	175,94	107,67
Y02	2,96	0,09	*98,77*	153,59	72,54	42,62	36,48	31,49	139,69	118,81	128,01
Y26	2,87	0,10	*99,33*	160,05	97,63	46,17	42,80	41,95	102,35	121,06	133,76
A01	2,70	0,09	*97,68*	157,51	94,13	32,98	38,10	80,06	109,86	106,42	90,06
A03	2,62	0,07	*97,80*	157,00	92,73	38,61	44,42	27,42	98,47	116,38	64,21
A07	2,68	0,06	*97,44*	136,67	85,67	34,19	38,78	30,90	86,81	112,95	77,85
A08	2,18	0,11	*97,58*	186,90	111,84	46,50	43,77	23,08	149,41	94,42	223,38
A09	2,30	0,17	*97,28*	182,41	160,85	43,82	51,56	46,13	567,57	96,67	207,50
A11	2,08	0,13	*98,10*	231,69	108,66	55,01	50,47	43,94	123,50	93,16	142,75
A12	2,15	0,12	*99,26*	172,65	100,38	41,73	42,14	34,77	140,23	90,24	165,87
A13	2,71	0,06	*98,03*	145,36	88,94	28,69	23,84	23,69	130,52	102,88	156,12
M01	5,37	0,09	*98,01*	131,14	27,14	32,62	34,34	22,28	80,42	286,69	104,90
M04	3,18	0,15	*99,32*	364,99	69,91	55,79	33,96	25,42	116,03	184,49	143,97
M16	3,92	0,10	*99,32*	158,08	67,30	37,78	33,01	38,63	215,79	197,39	130,78
M18	3,26	0,13	*99,27*	192,96	81,66	40,11	37,67	71,09	247,58	159,90	151,06
I01	6,22	0,07	*98,01*	82,43	15,59	16,23	34,46	4,98	48,41	340,75	120,85
I02	6,26	0,03	*97,89*	85,91	16,61	14,81	30,45	6,98	48,27	324,55	107,58
I05	5,87	0,04	*98,01*	89,52	18,89	15,37	29,15	11,58	49,65	308,36	103,59
I09	5,16	0,07	*97,84*	128,76	32,12	29,24	30,56	11,87	70,95	272,06	116,99
I13	5,69	0,06	*97,86*	109,74	25,90	25,06	27,05	17,67	56,24	280,31	99,29
I22	4,44	0,11	*98,22*	145,72	41,43	33,21	33,86	23,36	102,50	251,32	143,68
K01	3,02	0,04	*98,33*	98,88	45,75	17,75	18,53	13,50	56,84	106,78	114,77
K02	2,96	0,05	*97,59*	99,97	51,69	17,21	22,49	15,49	60,30	107,48	95,64
K03	3,14	0,05	*97,49*	109,95	59,01	18,56	21,37	17,53	61,42	109,15	90,56
K05	3,31	0,14	*97,98*	150,92	76,64	39,95	44,73	40,89	151,27	134,19	108,62
K06	2,58	0,09	*97,42*	248,35	141,80	42,47	39,00	53,30	106,59	100,82	139,19
K08	2,35	0,07	*97,72*	228,62	143,91	32,34	26,52	36,35	78,87	83,31	137,90
K12	2,63	0,09	*97,38*	145,38	71,04	29,35	28,09	27,43	104,71	97,52	119,97
T04	3,59	0,12	*98,58*	174,29	79,00	40,93	40,14	31,44	129,22	149,07	102,99
T09	2,99	0,10	*98,58*	166,20	96,79	36,46	36,90	34,03	114,08	117,25	86,86
T10	2,17	0,08	*98,41*	162,21	116,26	37,73	36,01	23,86	101,36	85,79	143,78
T14	1,93	0,06	*97,81*	166,95	115,71	34,70	35,66	20,75	74,90	89,04	109,42
T15	2,69	0,13	*98,21*	179,85	100,19	53,73	54,79	47,93	124,43	115,19	227,23
T17	2,96	0,11	*97,92*	183,40	114,15	41,59	41,27	39,20	125,87	115,30	80,89
N01	2,92	0,09	*99,35*	109,07	39,14	32,98	37,74	52,99	246,86	158,24	157,23
N02	2,83	0,02	*99,30*	59,87	12,59	20,19	28,59	5,17	136,44	161,36	104,98
N03	3,29	0,03	*98,97*	58,45	8,93	16,41	19,47	11,71	108,63	154,41	97,05
IN3	3,07	0,05	*98,08*	96,70	39,89	22,45	21,06	41,46	155,15	127,07	104,12
IN7	2,78	0,14	*97,73*	115,31	65,35	34,70	40,38	93,29	247,69	133,08	148,32
IN9	2,77	0,22	*97,85*	96,89	47,51	28,47	21,29	41,11	167,23	119,80	103,89

Sample	Y ppm	Zr ppm	Nb ppm	Ba ppm	La ppm	Ce ppm	Nd ppm	Pb ppm	Th ppm
Y02	39,08	222,74	11,55	373,88	25,80	31,78	16,02	17,10	5,25
Y08	61,69	268,31	19,56	386,65	38,94	50,83	26,43	32,58	9,46
Y10	63,89	231,64	15,18	579,76	30,88	28,65	19,81	23,58	11,35
Y12	99,82	462,34	24,60	792,83	76,86	66,74	44,82	25,86	16,15
Y02	47,11	244,94	13,92	485,32	37,07	46,65	20,87	12,25	8,39
Y26	46,56	236,50	12,18	431,37	34,79	36,87	21,48	15,24	6,46
A01	42,23	224,12	15,91	404,14	25,01	34,91	17,24	8,67	7,21
A03	47,03	236,10	17,38	383,44	30,19	43,12	20,72	12,26	9,13
A07	42,83	217,85	13,80	359,25	29,76	41,50	17,03	10,08	8,07
A08	40,59	262,57	12,63	353,75	30,50	37,27	20,92	23,95	7,21
A09	43,74	249,57	13,74	343,58	31,60	34,68	20,81	28,13	7,17
A11	42,88	232,40	17,69	310,83	31,86	30,82	19,79	11,78	7,34
A12	40,30	225,08	13,99	352,40	36,70	36,50	20,13	12,20	7,26
A13	35,59	391,05	16,49	406,23	27,46	37,60	19,18	7,91	9,90
M01	95,40	313,47	19,22	382,78	36,53	40,78	26,97	10,22	29,25
M04	82,76	765,24	42,21	28,76	48,23	67,83	43,11	11,00	37,93
M16	68,24	284,87	16,92	335,62	25,74	31,87	20,24	17,73	20,01
M18	62,02	363,61	21,07	280,35	36,94	43,51	25,40	44,28	18,33
I01	108,64	377,00	17,66	455,66	39,71	55,10	29,39	9,00	40,25
I02	99,66	461,36	19,13	424,51	26,95	38,19	22,78	8,02	25,76
I05	93,75	355,96	18,05	406,22	25,95	39,34	19,43	8,39	37,18
I09	89,34	343,28	18,02	347,92	26,52	38,07	22,93	7,83	34,35
I13	88,03	339,16	16,79	472,80	21,40	32,83	20,90	6,99	24,58
I22	93,61	552,95	19,92	310,21	35,26	56,64	34,54	10,50	34,70
K01	36,69	214,63	10,18	511,11	24,65	29,77	15,61	7,04	5,77
K02	39,17	215,80	10,78	488,89	36,02	30,30	21,08	7,68	6,23
K03	40,23	210,90	11,38	463,93	33,76	25,78	20,13	7,69	5,53
K05	66,02	265,20	16,90	514,42	90,09	23,97	48,43	18,08	9,94
K06	46,34	582,55	26,72	263,79	41,97	48,90	34,02	73,66	12,60
K08	36,96	434,94	21,71	227,18	35,79	37,44	21,00	18,94	10,02
K12	37,84	225,60	14,29	425,16	28,71	28,12	17,81	16,66	7,13
T04	61,27	253,22	17,79	485,09	52,33	46,24	30,89	17,14	9,96
T09	46,37	230,98	16,58	353,32	31,07	38,34	20,92	9,34	8,28
T10	37,44	219,61	11,68	310,85	28,19	26,66	19,94	9,26	5,99
T14	41,07	243,93	12,99	206,45	26,53	32,54	19,03	8,44	6,21
T15	50,80	215,78	14,45	406,57	37,50	40,65	25,55	10,12	7,86
T17	47,68	249,05	19,01	330,04	33,81	36,81	22,72	10,92	8,37
N01	78,72	623,23	34,53	410,10	72,46	60,57	46,84	18,88	20,57
N02	82,83	692,86	34,79	406,02	71,32	64,10	49,34	20,65	24,53
N03	64,75	584,68	26,17	490,40	36,43	52,12	30,91	11,66	19,98
IN3	50,56	266,18	25,44	469,68	25,88	35,98	19,71	15,01	8,82
IN7	63,36	312,32	18,46	404,34	42,72	47,58	32,45	27,93	12,94
IN9	47,41	290,09	16,25	501,19	34,40	41,29	21,05	17,58	9,54